Molecular characterization of hair cell metabolism and tip link damage

by

Kateri J. Spinelli

A dissertation in partial fulfillment of the requirements for the degree of

Doctor of Philosophy

Presented to the Neuroscience Graduate Program

Oregon Health & Science University

School of Medicine

February 2012

School of Medicine

Oregon Health & Science University

_____

CERTIFICATE OF APPROVAL

_____

This is to certify that the Ph.D. dissertation of

KATERI J. SPINELLI

has been approved on February 8, 2012

_____

Advisor, Peter Gillespie, PhD

_____

Member and Chair, Teresa Nicolson, PhD

_____

Member, Gary Banker, PhD

_____

Member, Anthony Ricci, PhD

_____

Member, Gary Westbrook, MD

Table of Contents

List of Figures

Acknowledgments

I thank Dr. Peter Gillespie for his keen guidance and thoughtful intellectual contributions to my thesis work over the last 5 years. Peter has taught me to think deeply about a scientific problem, to critically evaluate my work and the work of others, and to carefully and thoughtfully perform experiments in the laboratory. I appreciate him including me in peer reviews of outside manuscripts, written reviews of published work, and dinners with fellow hair-cell scientists. I am particularly gratefully that he encouraged and supported my summer science adventure at Marine Biological Laboratories. I also thank him for the freedom to pursue projects of my own desire and design, and for his substantial contribution to the mass spectrometry and microarray analyzes.

I thank my committee members, Dr. Teresa Nicolson, Dr. Gary Banker, and Dr. Tony Ricci. Because Teresa's lab is interested in tip links and calcium imaging, she and her post-docs became great resources for exchanging experimental ideas. Gary was instrumental in advising my post-doc search and offering advice on alternative careers. Tony was gracious enough to work with me directly at his laboratory at Stanford to attempt mechanotransduction recordings in the chicken cochlea. He also provided much guidance and advice on the calcium-imaging portion of my project.

Dr. Larry David and John Klimek performed mass spectrometry experiments, and I thank them for this invaluable contribution to my thesis work. I would like to further acknowledge Dr. Stefanie Kaech-Petrie, Aurelie Snyder, Dr. Joe Trapani, and Dr. Kevin

Abstract

Inner ear hair cells are required for our senses of hearing, balance, and acceleration. Because hair cells do not regenerate in humans, life-long maintenance and repair of these cells directly influences age-related hearing loss, yet we do not fully understand the molecular processes that govern normal cellular activity or a cell's response to and recovery from damage. This thesis characterizes hair-cell energy metabolism in chicken auditory and vestibular organs, and explores the cellular response to hair-bundle tip link damage. Chapter 1 gives a background of the relevant literature on energy metabolism and the tip link, highlighting what information is lacking and how the experiments on this thesis will advance our understanding. Chapter 2 presents a complete molecular characterization of the utricle and cochlear epithelium, which revealed that the cochlea up-regulates the glycolytic energy production pathway. Chapter 3 presents data on the fate of the tip link proteins CDH23 and PCDH15 following tip link breakage, using immunohistochemistry and scanning electron microscopy to examine tip links. Evidence is presented for the redistribution and intracellular co-localization of CDH23 and PCDH15 upon tip link breakage. Chapter 4 describes a novel method of calcium imaging in the chicken cochlea, using a cell-permeable dye to simultaneously monitor intracellular calcium in many hair cells following tip link breakage and pharmacological manipulation. Combined, this thesis uncovers tissue-specific pathways for inner ear energy metabolism and provides new evidence for how the hair cell responds to damage of the mechanosensory organ.

Chapter 1 – Introduction

Hair cells: highly specialized in structure and function

Inner ear hair cells are elegantly designed to carry out one task: convert sound-induced mechanical displacements of less than 1 nm into a chemical signal conveyed to the auditory nerve. This process is fast, with sub-millisecond responses at the level of the mechanosensory organ, called the hair bundle. To maximize sensitivity, the hair bundle has a quick reset button – in a process called adaptation, the mechanosensitive channel partially closes, and is thus able to respond to a second stimulation within a few milliseconds of the initial stimulation. Through active mechanisms in the cochlea, a non-linear sensitivity gain enhances signals at low sound pressure levels, ensuring that quiet sounds are amplified (for review, see (1, 2)). These features of the cochlea, combined with the faithful transfer of information through the ascending auditory pathway, results in a remarkably short delay at the level of auditory perception – the human cortex has the astounding ability to resolve individual click stimuli that are separated by just 15 milliseconds (3).

To achieve such precision and speed, hair cells require a unique cellular architecture. The sensory hair bundle is composed of an array of actin-filled stereocilia, arranged in a staircase pattern of increasing height. The rigid stereocilia core, filled with actin filaments and cross-linkers, ensures that the bundle can withstand force displacements of up to 100 pN. Tight coupling between stereocilia by extracellular

filaments and cohesive forces allow the stereocilia to move as one, resulting in precise timing of the gating and reset elements (4). Continuous, graded neurotransmitter release in the absence of stimulation ensures that the synapse is primed for synaptic transmission when a mechanosensory event occurs at the bundle. Electron-dense ribbon structures in the synaptic region supply a plethora of synaptic vesicles to the active zone, rapidly replenishing the readily releasable pool. Even the small cell body of the hair cell encourages a speedy response – decreased capacitance ensures that changes in membrane voltage necessary to trigger neurotransmitter release are rapidly conveyed to synaptic release sites (5).

Energy demand is substantial for the hair cell to operate under these stringent timing requirements. In the hair bundle, the major consumer of ATP is the plasma membrane calcium pump (PMCA2a) (6, 7). Calcium enters the hair bundle through the transduction channel, and is extruded from the bundle by PMCA2a at a rate of 3.7 fmol/second (8). Myosin motors, important for adaption of the transduction complex, and actin treadmilling are other sources of energy demand in the bundle. By examining the protein complement of isolated hair bundles by mass spectrometry (MS), our lab found that energy metabolism proteins are prominent in vestibular hair bundles, second only to cytoskeletal proteins (7). The bundle houses many enzymes involved in glycolysis, and inhibiting activity of this metabolic pathway reduces ATP levels and decreases transduction channel adaptation. Brain creatine kinase (CKB), the second most abundant hair-bundle protein, was proposed to act as the primary source of hair-bundle energy. Modeling shows that levels of ATP necessary for maintaining bundle

PMCA2a activity can only be achieved with the work of a BCK/phosphocreatine shuttle from mitochondria in the cell body. Further support for the essential role of BCK in mechanotransduction comes from BCK knockout mice, which have reduced hearing sensitivity and vestibular dysfunction (7).

At the level of the epithelium, enzymatic experiments from the 1970s directly measured metabolism molecules in acutely dissected organs. Using amplification by enzyme cycling followed by fluorometry, Thalmann and colleagues found that glucose and glycogen are much higher in the guinea pig cochlea compared to the vestibular organs of the sacculus, utricle, and semi-circular canals (9). Differences in vascularization also exist between the auditory and vestibular organs, with the cochlea showing decreased vascularization compared to the vestibule (10). Indeed, the drastic difference in blood vessel infiltration between these organs is what prompted the authors to investigate energy metabolism molecules.

To expand on and further explore these differences between the auditory and vestibular organs, we have performed quantitative MS on chicken cochlear and utricular epithelia. Pairing MS with gene microarrays provided the sensitivity and dynamic range to thoroughly evaluate the molecular composition of each organ. Chapter 2 describes our findings, including differences in proteins and transcripts of the glycolytic and oxidative phosphorylation pathways, which provide further support for the original reports on the prominence of glycolysis in the auditory system.

Tip link proteins and mechanotransduction

Cochlear mechanotransduction occurs when a sound stimulus deflects the hair bundle, which increases tension on extracellular tip link proteins to open the transduction channel. The tip link stretches from the tip of a short stereocilium to the side of the next tallest stereocilium in the staircase. Transduction channels have been localized to the lower end of the tip link, however the molecular identity of the channel is unknown, making it difficult to test the mechanism of channel gating (8). Possible gating mechanisms include a direct interaction of the tip link and channel, an indirect interaction through auxiliary proteins, or gating of the channel through membrane tension from tip link exerted force on the membrane (1, 11).

Tip links are only visible under the scanning and transmission electron microscopes, where structural analysis gives diameter and length estimates of 5-10 nm and 150-200 nm, respectively (12, 13). Tip link filaments have a helical structure and appear to be composed of two tightly coiled molecules that sometimes branch at the stereocilia insertion points (12, 13). The tip links' dependence on calcium for proper structure and function is well documented. Chelating extracellular calcium leads to loss of tip links and an inability to mechanically gate the transduction channel, providing support for the tip link as an essential element of channel gating (14-19).

Mounting evidence suggests that the tip link is composed of two members of the cadherin family, cadherin 23 (CDH23) and protocadherin 15 (PCDH15) (20-27). These single-pass transmembrane proteins have large extracellular domains, with CDH23 containing 27 extracellular cadherin (EC) repeats and PCDH15 containing 11 EC repeats.

Human deafness disorders Usher syndrome type 1D (USH1D) and nonsyndromic deafness DFNB12 correspond to mutations in CDH23, whereas USH1F and DFNB23 map to mutations in PCDH15 (28-32). Mouse and zebrafish mutants of these proteins lead to defects in mechanotransduction and deafness (21, 25, 32, 33) (for review, see (34)). One recent study thoroughly examined two PCDH15 mutants and one CDH23 mutant using a number of different assays for tip links and transduction (27). The Ames waltzer *av6J* mutation results in deletion of part of the PCDH15 extracellular domain. These mice have fewer tip links and reduced transduction responses compared to control, suggesting that the tip link is functional but may be compromised. Ames waltzer *av3J* mice have a point mutation in PCDH15 that introduces a stop codon in the extracellular domain, resulting in loss of protein expression in the hair cell and a dramatic reduction in the number of tip links. Mechanotransduction is abnormal in these mice, and the uptake of FM1-43 and gentamicin is impaired; under normal conditions, these molecules enter the cell through transduction channels open at rest. The waltzer *v2J* mutation of CDH23 results in a premature stop codon and loss of protein expression. These mice do not have tip links and exhibit many signs of impaired mechanotransduction, including loss of FM1-43 loading and abnormal transduction channel response (27).

Because the tip link has been precisely localized to the stereocilia tips by electron microscopy, antibodies against tip link proteins should specifically localize to this region of the hair bundle. In the adult guinea pig and mouse, antibodies to the extracellular domains of CDH23 and PCDH15 localize to stereocilia tips in both

immunohistochemistry and immuno-electron microscopy (EM) experiments (23). There are at least 24 isoforms of PCHD15 in the mouse inner ear, however, making tip link isoform specificity difficult to determine (24). Moreover, many studies that examined the presence of CDH23 and PCDH15 in the tip link were performed in the early post-natal mouse cochlea (P3-P5), which contains numerous transient lateral links located near stereocilia tips that are also composed of these proteins (18, 24, 35). Because of the presence of these lateral links in proximity to the tip link, assessing antibody labeling and EM structure of the tip link in young animals is difficult. Furthermore, in the cochlea of these animals the bundle and mechanotransduction is still developing; thus, the relationship between tip links and mature transduction response is not definitive (36).

To eliminate complications of data interpretation that are inevitable in the early postnatal mouse cochlea, Chapter 3 of this thesis examines the tip link in late embryonic and early post-hatch chickens (E21/P0). In contrast to early post-natal mice, hair bundles in the chicken cochlea are almost fully mature at birth, with many components of the transduction apparatus in their proper location and mechanotransduction responses closely approximating adult (37). Tip links are clearly distinguishable at stereocilia tips, with few to no lateral links apparent in the bundle (38, 39). As in the mammalian cochlea, CDH23 and PCDH15 have been localized to stereocilia tips in the chicken cochlea and utricle (26). In Chapter 3, I use immunohistochemistry to localize CDH23 and PCDH15 to stereocilia tips in the chicken cochlea and utricle, using multiple antibodies to verify CDH23 staining.

Interaction of CDH23 and PCDH15 to form the tip link

Immuno-EM experiments show that the lower portion of the tip link is composed of CDH23 and the upper portion of PCDH15 (23, 26). More specifically, it is thought that a homodimer of CDH23 extends from the lower stereocilium to interact *in trans* with a PCDH15 homodimer attached to the taller stereocilium (23, 26). This interaction occurs at the N-terminus of each protein, consistent with the known interaction of classical cadherins. Unlike classical cadherins, however, tip link cadherins do not contain the typical N-terminal binding motifs that are known to mediate the strand-swapping trans interaction. Length estimates of purified, trans-interacting CDH23 and PCDH15 match measured tip link lengths, providing additional support for these two molecules as tip link proteins (23).

Recent structural studies of purified CDH23 EC1+2 domains reveal a novel calcium-binding site at the N-terminus of this protein (40, 41). When two of the polar amino acids that mediate calcium binding at this site are mutated to hydrophobic residues, CDH23 and PCDH15 no longer interact *in vitro*, implying that calcium binding at this site of CDH23 is necessary and sufficient for the interaction with PCDH15 (41). Although it is known that calcium binding at EC interdomains is essential for structural rigidity of cadherin molecules, this finding suggests that it is not simply the rigid tertiary structure of the entire extracellular domain that enables the CDH23/PCDH15 interaction, but specifically calcium bound to this novel site at the tip of CDH23. To what extent this lone calcium ion plays a role in tip link interaction in the hair cell is not yet known. Although these new structural studies shed light on potential trans-

interacting domains in the N-terminus of CDH23, more studies are necessary to

determine how CDH23/PCDH15 interact to form the unique structure of the hair-cell tip

link. A deeper understanding this interaction, in particular the role of calcium, will also

shed light on tip link breakage by calcium chelators.

Hair cell damage: tip link breakage

Chelating extracellular calcium with BAPTA or EGTA leads to rapid loss of tip links

and disruption of transduction channel activity (13-17, 35, 42). All cadherin molecules

rely on calcium bound at EC interdomains to retain their structural integrity, and thus

their function. But what exactly happens to the hair-cell tip link when calcium is

removed from the extracellular media? Without knowing the nature of the

CDH23/PCDH15 interaction in the tip link, this question is hard to answer. Perhaps the

EC domains of CDH23 and PCDH15 simply unfold, leaving the usually rigid tip link limp

such that it can no longer mechanically gate the channel. Alternatively, CDH23 and

PCDH15 N-termini may dissociate from one another in the absence of calcium, thus

severing the tip link. Another possibility is that calcium removal triggers an

intermediate step that in turn leads to tip link loss, for example reduction of a disulfide

bond or proteolytic cleavage of the tip link. In Chapter 3, I directly test the role of

proteases in tip link breakage by chelating extracellular calcium in the presence of an

array of protease inhibitors, and examining tip link presence.

Antibodies against CDH23 and PCDH15 can be used to monitor the location of

these two proteins after tip link breakage, but the literature concerning their fate

beyond breakage is contradictory. Using a cytoplasmic antibody against CDH23 in the

frog sacculus, one group reported that staining disappears from stereocilia tips after

BAPTA treatment, with an accompanied increase in cell body staining (20). In the guinea

pig cochlea, however, CDH23 staining with an extracellular antibody appears to stay in

place or move slightly upward along the stereocilia after BAPTA treatment (23).

Extracellular PCDH15 staining disappears from the stereocilia tips following tip link

breakage in the chicken utricle, a finding that is also seen in the early post-natal mouse

cochlea with an intracellular antibody against PCHD15 (24, 43). With yet another

antibody against the PCDH15 extracellular domain, this same study reported that

bundle staining is *enhanced* by BAPTA treatment (24). It was later discovered that post-

fix antibody labeling with extracellular tip link antibodies is enhanced by unmasking

epitopes with calcium chelators, so the authors speculate that the unmasking effect

contributes to the increase in staining after BAPTA (23, 24).

Given the number of different antibodies, organs, species, and animal ages used

in these experiments, it is difficult to make general conclusions about the mechanism

and effect of tip link breakage. Chapter 3 of this thesis focuses on tip link breakage in

one organ, the chicken cochlea, with supportive data from the chicken utricle. The

chicken cochlea is mature at birth, with few to no lateral links at stereocilia tips, making

this organ ideal for scanning electron microscopy (SEM) and immunohistochemical

characterization of tip links. A number of treatments were tested for their ability to

break or protect tip links, including mechanical displacement of the bundle and protease

inhibitors, respectively. Three antibodies against CDH23 were characterized by

immunohistochemistry and immunoblot for specificity in the chicken cochlea, and one previously characterized antibody against PCDH15 was used in parallel for double labeling experiments. These antibodies were used to explore the fate of these proteins after tip link breakage.

Recovery from damage: tip link regeneration

Exposure to loud sounds can result in temporary or permanent hearing loss. Hair cell death is thought to underlie permanent hearing loss, whereas hair bundle morphology is affected by stimuli that induce temporary hearing loss (44-46). Specifically, hair bundle stiffness decreases, and tip links disconnect or disappear (47-49). In the chicken cochlea, exposure to intense sound results in a loss of tip links in the region of damage, and tip links reappear if the animal is allowed to recover for 24-96 hours (50, 51). Typical recovery times from the temporary threshold shift (TTS) associated with noise-induced hearing loss in humans are less than 24 hours, similar to the time course for reappearance of tip links in animal models (52, 53). Combined, these findings indicate that restoration of broken tip links may underlie recovery from TTS associated with noise-induced hearing loss.

In the chicken cochlea *in vitro*, tip links broken by calcium chelation can regenerate over 6-12 hours in culture, and mechanotransduction returns after 24 hours (42). In the early post-natal mouse cochlea, small mechanotransduction responses can be recorded after 3 hours of recovery from calcium chelation, and gradually increase in amplitude to fully recover at 12 hours (54). This process can be blocked by incubation

with extracellular CDH23 and PCDH15 fragments, indicating that recovery of transduction is due to the reformation of tip links. Tip link regeneration is not dependent on new protein synthesis, as incubation with cyclohexamide to block protein translation has no effect (42). However, raising intracellular calcium with the calcium ionophore ionomycin does block regeneration, indicating that low intracellular calcium is required for regeneration of tip links.

A proposed model of tip link regeneration involves hair bundle calcium and myosin motors, as follows: the direct result of breaking tip links is transduction channel closure, which will eliminate calcium entry through transduction channels open at rest. When hair bundle calcium decreases, plus-end directed myosin motors that are normally inhibited by calcium entry in the vicinity of the channel could climb up actin filaments to the stereocilia tips. These motors could transport tip link proteins into the region where they must connect to each other and to the mechanotransduction complex (42).

In addition to a decrease in hair bundle calcium, tip link breakage likely results in a decrease in cell body calcium – voltage-gated calcium channels that are partially activated at resting membrane potentials will close when the cell hyperpolarizes as a result of transduction channel closure (55-57). Despite the apparent importance of low calcium for tip link regeneration, changes in hair bundle and cell body calcium following tip link breakage have not been directly measured. In chapter 4, I describe a method of labeling hair cells with a cell-permeable calcium dye. Control experiments verified that the hair bundle calcium signal originates from calcium entry through functional

transduction channels. Because this method labels all hair cells in an epithelium with limited disruption to the tissue, it will be a useful tool for studying intracellular calcium during tip link regeneration in a population of hair cells.

Overall goals

The overall goals of this thesis are to compare the molecular composition of the auditory and vestibular organs of the chicken, and to characterize cellular changes associated with hair-cell tip link breakage. In chapter 2, I characterize differences in genes and proteins expressed in the chicken cochlea and utricle, highlighting differences in energy metabolism and the potential biological reason for these differences. Chapter 3 describes the immunolocalization of CDH23 and PCDH15 following tip link breakage, and also includes experiments that test the mechanism of breakage. In chapter 4, I present a novel method for loading hair cells in the cochlea with a calcium indicator and describe a number of experiments that test the source of the hair-bundle calcium signal. Applicability of this method for studying tip link regeneration is discussed. Finally, in Chapter 5, I describe one pilot experiment regarding the mechanism of tip link regeneration, and discuss future experiments related to the discoveries made in this thesis.

Chapter 2 – Distinct energy metabolism of auditory and vestibular sensory epithelia revealed by quantitative mass spectrometry using MS2 intensities

Kateri J. Spinelli[a,b,*], John Klimek[c,*], Phillip A. Wilmarth[c], Jung-Bum Shin[a,b,†],

Dongseok Choi[d], Larry L. David[c,e,‡], and Peter G. Gillespie[a,b,‡,§]

[a]Oregon Hearing Research Center, [b]Vollum Institute, [c]Proteomics Shared Resource,

[d]Department of Public Health & Preventive Medicine, [e]Department of Biochemistry &

Molecular Biology, Oregon Health & Science University, Portland OR 97239, [†]Present

address: Department of Neuroscience, University of Virginia, Charlottesville, VA 22908

*K.S. and J.K. contributed equally to this work.

Abstract

Measuring the abundance of many proteins over a broad dynamic range requires accurate quantitation. We show empirically that in mass-spectrometry experiments, relative quantitation using summed dissociation-product (MS2) ion-current intensities is accurate, albeit variable from protein to protein, and outperforms spectral counting. Applying MS2 intensities to quantify proteins in two complex but related tissues, chick auditory and vestibular sensory epithelia, we find that glycolytic enzymes are enriched three-fold in auditory epithelia, while enzymes responsible for oxidative phosphorylation are elevated at least four-fold in vestibular epithelia. This striking difference in relative utilization of the two ATP-production pathways likely reflects the isolation of the auditory epithelium from its blood supply, necessary to prevent heartbeat-induced mechanical disruptions. The global view of protein expression afforded by label-free quantitation with a wide dynamic range reveals molecular specialization at a tissue or cellular level.

Introduction

Modern mass spectrometry methods allow parallel detection of thousands of proteins. With accurate proteome-wide quantitation, perturbation experiments that test functional interconnections of protein networks are feasible (58). While known proteins can be accurately quantified using directed and targeted mass spectrometry (59), these approaches require respectively high-resolution instruments or substantial experimental groundwork. By contrast, the protein landscape in many experiments is unknown, necessitating a shotgun (or discovery) proteomics approach (59), which does not assume prior knowledge of which proteins vary in concentration or modification.

While methods that require cotranslational (60) or post-translational (61, 62) labeling enjoy wide acceptance, not only can labeling be technically impractical for some experiments but these methods' accuracy is often no better than that of label-free methods (63). Several label-free methods have been introduced for mass-spectrometry quantitation, with spectral counting (64) in particular garnering wide acceptance.

A drawback for quantitation by spectral counts is that counts saturate for abundant proteins (65). To counter this compression, Shin et al. (7) summed collision-induced dissociation products (MS2 peaks) assigned to each protein. While two proteins of differing abundance, each detected by single peptides, are measured as equal in concentration by spectral counting, intensity-based methods in principle could yield greater accuracy if the intensity is proportional to peptide mass (Fig. 1a). Griffin and

colleagues introduced "spectral index" (66), essentially the same measure as proposed by Shin et al., and showed that it outperformed other label-free methods for quantitation. However, neither Shin et al. nor Griffin et al. demonstrated whether normalized MS2 intensities exactly reported the fraction of each protein analyzed.

In our experiments, we desired an accurate quantitation method for relative comparisons. Because varying peptide ionization, MS2 selection, and MS2 signal render the relationship between ion-current intensity and peptide abundance uncertain, we sought to empirically determine the suitability of MS2 intensity for protein quantitation under conditions of high protein complexity. Moreover, to verify our MS2 intensity quantitation methods, we sought a direct comparison of the molecular composition of two related but distinct biological tissues. Auditory and vestibular inner-ear organs contain highly specialized sensory epithelia, each consisting of sensory hair cells and supporting cells. While morphologically and functionally similar, auditory hair cells are stimulated by vibrations of the whole cochlear sensory epithelium and its underlying basilar membrane, while vestibular hair cells respond to movement of an overlying extracellular matrix structure. Our results show that MS2 intensity reports protein abundance more accurately than spectral counting, and that use of this quantitation method reveals biologically-relevant differences in energy utilization by auditory and vestibular epithelia.

Results

Label-free quantitation with MS2 intensities

We first sought to compare spectral counting to MS2-intensity quantitation under controlled conditions replicating typical experimental situations. We diluted a mixture of purified proteins into an *E. coli* protein extract (Experimental Procedures), carried out SDS-PAGE and in-gel tryptic digests, then subjected peptides to liquid chromatography tandem mass spectrometry (LC-MS/MS) using an LTQ ion-trap mass spectrometer. Following SEQUEST identification of peptides, proteins were identified and assigned summed spectral counts and MS2 intensities using the PAW results-processing pipeline (67).

We generated normalized spectral counts (*c*) and normalized MS2 intensities (*i*) by dividing counts or intensity for each protein by the sum of all counts or intensities for all detected proteins for each run. Spectral counts and intensities for peptides shared by more than one protein were divided amongst those proteins based on the relative counts or intensities of the unshared peptides (68). For each protein, *c* and *i* were averaged over five biological replicate runs. We plotted log *c* or log *i* against the log of the known mass fraction (w_i, the ratio of the mass for each spiked protein relative to the total protein mass injected; $w_i = m_i/m_{tot}$), fitting the data for all proteins linearly (Fig. 1b-c).

If *c* or *i* accurately reflects the mass fraction of the protein of interest, the slope of the log-log plot will equal 1 and the y-intercept 0. For spectral counting, the slope was

0.8 (Fig. 1b), indicating a systematic misrepresentation of protein abundance. By a one-sample t-test, the slope of the log w_i vs. log c plot was significantly different from 1 (p<0.00001) and outside the 95% confidence interval. By contrast, intensities correlated well with w_i (Fig. 1c); the slope of the log w_i vs. log i plot was 1.

The scatter in the data points of Fig. 1c indicates that calculating w_i from i in subsequent experiments should include an estimate of the uncertainty in w_i, which we determined from the inter-protein variability as follows. We assumed that i = 1 when w_i = 1, allowing us to fit log i vs. log w_i data for each protein linearly through the origin, with a slope of α (SI Appendix). Equation 1 can therefore be used to calculate w_i:

$$w_i = i^\alpha \hspace{3cm} \text{Equation 1}$$

Using either simple averaging or a linear mixed-effects model, α = 1.03 ± 0.12 (mean ± SD), with a 95%-confidence interval of 0.79-1.27.

The nonlinear relationship between normalized MS2 intensities and normalized spectral counts also held for *E. coli* proteins analyzed in these experiments (Fig. 1d). In general, the most abundant proteins had higher relative intensity than relative counts, while the converse was true for the least abundant proteins. The consequence of these systematic differences is that relative intensities cover a broader dynamic range than relative counts.

Quantitation of proteins in chick auditory and vestibular epithelia

To apply the intensity-based quantitation method in a cell-biological context, we compared expression of proteins in sensory epithelia of chick auditory (cochlea) and

vestibular (utricle) organs at embryonic day 20-21 (E20-E21), when structural and functional development of both organs is nearly complete (69-72). We chose chick because of the superb description of its hair-bundle development (73), its sequenced genome (74), and the ability to compare results with our hair-bundle proteomics data (7, 75).

We microdissected sensory epithelia of each organ (Fig. 2a,b), which contain pure populations of hair cells, the sensory cells of the inner ear, and their interdigitating supporting cells. Cochlear samples also contained the overlying acellular tectorial membrane, as its removal would have required a protease step that degrades surface proteins (Fig. 2c).

Samples were subjected to LC-MS/MS and i was calculated for each detected protein; we detected 2587 total proteins with a false-discovery rate (FDR) of 0.8% (Datasets S1-S3). We included in our subsequent analysis only the 1142 proteins detected with at least three total spectral counts arising from two or more separate replicates out of a total of 5 replicates for each sample (Dataset S4). Tectorin α and β (TECTA and TECTB) comprise almost all tectorial-membrane components detected in the cochlea and together accounted for ~45% of the total intensity (Fig. 2g). Because the tectorial membrane is an extracellular structure, proteins derived from it will artificially depress the normalized intensity values of cellular proteins; we therefore computationally removed the tectorins and proportionally increased the normalized intensities of all other proteins (Fig. 2h). Other extracellular matrix proteins contributed

much lower total intensity and had an insignificant effect on protein abundance calculations.

To confirm tissue-preparation and instrumentation reliability, we compared i for individual utricle proteins detected in two groups of four randomized utricle samples (Fig. 2d,e). Protein intensities were tightly correlated between the two groups and their ratios fell close to the unity line. Given the similarities between mass-spectrometry and microarray data (76), we used significance analysis of microarrays (SAM) (77), a stringent statistical test, to identify proteins with altered expression; we found no significant enrichment for any protein.

We then compared protein expression in cochlea and utricle. We assumed that the total protein concentration was identical in both organs (78, 79), so that differing relative intensities in the two organs reflected differences in protein concentration. i for individual proteins detected in utricle and cochlea samples were less well correlated than between the two utricle samples, showing biological variability in protein expression between these organs (Fig. 2e,f). SAM analysis identified 620 utricle-enriched proteins, but only 134 proteins enriched in cochlea. We attribute this difference to the reduced dynamic range in cochlea because of the large number of tectorin peptides analyzed.

Small, mobile calcium buffers were elevated 30-fold in cochlea over utricle. Indeed, calbindin (CALB1) was the second-most most abundant cellular protein in the cochlea epithelium. Intensity measurements also suggested that the utricle nuclear mass is greater than that of cochlea. Intensity assigned to histones was 2.5-fold greater

in utricle than in cochlea (Table 1); similarly, the nuclear lamins B1 and B2, the lamin-B

receptor, and summed intensities of the nuclear pore complex were 10-fold elevated in

utricle relative to cochlea. To verify that result, we used DAPI staining to estimate that

hair cells and supporting cell nuclei are ~4-fold denser in utricle than in cochlea. By

contrast, heat-shock proteins were equal in concentration in the two tissues (Table 1),

suggesting that they may better serve the role of "housekeeping proteins" for

standardization, at least for protein detection.

Verifying mass spectrometry quantitation

Because of its small size and abundance, CALB1 was resolved from other

proteins of the cochlea by SDS-PAGE, which allowed an independent comparison of the

accuracy of intensity and spectral count quantitation. By mass spectrometry, CALB1

accounted for 6.1 ± 0.4% of cochlea intensity (including the tectorins) but only

2.2 ± 0.2% of the spectral counts; scanning of SDS gels stained with Coomassie blue

indicated CALB1 accounted for 5.7 ± 0.8% of the cochlea protein stain (SI Appendix). By

a two-tailed t-test, intensity values were not significantly different than gel-staining

values (p = 0.72), while count values were significantly different (p < 0.005). In addition,

CALB1 accounts for ~12% of the tectorin-free cochlear protein mass; with an estimated

total protein concentration of ~200 mg/ml (78, 79), its cochlea concentration should be

~0.8 mM, very similar to previous estimates in hearing organs of chicken (80), turtle

(81), and rat (82).

To further test the veracity of *i* for quantitation, we used protein immunoblots to

determine relative COCH to UTR abundance of brain-type creatine kinase (CKB),

glyceraldehyde 3-phosphate dehydrogenase (GAPDH), and CALB1. We measured the

dependence of signal intensity on total protein from microdissected epithelial peels and

calculated the ratio of the slopes for linear fits (SI Appendix).

For GAPDH, COCH/UTR estimated by the slope ratio was 1.42 ± 0.15 (mean ± SD;

n=3), identical to the mass-spectrometry estimate of 1.42 ± 0.16 (n=5), assuming α = 1

(SI Appendix). These values have not been adjusted upwards to account for cochlea

tectorins. By contrast, the slope ratio for CKB was 0.13 ± 0.07 (n=3), substantially greater

than the mass spectrometry estimate of 0.016 ± 0.004 (n=5), just outside the range

generated using the two standard deviation span of α (SI Appendix).

Despite imperfect absolute agreement between quantitative western blot and

mass spectrometry ratio estimates, all differentially expressed proteins examined by

immunoblot follow the trends detected by mass spectrometry (see also Fig. 5). Mass

spectrometry and immunoblot quantitation most closely agrees for GAPDH, suggesting

that quantitation by MS2 intensities is most accurate for abundant proteins.

Comparing protein and mRNA abundance

Few studies compare global protein and transcript expression (76, 83-87). To

examine how well protein expression is predicted from transcript expression, we

correlated mass-spectrometry protein abundance to transcript abundance determined

from microarray hybridization data. We used four replicates each of cRNA derived from

utricle and cochlea epithelium mRNA to probe Affymetrix chicken genome chips; array

data were subjected to GC-RMA background correction, quantile normalization, and

median polish summarization using PM probes only (88, 89) (Dataset S5). Of the ~14,000

probesets with detectable signal in both tissues, corresponding to ~10,000 genes, almost 5000 probesets were significantly up-regulated in utricle or cochlea by SAM analysis (Fig. 3a); in addition, about 2000 probesets gave detectable signal only in either utricle or cochlea.

To correlate microarray and mass spectrometry abundance, we identified those genes detected by both analyses. Not all detected proteins and transcripts could be correlated; the dynamic range of mass spectrometry is limited, and the Affymetrix chicken array is based on an older, incomplete genome assembly (Ensembl v1, May 2004). Nevertheless, we were able to obtain correlative data corresponding to 947 genes (Fig. 3b).

Microarray signals are proportional to molar transcript abundance, dictating a molar abundance parameter for mass spectrometry, which we call normalized molar intensity (i_m). We calculated i_m for each protein by first dividing protein intensity by molecular mass, then dividing by the sum of intensity/mass for all detected proteins. Because microarray signals depend on probe position within the gene and hybridization efficiency, their relative intensity can vary substantially. i_m was poorly correlated with the microarray signal (SI Appendix) which was not unexpected; even the most rigorous comparisons of mRNA and protein levels show only a very rough correlation (90).

Most microarray studies compare expression ratios between conditions or tissues. Utricle-to-cochlea ratios were more broadly distributed for mass spectrometry data than for microarray data (Fig. 3c); only a small fraction of this variance derived from variance in α, the mass-spectrometry calibration coefficient. Regardless, relative

transcript and protein expression were reasonably well correlated for the most enriched

proteins and transcripts in the two tissues (Fig. 3d).

Auditory and vestibular epithelia differ in their use of glycolysis and oxidative

phosphorylation. Mass spectrometry suggested that energy metabolism differed

significantly in the two inner-ear tissues. Intensities assigned to glycolytic and

gluconeogenesis enzymes were 3-fold greater in cochlea than in utricle; by contrast,

summed intensities were higher in utricle for enzymes of the citric-acid cycle (4-fold

over cochlea), enzymes of the electron-transport chain (10-fold), and mitochondrial F-

ATPase components (4-fold) (Table 1 and SI Appendix). In almost every case, there were

more peptides detected for glycolytic enzymes in the cochlea and more peptides

detected for oxidative phosphorylation enzymes in the utricle (Fig. 4a). Moreover,

peptides derived from enzymes of both pathways were detected in each organ,

demonstrating that differential expression was not an artifact of poor detection in one

of the organs.

Strikingly, while transcript levels for glycolytic enzymes were elevated ~2-fold

(Fig. 4c), transcripts for those involved in oxidative metabolism were at similar levels in

utricle and cochlea, despite substantially elevated protein concentrations in utricle. This

result suggests that the cochlea up-regulates glycolysis transcriptionally, while

regulation of energy metabolism in the utricle is translational or post-translational.

All elements of the glycolytic pathway, including the glucose transporters

SLCA2A1 and SLC2A3 and the lactate transporter SLC16A3 (MCT4), were up-regulated in

cochlea by mass spectrometry or, if not detected there, by microarray analysis (Fig. 4d).

Moreover, enzymes involved in glycogen synthesis and liberation were also up-regulated in cochlea (Fig. 4d). The glycolytic enzymes are all controlled by the transcription factor hypoxia induction factor α (HIF1A), which is stabilized by low oxygen tension and coordinately controls expression of a wide array of genes (91). Consistent with HIF1A regulation, transcripts for pyruvate dehydrogenase kinase 1 (PDK1), which blocks oxidative phosphorylation (92), and BNIP3, a master regulator of mitochondria catabolism or mitophagy (93), were elevated in cochlea (Fig. 4c,d). As HIF1A protein is degraded within 10 minutes under normoxic conditions (137), it was not surprising that we did not detect it in our mass spectrometry analysis.

To verify differences in energy metabolism using independent methods, we examined proteins involved in glycolysis and mitochondrial energy production by protein immunoblot analysis. As expected, the glycolytic proteins GAPDH and enolase 1 (ENO1) were increased in expression in the cochlea, while malate dehydrogenase 2 (MDH2), a citric acid cycle enzyme, cytochrome c (CYCS), an electron transport chain enzyme, and the F_1-ATPase α1 subunit (ATP5A1) were all more abundant in the utricle (Fig. 5a). Immunocytochemistry confirmed that these proteins are expressed in hair cells (Fig 5c-j).

Glycolytic rate is increased in the cochlea

We measured glycolysis directly in the two tissues by adding [^{3}H]glucose to cochlear and utricular epithelia in the presence of high-glucose saline, then quantified the amount of [^{3}H]H$_2$O released during the enolase step of glycolysis (94). The glycolytic rate was 1.55 ± 0.08 pmol/min/µg in the cochlea and 0.42 ± 0.05 in the utricle

(mean ± SEM, n = 4, difference significant at p<0.0001), yielding an average COCH:UTR

glycolysis ratio of 4.1 ± 0.4 (statistically significant from an average of 1 at p<0.05) (Fig.

5b). For comparison, at 0.75 ± 0.14 pmol/min/µg, the rate of glycolysis in chick brain

was in the same range as inner ear organs. Thus, the 3-fold enrichment of glycolytic

enzymes in the cochlea predicted by mass spectrometry was accurately reflected in the

cellular biology of the auditory system.

Angiogenesis inhibitors are elevated in cochlea

Apparent HIF1A-dependent regulation suggests that oxygen tension is low in the

cochlea, presumably because blood vessels are distant from the epithelium (10).

Morphological analysis shows many blood vessels in close proximity to the utricular

epithelium, while the cochlear epithelium is significantly less vascularized (Fig. 6).

Remarkably, transcript levels for at least five anti-angiogenesis factors operating via

different mechanisms—TIMP3 (95), TSP2 (96), NR2F2 (97), BMP6 (98), and WIF1 (99)—

were elevated at least 40-fold in cochlea over utricle (Table 2). These data imply that the

cochlea actively inhibits vascularization, and therefore must rely more heavily on energy

production through glycolysis.

Discussion

Protein quantitation with MS2 intensities

By summing ion-current intensities of peptide fragments detected by mass spectrometry, we accurately quantify individual proteins in a complex mixture. Because mass spectrometers do not operate in the ideal manner depicted in Fig. 1a, real-world factors like dynamic exclusion could affect the relationship between MS2 quantitation and protein concentration. However, we show here empirically that MS2 quantitation is accurate and outperforms spectral counting for estimating true protein abundances.

For accurate relative quantitation of a protein population, it is not sufficient for a quantitative measure to be linearly related to protein abundance; an accurate relative quantitative measure must *equal* the mass fraction for each protein (i.e., slope equal to 1 and intercept equal to 0 for a linear fit). This requirement is rarely tested, particularly over a wide concentration range and in the presence of a complex protein mixture. Using standard proteins diluted over four orders of magnitude and quantifying with MS2 intensity, the calibration coefficient α was ~1, suggesting that on average protein abundance was accurately determined.

Protein-to-protein variance in α indicates, however, that the abundance of any one protein may be over- or underestimated. Although this variability is inherent in most quantitative methods, reinforcing the necessity to confirm interesting results using alternative methods (100), label-free methods enable the essential step of discovery,

allowing shotgun proteomics experiments to provide initial evidence needed prior to

focused experiments.

To overcome the variability in α, conclusions about biological function can be

drawn by assessing expression levels of many proteins in a pathway. Indeed, we show

here directly that the 3-fold up-regulation in glycolytic enzymes in the cochlea is

paralleled by a 4-fold higher glycolytic rate as compared to utricle. Differences in

energy-metabolism pathways detected by mass spectrometry are thus biologically

relevant to sensory epithelia, presumably especially hair cells. Thus we believe that MS2

quantitation, more accurate than spectral-counting quantitation, will be broadly useful

for simultaneously estimating approximate concentrations of a large number of proteins

in parallel.

Protein abundance in cochlea and utricle

The distribution of cochlea-to-utricle abundance enrichment is skewed with

most proteins having modestly elevated levels in utricle (Fig. 2e). While measurement or

normalization errors plausibly could explain this discrepancy, the systematic differential

expression of distinct protein groups (e.g., glycolytic, mitochondrial, nuclear) argues for

biological relevance. Indeed, elevated expression of CALB1 and glycolytic enzymes may

by necessity depress expression levels of all other proteins in cochlear cells. Proteins in

the cytoplasm experience only modestly more hydration than when they are in crystals,

suggesting that total protein concentration is near a physical limit, thought to be

~200 mg/ml (78, 79). If we recalculate cochlea normalized intensities after adjusting i of

CALB1 and the most abundant glycolytic enzymes in cochlea to their utricle values, the

average protein's cochlea-to-utricle ratio is very nearly 1 ("COCH$_{adj}$/UTR"), Fig. 2e). This observation supports our contention that our global view of protein abundance is accurate.

Energy metabolism in auditory and vestibular end organs

Multiple lines of evidence reported here show that auditory tissues are biased towards ATP generation by glycolysis and vestibular tissues by oxidative phosphorylation. Using elegant microdissection and enzymatic cycling techniques, Thalmann and colleagues drew similar conclusions for the mammalian inner ear (9). The combination of mass spectrometry and microarrays used here offers a much more comprehensive view of energy metabolism in these tissues, however, and suggest the mechanism by which the cochlea controls vascularization. Both methods were essential; microarray analysis did not detect the reduced levels of oxidative phosphorylation enzymes in cochlea, consistent with destruction of mitochondria by mitophagy, and mass spectrometry lacks the sensitivity of microarrays and missed the striking up-regulation of anti-angiogenesis factors.

Elevation of glycolytic enzymes in the cochlea is unlikely to be an example of the Warburg effect, where aerobic glycolysis enables the high proliferative needs of cancer cells (101); the cochlear sensory epithelium is at its mature size at E20, while the utricle exhibits very slow postnatal growth (70). Moreover, the endoplasmic reticulum enzyme ENTPD5, which favors aerobic glycolysis (102), was detected in utricle but not cochlea by mass spectrometry.

The chick cochlea likely favors glycolysis over oxidative phosphorylation for one of at least three reasons: (1) auditory energy demand is lower, allowing less-efficient glycolysis to suffice; (2) oxidative metabolism is particularly damaging to auditory hair cells; or (3) O_2 diffusion to the cochlea is limited, preventing efficient oxidative phosphorylation.

Reason (1) seems unlikely. If removal of Ca^{2+} entering through transduction channels is the major energetic demand on hair cells (7), it is unlikely that the cochlea has a lower need for energy than the utricle. Cochlear hair cells have on average more stereocilia than do utricular hair cells, indicating that they have more transduction channels and hence a higher resting Ca^{2+} flux. In hair cells, removal of incoming Ca^{2+} is energetically expensive, as it must be pumped back into the Na^+-poor endolymph by the plasma-membrane Ca^{2+} pump at the cost of one ATP per Ca^{2+} (6). In addition, although oxidative metabolism could damage auditory hair cells more readily than vestibular hair cells (reason 2), there is little evidence for that hypothesis.

By contrast, it is quite possible that cochlear hair cells experience low O_2 tension (reason 3). In the bird auditory system, no cochlear blood vessels are adjacent to the hair cells, being instead restricted to cartilage, the nerve ganglion, and the overlying tegmentum vasculosum (Fig. 6) (10). By contrast, vestibular end-organs like the utricle are richly endowed with an extensive capillary bed within the stroma, just below the sensory epithelium (Fig. 6) (10). Thus the chicken cochlea may be forced to rely on glycolysis if the O_2 supply is insufficient to maintain oxidative phosphorylation.

Low O_2 tension in the cochlea is likely a design feature. Auditory tissues apparently express multiple anti-angiogenesis factors, preventing capillary infiltration; in turn, low oxygen tension likely activates HIF1A, which induces transcription of genes for glycolytic enzymes and those that inhibit mitochondrial function. While this metabolic shift renders auditory tissues susceptible to energy depletion, sensory sensitivity is apparently preserved by preventing heartbeat-induced mechanical disruption of the organ (9)—not a problem for vestibular organs because the stroma can be mechanically much more rigid than the cochlea's basilar membrane.

Experimental Procedures

Animals. Inner ear organs from E20-21 *Gallus domesticus* embryos were dissected in chicken saline as previously described (7). After removal of the otoconia and otolithic membrane of the utricle, the sensory epithelium was peeled off the basement membrane using an eyelash. In a separate dish, the tegmentum vasculosum was removed from the cochlea and the sensory epithelium, including the overlying tectorial membrane, was peeled off using an eyelash.

Mass spectrometry. To assess mass-spectrometry quantitation, we analyzed ten proteins purchased from Sigma-Aldrich (St. Louis, MO): bovine serum albumin, carbonic anhydrase, catalase, cytochrome c, transferrin, α-lactalbumin, and β-lactoglobulin; chicken ovalbumin; rabbit phosphorylase; and *B. licheniformis* α-amylase. Following amino-acid analysis, proteins combined to make mixes A & B (SI Appendix). To prepare final mixtures for analysis, aliquots of mixes A & B were diluted with protein extracts of BL21 (DE3) *E. coli* cells. Mix A was diluted 1:2 (wt/wt) with the *E. coli* lysate; mix B was serially diluted with the *E. coli* lysate at 1:9, 1:29, 1:99, 1:299 and 1:999. These six dilutions were each run in triplicate for the experiment of Fig. 1.

For inner-ear analysis, 10-30 utricle or cochlea epithelia were pooled, pelleted, and stored at -80°C. Five separate pooled samples were run in parallel; epithelia were resuspended and homogenized in water, and total protein concentration was assayed using the CBQCA protein quantitation kit (Invitrogen).

Samples were separated by a short SDS-PAGE run; after staining with Imperial

Protein Stain (Thermo Scientific, San Jose, CA), the ~1 cm distance of gel traversed by

the proteins was divided evenly into six segments spanning from the well bottom to the

dye front (75, 103). After washing, each gel segment was treated with dithiothreitol and

iodoacetic acid before digesting overnight with trypsin (75). After digestion peptides

were extracted and passed through a 0.45 µm filter (Millipore Billerica, MA) via

centrifugation. Filtered extracts were lyophilized before being re-suspended in 5%

formic acid for analysis on the mass spectrometer.

Protein digests were analyzed by LC-MS/MS using an Agilent 1100 series capillary

LC system (Agilent Technologies Inc., Santa Clara, CA) and an LTQ linear ion trap mass

spectrometer (Thermo Scientific). Electrospray ionization was performed with an ion

max source fitted with a 34 gauge metal needle (Thermo Fisher, cat. no. 97144-20040)

and 2.7 kV source voltage. Samples were applied at 20 ml/min to a trap cartridge

(Michrom BioResources, Inc., Auburn, CA), and then switched onto a 0.5 x 250 mm

Zorbax SB-C18 column with 5 µm particles (Agilent Technologies) using a mobile phase

containing 0.1% formic acid, 7-30% acetonitrile gradient over 195 min, and 10 µl/min

flow rate. Data-dependent collection of MS2 spectra used dynamic exclusion (repeat

count equal to 1, exclusion list size of 50, exclusion duration of 30 sec, and exclusion

mass width of -1 to +4) to obtain MS2 spectra of the three most abundant parent ions

following each survey scan from m/z 400-2000. The tune file was configured with no

averaging of microscans, a maximum inject time of 200 msec, and AGC targets of 3×10^4

in MS1 mode and 1×10^4 in MSN mode.

RAW data from the LTQ mass spectrometer was converted to DTA files representing individual MS2 spectra using extract_msn.exe version 4.0 included with Bioworks (version 3.3; Thermo Scientific). We used SEQUEST to search the Ensembl Chicken v53 database (22,194 entries); to facilitate error estimates, 179 common contaminant entries were added and all forward entries appended with sequence-reversed entries using software available at www.ProteomicAnalysisWorkbench.com. SEQUEST search parameters were: parent ion tolerance of 2.5 Da, fragment ion tolerance of 1.0 Da, average parent ion masses, monoisotopic fragment ion masses, differential methionine oxidation of +16 Da, static cysteine modification of +57 Da, maximum of two missed cleavages, and no enzyme cleavage specificity.

We used a linear discriminant transformation to improve the identification sensitivity from the SEQUEST analysis (67, 104), using reversed databases to estimate error thresholds (105). Discriminant function thresholds were set independently by peptide charge and number of tryptic termini to control peptide false discovery rates (67). Peptide identification lists are reported in Supplemental Tables 1 and 2. Protein identification lists of Supplemental Table 3 were prepared using a peptide subset-removal parsimony filtering and proteins were considered present in a given sample if they had two or more peptides with distinct sequences, having a unique count greater than or equal to one in the respective sample. For the quantitative analysis of Supplemental Table 4, proteins were considered present in a given sample if they had two or more peptides with distinct sequences, were detected in two or more separate

runs, and having a total spectral count of 3 or greater in the combined runs for each tissue.

We quantified proteins using summed MS2 intensities of peptides identified by SEQUEST. Peptide intensities were extracted from DTA files; the top 50 values were summed (or all values if there were between 25 and 50 values). MS2 intensities from all runs were combined to give the each protein's total intensity value.

Microarray. Total RNA was isolated from 10-20 pooled utricle or cochlear epithelia using Trizol and RNeasy MinElute Cleanup Kit (Qiagen). RNA concentration and quality were assessed using a NanoDrop-8000 spectrophotometer and fluorescence-based capillary electrophoresis with an Agilent 2100 Bioanalyzer. For each sample, labeled cRNA was synthesized in vitro (MessageAmp Premier RNA Amplification kit; Ambion) using 80 ng of RNA, hybridized to the Whole Chicken Genome Array (Affymetrix), then incubated, washed, and read by a Microcon Array imager. Microarray assays were performed in the Affymetrix Microarray Core of the OHSU Gene Microarray Shared Resource.

Affymetrix software was used to determine whether probe sets detected expression. Image processing and initial expression analysis were performed using Affymetrix GeneChip Command Console (AGCC) v. 2.0.0.1029 and Affymetrix Expression Console v. 1.1 software, respectively. An absolute expression analysis was performed using the Affymetrix analysis algorithm, MAS 5.0 (Microarray Suite 5.0) for each GeneChip genome array hybridization. Global scaling was used to an average target intensity of 250; the parameters α_1 and α_2 were set to 0.05 and 0.065, respectively.

Transcripts detected with each probe set were called as present (P), marginal (M), or undetectable (A); these calls are based on the detection p-value of the probe set. To determine whether a gene was expressed in a particular tissue, summed probe sets corresponding to that gene were required to have at least 50% P calls in that tissue.

For quantitative analysis, the cell fluorescence intensity (CEL) files were imported into the R statistical language environment (106) for data preprocessing. We employed the GC robust multi-array average (GC-RMA) developed by Wu and co-workers (88) to correct background noise in perfect match (PM) probe data. The background corrected intensity data were further normalized by quantile normalization and the gene expression levels were summarized using a linear model estimated by the median polish algorithm (89).

Antibodies. The following primary antibodies were used at 1:300 for protein immunoblots and 1:300 for immunocytochemistry: mouse anti-rabbit GAPDH (Chemicon), rabbit anti-chicken CKB (courtesy of T. Walliman), mouse anti-chicken calbindin D-28k (Swant), rabbit anti-chicken calretinin (courtesy of J.H. Rogers). Rabbit anti-human ENO1 (Santa Cruz), rabbit anti-human MDH2 (Sigma Prestige), mouse anti-pigeon CYCS (BD Pharmingen), and mouse anti-human ATP5A1 (BD Transduction) were used at 1:200 for immunoblot and 1:200 for immunocytochemistry. For immunoblots, secondary antibodies goat anti-rabbit-HRP or goat anti-mouse-HRP were used at 1:5000 (Jackson Labs). Secondary antibodies for immunocytochemistry were donkey anti-rabbit-Alexa 555 or donkey anti-mouse-Alexa 555 at 1:300; all secondary incubations included Alexa 488-phalloidin at 1:200 and DAPI at 1:500 (Invitrogen).

Protein immunoblots. Three pooled utricle and three pooled cochlear samples were used for independent immunoblot analysis. We quantified total protein in each sample using the CBQCA kit (Invitrogen), and confirmed our measurements with silver- and Coomassie-stained gels. Bis-Tris 4-12% gradient gels (Invitrogen) were run at 100 V for 2.5 hrs on ice in MOPS buffer, then transferred onto PVDF membranes. Blots were blocked in 5% liquid block (GE Healthcare) for 1 hr, probed with primary antibodies for 1-2 hrs, washed, and probed with secondary antibodies for 0.5-1 hr. HRP signal was detected using SuperSignal West Pico Chemiluminescent reagents (Thermo Scientific) and the FujiFilm LAS 3000 Image Reader. Band intensities were quantified with Image Reader software, and blot background was subtracted for each band.

Cryosection immunocytochemistry. Cochlear and utricular epithelia were dissected in chicken saline and fixed in 4% formaldehyde, washed in PBS, and stored at 4°C. Organs were sequentially embedded in 8% gelatin/8% sucrose, 15% gelatin/15% sucrose, and 25% gelatin/15% sucrose for 5-12 hrs at room temperature for each solution, while nutating. Separate organs were frozen in molds in the final solution, then embedded in OCT and cut into 16 μm sections on a cryostat. After drying for 2 hrs at 50°C, slides were stored desiccated and sealed at -80°C until use. For immunocytochemistry, sections were blocked with 3% normal serum, 2% BSA, 0.2% saponin for 2-3 hrs, incubated with primary antibodies in block overnight at 4°C, washed, and incubated with secondary antibodies for 2 hrs. After washing and mounting in Vectashield, sections were imaged on an Olympus Fluoview 1000 confocal

microscope and processed using ImageJ and Photoshop software. Only linear slope transformations were performed on the images.

Glycolytic rate assay. To measure glycolysis, the method of Ashcroft et al. was used (94). Brain temporal lobe or seven to eight cochlear or utricular epithelia were pooled after dissection in saline with 10 mM glucose. [^{3}H]glucose was added to a final specific activity of 3.6 ± 0.2 cpm/mmol (mean ± SEM); samples were incubated at 37°C for 30 min. Reactions were stopped with HCl; after a 5 min microfuge spin, 10 µl of the supernatant was transferred to a new tube, which was placed inside a scintillation vial filled with 0.25 ml water. After 42 hrs, [^{3}H]water in the sample arising from glycolysis had equilibrated with water in the scintillation vial, which was counted to determine glycolytic rate.

Acknowledgements
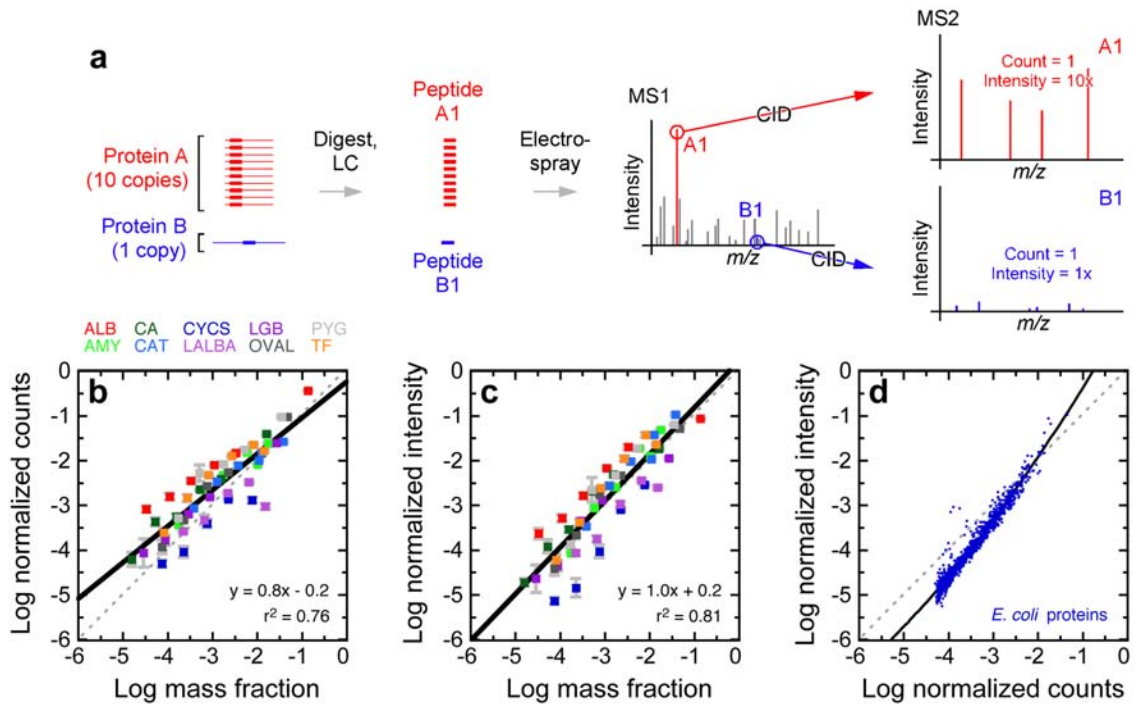
Figure 2.1 - Quantitation with MS2 intensities.

(**a**) Cartoon depicting spectral counts and intensities from two peptides (A1 and B1), each derived from a different protein, one of ten-fold greater abundance. If digest efficiency, chromatography behavior, ionization, and charge are equal, peptide A1 will have 10x greater MS1 intensity than peptide B1. In MS2 spectra, A1 and B1 are both counted as one spectral count; by contrast, if sampling, collision efficiency, and ion purity are similar, then peptide A1 will produce 10x more total MS2 intensity than peptide B1. LC, liquid chromatography; CID, collision-induced dissociation. (**b-c**) Detection of spiked proteins in complex protein mixture. Ten purified proteins (ALB, serum albumin; AMY, a-amylase; CA, carbonic anhydrase; CAT, catalase; CYC, cytochrome c; LACTA, a-lactalbumin; LGB, b-lactoglobulin; OVAL, ovalbumin; PYG, phosphorylase; TF, transferrin) were added in various mass ratios to an *E. coli* extract (total protein 30 μg) and the mixture was subjected to LC-MS/MS. Normalized spectral counts (**b**) and normalized intensity (**c**) were calculated for each protein at each dilution. Perfect correspondence between the amount spiked and the normalized detection value gives the unity line (dashed). (**d**) Relationship between normalized counts and normalized intensity for 1018 *E. coli* proteins detected in at least 3/15 runs from the experiment of **b-c**. Fit is a second-order polynomial ($i = 1.3 + 1.8\,c + 0.07\,c2$).
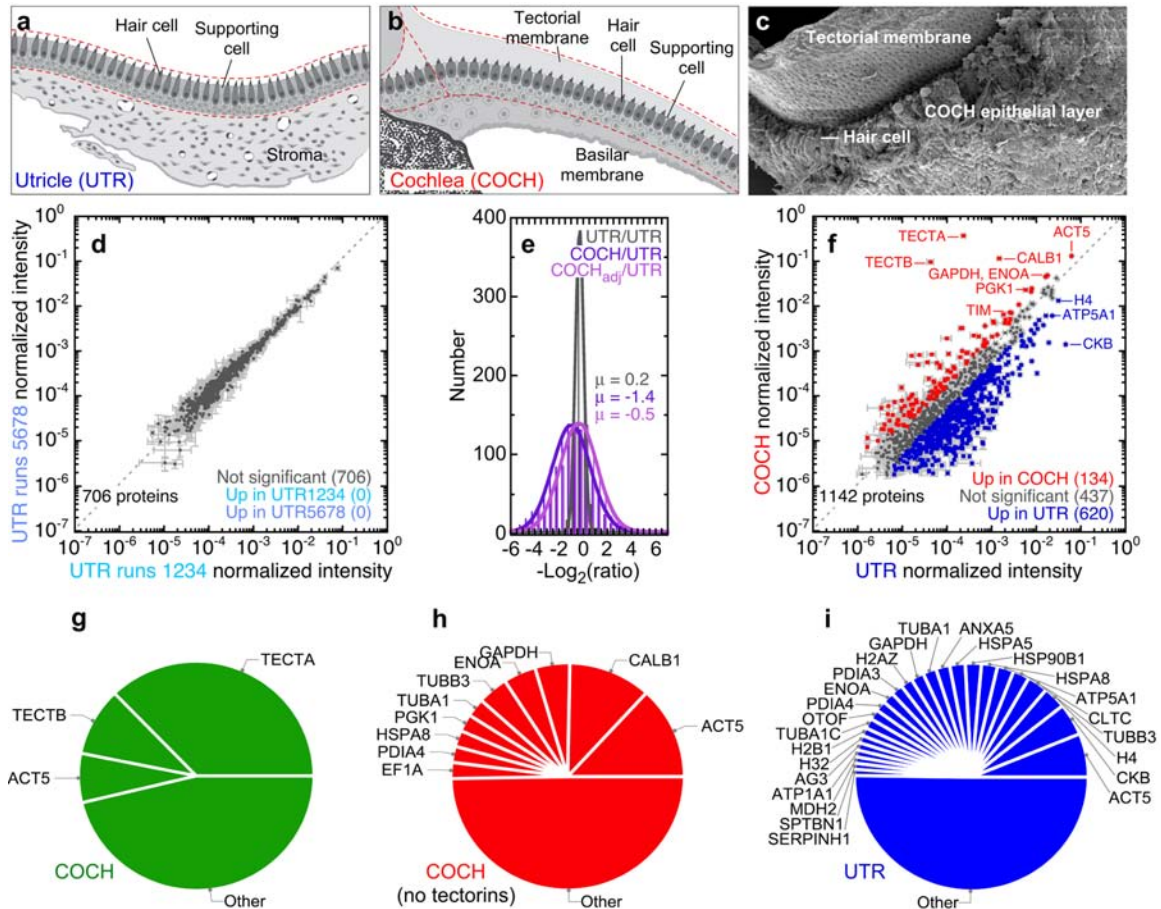
Figure 2.2 – Protein abundance in chick auditory and vestibular epithelia.

(a-c) Morphology of utricle (a; UTR) and cochlea (b; COCH). Red dashed lines in a and b indicate approximately where tissue peels were taken. Scanning electron micrograph of peeled COCH preparation (c) shows the tectorial membrane. (d) Reproducibility of mass spectrometry quantitation. Eight UTR samples were randomized into two groups; normalized intensities were plotted for each detected protein where SEM/mean<0.5. No proteins were significantly enriched (SAM analysis; all q-values >75%). (e) Sample-to-sample variation for a given protein varies more widely for the between-tissue (COCH/UTR) comparison than for the in-tissue (UTR/UTR) comparison. "COCH adj/UTR" shows distribution after CALB1 and glycolytic enzyme i values were adjusted in COCH to the UTR levels and all i values were recalculated. μ is midpoint of Gaussian fit to data. (f) Quantitation of individual proteins detected both in cochlea and utricle samples. Normalized intensities after tectorins were removed are plotted for each protein; TECTA and TECTB intensities are also plotted to illustrate their enrichment in cochlea. Dashed line is unity line. Points are colored if SAM analysis indicated significant enrichment and enrichment >2-fold. Only data with SEM/mean<0.5 displayed. (g) Relative mass-abundances of cochlea proteins. (h) Relative mass-abundances of cochlea proteins with tectorins removed. (i) Relative mass-abundances of utricle proteins. While not all labels are legible, the data are present in Suppl. Table 4.

40
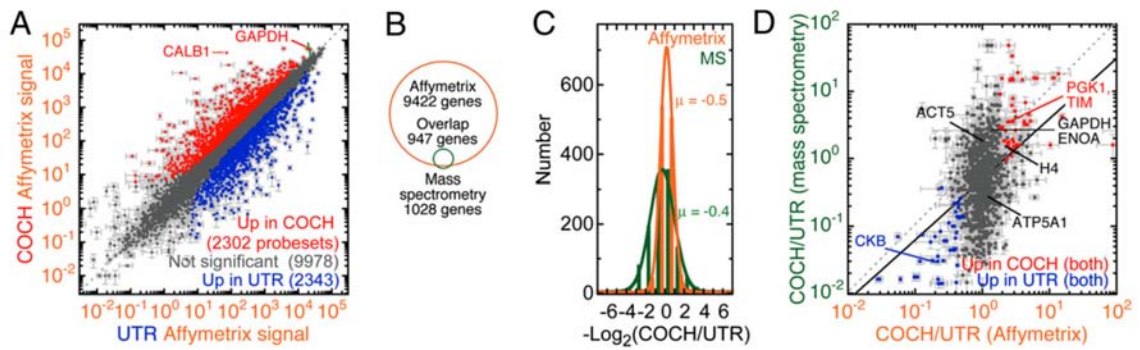
Figure 2.3 – Comparison of mass-spectrometry and microarray quantitation.

(a) Quantitation of individual transcripts detected both in cochlea and utricle samples. Points are colored if SAM analysis indicated significant enrichment and enrichment is >2-fold. Mean ± SEM are plotted. (b) Venn diagram showing overlap of detection by Affymetrix arrays and mass spectrometry. Affymetrix: 13,078 probesets mapping to 9422 genes. Mass spectrometry: 1029 proteins from 1028 genes, mapping to 1715 probesets. (c) Distribution of UTR/COCH ratios for entries detected by Affymetrix microarrays and mass spectrometry. (d) Correlation between UTR/COCH ratio measured by Affymetrix array and by mass spectrometry.

Figure 2.4 – Up-regulation of glycolysis and down-regulation of oxidative phosphorylation in auditory sensory epithelium.

(a-b) Distribution of peptides detected in cochlea (red) or utricle (blue) for proteins of glycolytic (a) and mitochondrial energy metabolism (b) pathways. Bar height indicates summed intensity for all peptides detected that span the indicated amino acid residues. Dashed lines indicate length of protein in amino acids. (c) Selected microarray cochlea:utricle expression levels. If up-regulation in cochlea or utricle is significant by SAM analysis, bar is colored respectively red or blue. Dashed line indicates two-fold up-regulation in cochlea. (d) Flowchart of glycolysis, glycogen metabolism, mitochondrial energy production, and mitophagy. Legend indicates up-regulation detected by mass spectrometry and/or microarray. Genes regulated by HIF1A are indicated.
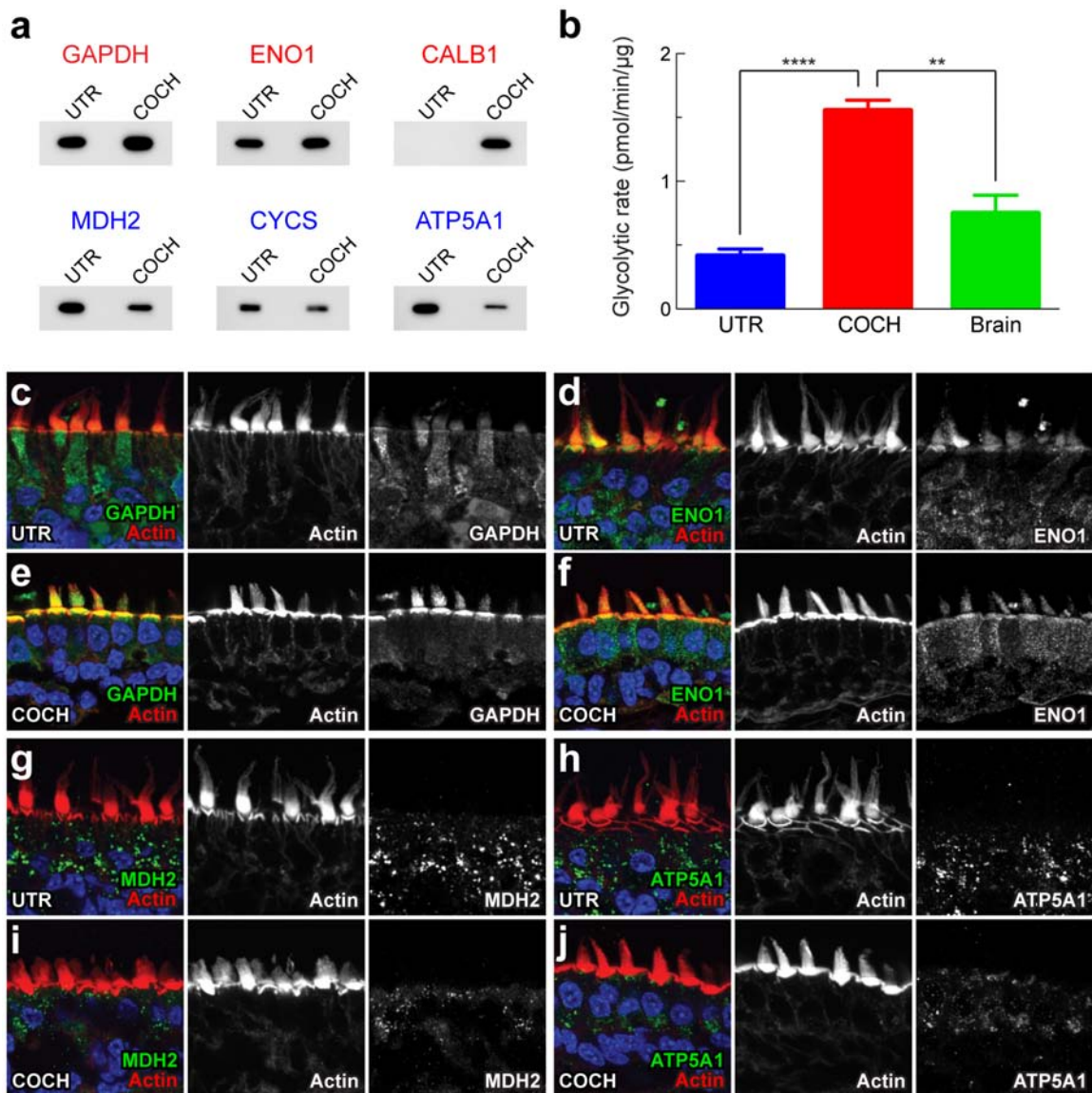
Figure 2.5 – Glycolytic protein expression and rate of glycolysis are increased in auditory sensory epithelium.

(a) Protein immunoblot for glycolytic proteins GAPDH and ENO1, mitochondrial proteins MDH2, CYCS, and ATP5A1, and calcium buffer CALB1 as a positive control. (b) Glycolytic rates in utricle, cochlea, and brain measured by [3H]glucose utilization, normalized to total protein; cochlea specific activity is significantly different from utricle and brain (two-tailed t-test; **p<0.005, ****p<0.0001). (c-j) Immunocytochemical detection of glycolytic and mitochondrial energy metabolism proteins in utricle (c, d, g, h) and cochlea (e, f, i, j). For each antibody, merge is on the left, actin counterstain in the middle, and antibody labeling on the right.
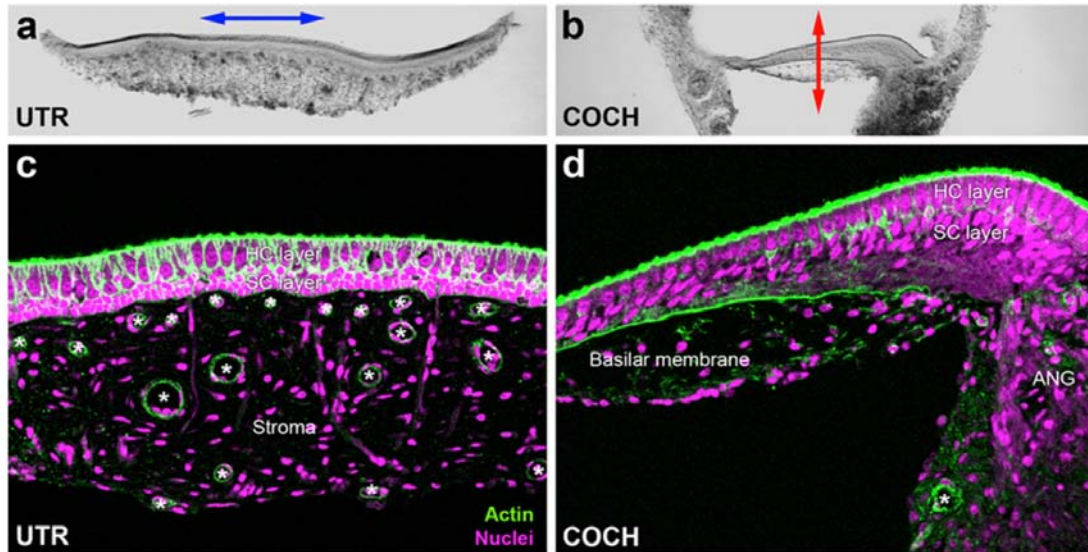
Figure 2.6 – Relationship of blood vessels to vestibular and auditory sensory epithelia.

(a-b) Nomarski images of chick utricle (a) and cochlea (b). Tectorial membrane has been removed. Arrows indicate direction of mechanical stimulus. Panels are 1272 μm wide. (c-d) Chick utricle (c) and cochlea (d) stained with phalloidin (to detect actin) and DAPI (to detect nuclei). Hair cell (HC) and supporting cell (SC) layers are indicated, as is stroma in utricle, and basilar membrane and auditory nerve ganglion (ANG) in cochlea. Yellow asterisks indicate blood vessels. Panels are 317 μm wide.

Table 1. Abundance and tissue ratios for classified protein groups

Abbreviation	Description	UTR mean i_{all}	COCH mean i_{all}	UTR/COCH mean	COCH/UTR mean
CAB	Mobile calcium buffers	$4.17 \pm 0.14 \times 10^{-3}$	$1.17 \pm 0.04 \times 10^{-1}$	0.036 ± 0.002	28.0 ± 1.4
Glycogen	Glycogen storage and liberation	$1.18 \pm 0.13 \times 10^{-3}$	$3.71 \pm 0.16 \times 10^{-3}$	0.32 ± 0.04	3.2 ± 0.4
Gly	Glycolysis	$6.32 \pm 0.12 \times 10^{-2}$	$1.67 \pm 0.03 \times 10^{-1}$	0.38 ± 0.01	2.6 ± 0.1
SLC	Solute carriers (nonmitochondrial)	$2.95 \pm 0.15 \times 10^{-4}$	$6.86 \pm 0.72 \times 10^{-4}$	0.43 ± 0.05	2.3 ± 0.3
LDH	Lactate dehydrogenases A and B	$8.99 \pm 0.39 \times 10^{-3}$	$1.39 \pm 0.03 \times 10^{-2}$	0.65 ± 0.03	1.5 ± 0.1
HSP	Heat shock proteins	$4.23 \pm 0.27 \times 10^{-2}$	$4.23 \pm 0.09 \times 10^{-2}$	1.00 ± 0.07	1.00 ± 0.07
HIST	Histones	$8.26 \pm 0.35 \times 10^{-2}$	$3.28 \pm 0.06 \times 10^{-2}$	2.5 ± 0.1	0.40 ± 0.02
Ion ATPase	ATP-dependent ion pumps	$1.93 \pm 0.05 \times 10^{-2}$	$7.09 \pm 0.25 \times 10^{-3}$	2.7 ± 0.1	0.37 ± 0.02
CAC	Citric acid cycle	$2.04 \pm 0.05 \times 10^{-2}$	$5.06 \pm 0.18 \times 10^{-3}$	4.0 ± 0.2	0.25 ± 0.02
F-ATPase	F-ATPase	$4.01 \pm 0.08 \times 10^{-2}$	$9.36 \pm 0.19 \times 10^{-3}$	4.3 ± 0.1	0.23 ± 0.01
NUP	Nuclear pore complex	$8.56 \pm 0.19 \times 10^{-4}$	$8.34 \pm 0.88 \times 10^{-5}$	10.3 ± 1.1	0.10 ± 0.01
ETC	Electron transport chain	$1.52 \pm 0.06 \times 10^{-2}$	$1.47 \pm 0.06 \times 10^{-3}$	10.4 ± 0.6	0.10 ± 0.01

Table 2.1 – Abundance and tissue ratios for classified protein groups.

Summed intensities (i_{all}) for individual runs for all proteins in indicated classes were adjusted for tectorins, then were averaged across runs. Entries contributing to each class are flagged in Dataset S4.2 by the abbreviation listed below.

Table 2. Microarray-detected angiogenesis inhibitors up-regulated in cochlea

Affymetrix probe set	Identifier	Description	Abbreviation	COCH/UTR
Gga.2827.2.S1_a_at	ENSGALG00000012568	Metalloproteinase inhibitor 3	TIMP3	56 ± 11
GgaAffx.21822.1.S1_s_at	ENSGALG00000011200	Thrombospondin-2	TSP2	66 ± 12
Gga.4445.1.S1_at	ENSGALG00000007000	COUP transcription factor 2	COT2	218 ± 91
GgaAffx.23995.1.S1_at	ENSGALG00000012787	Bone morphogenetic protein 6	BMP6	210 ± 43
Gga.11611.1.S1_at	ENSGALG00000009867	WNT inhibitory factor 1	WIF1	35 ± 27

Table 2.2 – Microarray-detected angiogenesis inhibitors up-regulated in cochlea.

Transcripts are displayed here that show very high cochlea-to-utricle up-regulation and have been reported to be antiangiogenesis factors.
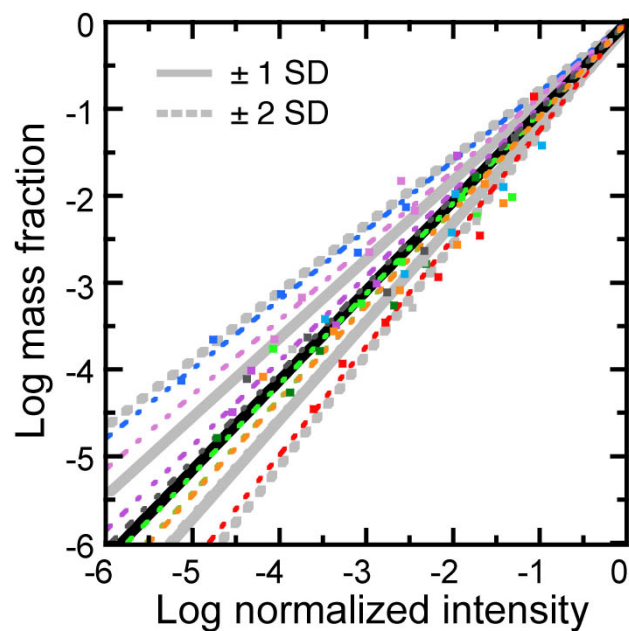
Figure S-2.1 – Determination of quantitation calibration factor α.

Data from Fig. 1d replotted; axes were transposed. Each protein's data points were fit with a linear function through the 0,0 point (f = α i). Colored dashed lines indicate fit through each data set. Solid black line indicates the average slope (1.03 ± 0.12); solid and dashed gray lines indicate one and two standard deviations. Color scheme is the same as in Fig. 1.
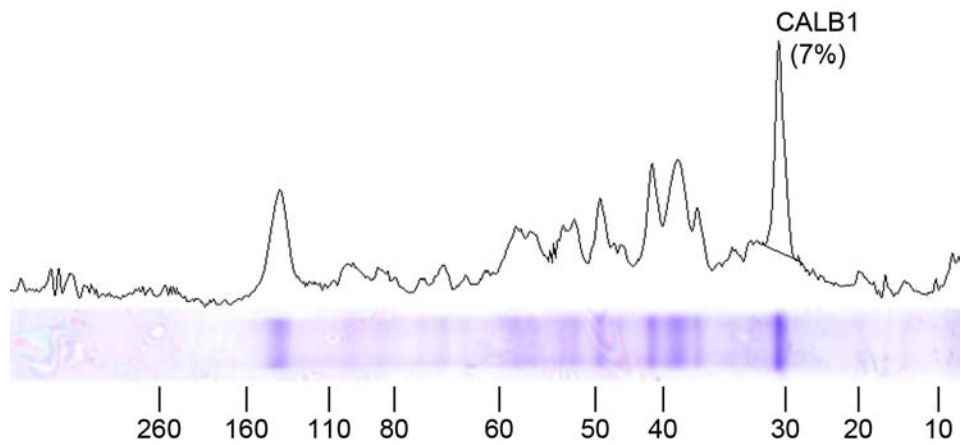
Figure S-2.2 – Gel scan quantitation of CALB1.

Four chick cochlea protein samples were run on SDS-PAGE, then stained with Imperial Protein Stain (bottom). Cochlea lanes and blank lanes were scanned and quantified using ImageJ (top). In this example, CALB1 (peak indicated) accounted
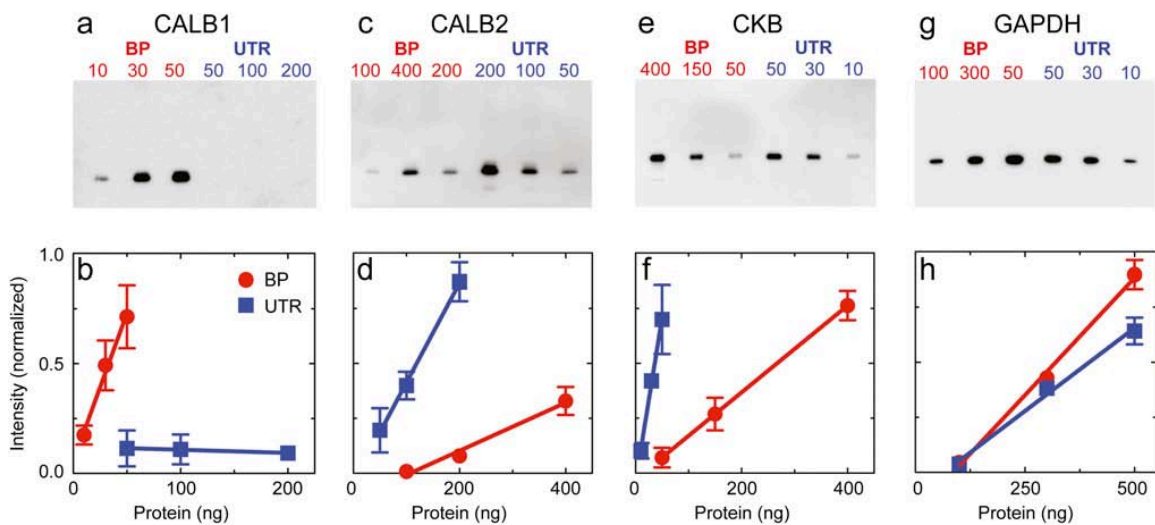
Figure S-2.3 – Quantitative protein immunoblots comparing cochlea and utricle expression.

(A-C) Representative protein immunoblots with dilutions of each tissue, detected by the indicated antibody. Values below cochlea (BP) and utricle (UTR) labels indicate total nanograms of protein loaded per lane. (D-F) Triplicate quantification of indicated proteins.
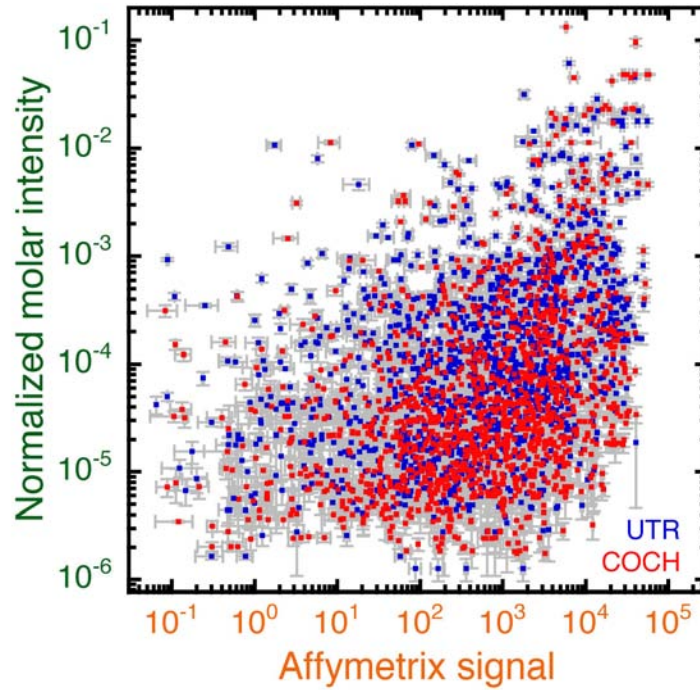
Figure S-2.4 – Poor correlation between Affymetrix signal and mass spectrometry normalized molar intensity.

Noise-corrected, normalized Affymetrix signal for each probeset was compared with normalized molar intensity values for the corresponding gene.
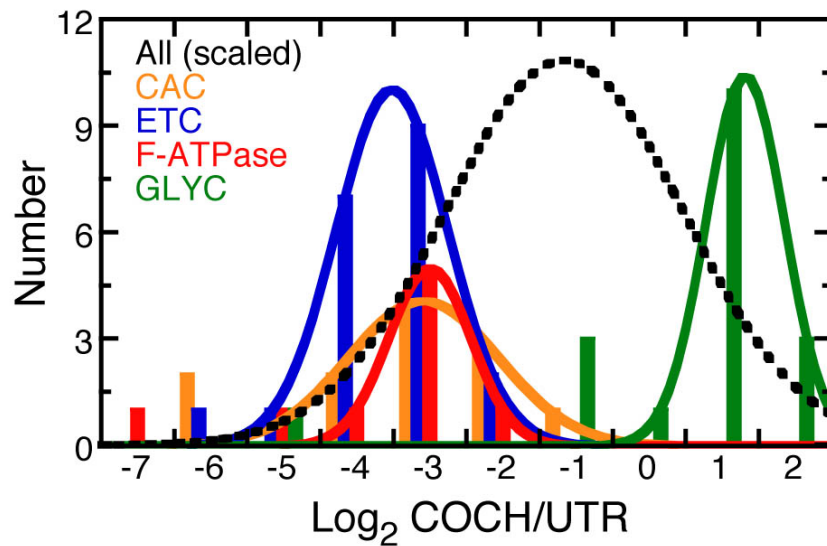
Figure S-2.5 – Distribution of cochlea-to-utricle ratios for glycolysis and oxidative phosphorylation enzymes.

Log2-transformed ratios for proteins assigned to the indicated classes were binned and plotted; data were fit with Gaussian functions. A scaled version of the Gaussian fit to the entire data set was also plotted (black dashed line).

Protein	Enriched organ	Enrichment by MS2 intensities (range)		Enrichment by protein IB with tectorin	Enrichment by microarray
		No tectorin	With tectorin		
CALB1	COCH	78 (27-220)	41 (17-99)	∞	1486
CKB	UTR	33 (14-75)	62 (23-166)	7.6	3.9
GAPDH	COCH	2.7 (2.1–3.4)	1.42 (1.31–1.55)	1.41	1.51

Table S-2.1 – Comparison of enrichment values.

Fold-enrichment values by mass spectrometry MS2 intensities (with and without tectorins), quantitative protein immunoblot, and microarray analysis. Range in mass spectrometry data is two standard deviation range of α. *only 1 count for CALB2 in COCH.

Protein	Mix A				Mix B			
	Molar ratio	Mass fraction	pmol	µg	Molar ratio	Mass fraction	pmol	µg
Serum albumin (bovine)	12	0.412	601	39.8	1	0.033	50.1	3.32
Carbonic anhydrase (bovine)	3	0.049	163	4.74	1	0.016	54.2	1.58
Catalase (bovine)	1	0.033	52.8	3.16	12	0.378	633	38.0
Cytochrome C (bovine)	1	0.023	193	2.25	1	0.022	193	2.25
Egg white albumin (chicken)	6	0.140	315	13.5	1	0.022	52.5	2.25
Phosphorylase B (rabbit)	2	0.107	106	10.3	1	0.051	53.0	5.16
Apo-transferrin (bovine)	1	0.043	53.0	4.12	2	0.082	106	8.23
α-Amylase (*Bacillus licheniformis*)	1	0.030	50.3	2.94	6	0.176	302	17.7
β-Casein (bovine)	1	0.014	54.5	1.37	9	0.123	491	12.3
β-Lactoglobulin (bovine)	9	0.081	429	7.84	1	0.009	47.7	0.871
α-Lactalbumin (bovine)	6	0.046	272	4.42	9	0.066	407.67	6.62
Phosphomannose isomerase (*Escherichia coli*)	1	0.023	51.6	2.21	1	0.022	51.6	2.21
Total	—	—	—	96.7	—	—	—	100

Table S-2.2 – Protein mixes.

Concentrations of individual proteins were measured using amino-acid analysis prior to mixing. Mass fractions are of undiluted mixes; mix A was diluted 1:2, while Mix B was diluted 1:9, 1:29, 1:99, 1:299 and 1:999 prior analysis of 30 µg total by LC-MS/MS.

Other Supporting Information Files:

Dataset S1 (XLS)

Dataset S2 (XLS)

Dataset S3 (XLS)

Dataset S4 (XLS)

Dataset S5 (XLS)

Chapter 3 – Damage to the hair bundle: Tip link breakage

Kateri J. Spinelli and Peter G. Gillespie

Unpublished data.

Abstract

Proper hair cell function requires the gating of transduction channels by extracellular tip links. Tip links can be broken by chelating extracellular calcium, but the underlying molecular mechanism of tip link breakage and the effect on tip link proteins is not well understood. I used immunohistochemistry to characterize the location of CDH23 and PCDH15 after breaking tip links in the chicken cochlea. Using antibodies against both the intracellular and extracellular domains, I found that tip link breakage caused a decrease in hair bundle CDH23 staining. Furthermore, CDH23 co-localized with PCDH15 in the cell body after breaking tip links. These data are supported by data from the utricle, where breaking the tip links and kinocilial links with calcium chelation resulted in a similar decrease in CDH23 and PCDH15 bundle staining and co-localization in the cell body. I also tested two new mechanisms of tip link breakage, using SEM to monitor the presence and number of tip inks. I found that calcium chelators did not break the tip link through at intermediate protease step, and that rough mechanical removal of the overlying tectorial membrane is not sufficient to cause tip link breakage.

Introduction

Extracellular tip link filaments that gate the mechanotransduction channel are susceptible to damage by calcium chelators (13-17, 35, 42). Controversy exists in the literature regarding the location of tip link proteins CDH23 and PCDH15 following breakage. A number of groups have reported that immunostaining for both proteins disappears from the stereocilia tips upon tip link breakage (20, 24, 43), however other studies report that these proteins did not change location (23, 24). Experiments that address the post-EGTA location of CDH23 and PCDH15 span across species and organs, and include hair bundles at various stages of development stained with many different antibodies. These differences between studies make the inconsistencies hard to interpret.

The chicken cochlea is an ideal organ in which to study the tip link. Morphologically, the bundle is relatively flat in the XY-plane, in contrast to the W-shaped bundles in the mammalian cochlea, and tip links are easily visible by SEM. Importantly, early post-hatch chicken cochlear bundles are relatively mature, which is in stark contrast with much of the immunohistochemistry work that reported on CDH23 and PCDH15 localization in the immature, early post-natal mouse cochlea (35-37). In the chicken cochlea, there are no lateral links at stereocilia tips, ensuring that CDH23 and PCDH15 antibodies do not label transient lateral links, which is the case in the early post-natal mouse cochlea.

CDH23 and PCDH15 localize to stereocilia tips in the chicken cochlea and utricle (26). Using a monoclonal antibody against PCDH15 (G19) and an extracellular CDH23 antibody, the authors showed labeling of every stereocilia tip in one hair bundle of the chicken cochlea at P2-P7. This study went on to characterize the orientation of CDH23 and PCDH15 in the kinocilial links of the chicken utricle, using both immunohistochemistry and immuno-EM. It is clear from these data that much of PCDH15 and CDH23 in the utricle bundle is in the kinocilial links, which are also disrupted by calcium chelation (43). To avoid confusion with kinocilial links, I focused on immunolabeling in the cochlea, while providing supporting data from the utricle.

I characterized three antibodies against CDH23 by immunohistochemistry and immunoblot for specificity in the chicken cochlea. One previously characterized antibody against PCDH15 was used in parallel for double labeling experiments. Staining patterns for these two tip link proteins were analyzed and quantified after tip link breakage in both the utricle and cochlea, with a focus on the cochlea. One major conclusion of this work is that CDH23 and PCDH15 co-localize in the cell body after BAPTA treatment; the implications of this finding are discussed.

Various treatments have been tested for their ability to break the tip link. In addition to chelating extracellular calcium, incubation with lanthanum ions and enzymatic treatment with elastase both disrupt the tip link (13, 20, 107). In the chicken cochlea, elastase cleavage requires pre-treatment with *N*-glycosidase F, which suggests the tip link must be de-glycosylated to be susceptible to enzymatic degradation (13). The tip link is insensitive to cleavage by subtilisin protease, which cleaves ankle links of

the hair bundle (35). To expand upon what is known about tip link breakage, I tested

whether a rough, mechanical displacement of the overlying tectorial membrane would

break tip links in the chicken cochlea. I also tested the hypothesis that calcium chelation

activates a protease that cleaves the tip link by determining if protease inhibitors had a

protective effect on BAPTA-treated epithelium. For both conditions, I assessed tip link

presence and number using SEM.

Results

Breaking the tip link

In order to study the tip link, I first designed and optimized a scanning EM (SEM) protocol for our lab. SEM sample preparation is tumultuous and may break fragile extracellular tip links that may were intact at the time of fixation. In EM tomography experiments, Auer et al. have reported that tip link preservation was improved by sequentially cooling the sample during the dehydration steps (108). Presumably if one dehydrates too quickly, single-pass transmembrane proteins like the tip link can be damaged due to rapid extraction of lipid molecules on the membrane. By dehydrating with long progressive cooling steps, the lipid molecules are less likely to be violently extracted, and tip link number is substantially increased. In my studies, dehydration with progressive cooling yielded a tip link count of 92 ± 1 % of tip links in expected positions (Figure 3.1a,e; mean ± SEM, n = 16 bundles). Importantly, these data also show that the majority of tip links are maintained through my dissection technique.

In early experiments, I tested the osmium/thiocarbohydrazide method of osmium cross-bridging (OTOTO), which is often used in the mammalian cochlea to replace sputter coating, but this method did not result in a significant improvement in tip link imaging (data not shown). Therefore in all experiments presented here, samples were post-fixed and stained with a 15 minute osmium step, and sputter coated with ~10 nm gold/palladium before imaging. Sputter coating with gold alone was also tested, but

these samples showed substantially more electrical charging than samples coated in the gold/palladium mix.

I next examined the effect of calcium chelators on tip link presence and number. As in control, organs were acutely dissected in HEPES-buffered HBSS at room temperature, and the tectorial membrane that overlies the hair bundle was removed after incubation with subtilisin protease. Organs were then incubated in either 5 mM EGTA or 5 mM BAPTA in calcium-free HBSS for 5 minutes, and returned to calcium-containing media for wash and fixation steps. Calcium chelation reduced tip link presence to 7 ± 1 %, a significant decrease compared to control (Figure 3.1b,e; n = 15 bundles; p < 0.0001). I did not observe a difference in the ability of EGTA or BAPTA to break the tip link; both worked sufficiently well (data not shown). I occasionally observed some tip links remaining after treatment with calcium chelators. In experiments where BAPTA was added to the hair bundle while recording transduction currents, a mechanical displacement in the presence of BAPTA was sometimes needed to disrupt the transduction channel response ((14) and Ricci A., personal communication). To ensure that tip links were obliterated in my experiments, I provided a mechanical displacement in the presence of BAPTA/EGTA by gently shaking the dish containing the cochlea. In immunohistochemistry experiments, where one does not have the luxury of directly observing tip link presence, I sometimes used a stronger mechanical displacement in the presence of BAPTA to ensure that the tip links were indeed lost after calcium chelation (see "Antibody staining after tip link breakage").

I performed a number of experiments to further address the question of tip link breakage. To test whether the tip link is cleaved by a protease upon calcium chelation, I pre-treated the cochlea with a protease inhibitor cocktail for 5 minutes before EGTA treatment, and included the inhibitors in the EGTA and wash steps. In these hair cells, tip link number was reduced to 6 ± 2 %, which was not significantly different from EGTA treated cells (Figure 3.1d,e; n = 7 bundles; p = 0.69). I also separately tested calpain inhibitor type I, because calpain is a calcium-dependent protease detected in hair bundles by mass spectrometry (Gillespie P., personal communication). However, I did not see a protective effect of pre-treatment with calpain inhibitor. These results indicate that EGTA does not cleave the tip link through activation of calpain or one of the proteases sensitive to the inhibitor cocktail. In agreement with this finding, EGTA-treated epithelium did not show an obvious increase in low molecular weight CDH23 species by western blot, which would indicate proteolysis (data not shown). Combined, these results indicate that extracellular calcium chelation does not cause proteolytic cleavage of the tip link.

In most experiments in the chicken cochlea, the organ is incubated in subtilisin protease to detach the bundle-tectorial membrane connections and allow for the gentle removal of this overlying structure. However, *in vivo* tip link damage due to noise exposure could act by mechanically damaging the bundle and tip link. In an attempt to mimic this potential mechanical damage, I roughly removed the tectorial membrane without pre-treating with subtilisin. Although some of the hair cells were ripped out of the sensory epithelium by this treatment, the hair cells that remained did have tip link

numbers similar to control (Figure 3.1c,e; 80 ± 5 %, n = 5 bundles; p < 0.005). Note that

the extracellular matrix that is usually degraded by subtilisin was clearly visible on these

hair bundles and surrounding the apical cell surface.

Developing antibodies against tip link proteins

Robust antibodies against CDH23 and PCDH15 are essential tools for studying

the tip link. Over the course of this thesis work, I have tested 9 antibodies against

CDH23 and 5 antibodies against PCDH15, with most antibodies giving unsatisfactory

staining patterns. One monoclonal antibody against PCDH15, called G19, has been

extensively characterized by Guy Richardson's laboratory (24, 26). G19 recognizes part

of the extracellular domain of PCDH15, although the exact epitope is not known (Figure

3.2). In P2-P7 animals, this antibody labels stereocilia tips in the chicken utricle and

cochlea, and kinocilial links in the utricle (26). This antibody showed good staining in the

utricle where there are many kinocilial links, but stained less than half of the stereocilia

tips in the cochlea of E21/P0 chickens (see "Other experiments related to tip link

breakage" for an explanation of this discrepancy) (Figures 3.4d and 3.5d).

Three antibodies worked well for detecting CDH23 in the chicken inner ear

(Figure 3.2). Given the difficulty with immunolocalization of CDH23 in the hair cell field

at large, I have separately used all three antibodies to study the tip link so that the data

and conclusions will be more believable. For the two extracellular domain antibodies,

all immunohistochemistry steps were carried out in EGTA buffer, which is thought to

unfold the EC domains to increase antibody accessibility (23, 26).

The first CDH23 antibody is a peptide antibody against the EC15/EC16 interdomain boundary, which was designed and purified by Peter and me (CEC15, Figure 3.2). This antibody showed a beautiful staining pattern at the tips of stereocilia in the chicken cochlea, and this staining was blocked by pre-treatment with the antigenic peptide (Figure 3.3). Although this antibody initially worked well for detecting CDH23 at stereocilia tips, it was not stable when stored in glycerol at -80°C and had to be re-purified after 4-5 months. In addition, CEC15 failed to detect CDH23 at stereocilia tips when the organ was treated with the protease subtilisin, which is an essential step for removal of the tectorial membrane. Other CDH23 antibodies have shown substantially reduced staining after treatment with this protease, even though the tip link remains intact (Richardson G., personal communication). Subtilisin treatment is required for good morphology of the hair bundle for immunohistochemistry – leaving the membrane on during staining results in reduced antibody penetration to the hair bundles near the neural edge of the cochlea, and removing the membrane after fixation causes damage to the bundles (data not shown). Because of the storage problem and subtilisin sensitivity, this antibody had limited utility for my research, but data for this antibody did support results obtained with other CDH23 antibodies.

Another CDH23 antibody that is well documented in the literature is designed against the cytoplasmic domain of CDH23, including exon 68, which is the isoform that forms the tip link (20) (C-cyto, Figure 3.2). This antibody worked well for detecting CDH23 in the chicken utricle, where it stained some stereocilia tips and the kinocilial

links (Figure 3.4c, see also Figure 3.9c). C-cyto antibody also strongly detected full-length CDH23 by western blot (Figure 3.6a).

We recently developed another CDH23 antibody against the EC15/16 interdomain that is not sensitive to subtilisin protease (C2367, Figure 3.2). This peptide antibody against the mouse sequence was generated in goat instead of rabbit, increasing its usability in double and triple labeling experiments. Because C2367 is insensitive to subtilisin, it could be used after enzyme treatment and pre-fixative removal of the tectorial membrane, thus greatly improving hair bundle morphology and, importantly, mimicking dissection conditions used for recording transduction currents and examining tip links by SEM. C2367 stained the tips of stereocilia in the cochlea, and showed a more diffuse staining pattern throughout the utricle bundle (Figure 3.5c and Figure 3.7c, see also Figure 3.13a). This antibody weakly detected full-length CDH23 in immunoblots of chicken ears, with an increase in band intensity in epithelial peels compared to total inner ear, reflecting CDH23 enrichment in the epithelium. C2367 also detected a number of lower molecular weight bands that could represent proteolytic cleavage or splice variants of CDH23 (Figure 3.6b). In tissue culture cells expressing CDH23, C2367 detected only one band corresponding to full-length protein by western blot, indicating antibody specificity for full-length CDH23 (data not shown).

Antibody staining after tip link breakage in the utricle

Given the contradicting evidence in the literature regarding CDH23 and PCDH15 staining after tip link breakage, I used the three CDH23 antibodies and one PCDH15 antibody described above to examine staining patterns of these proteins after breaking

tip links. To ensure that tip links were broken during the calcium chelation step, in some experiments I added a mechanical displacement in the presence of BAPTA by using a 15 gauge needle and syringe to perfuse BAPTA solution directly over the sensory epithelium to displace the bundles.

In the utricle, incubating the organs in 5 mM BAPTA for 5 minutes caused a decrease in CDH23 and PCDH15 hair bundle staining as detected by C2367 and G19 antibodies (Figure 3.7). To quantify the change in fluorescence, individual hair bundle regions of interest (ROIs) were selected and analyzed for mean fluorescence intensity of CDH23 and PCDH15, normalized to phalloidin (Figure 3.8a,b), then normalized again to the mean fluorescence in control samples. Normalization to phalloidin was essential to account for differences in the plane of focus between ROIs, as well as for internal normalization of CDH23 and PCDH15 signal in each ROI. CDH23 hair bundle fluorescence decreased 1.5-fold, from 1.00 ± 0.02 arbitrary units (au) to 0.670 ± 0.001 au after BAPTA treatment, and PCDH15 hair bundle fluorescence decreased 2.7-fold, from 1.00 ± 0.03 au to 0.37 ± 0.01 au (n = 178 in control, n = 157 in BAPTA; $p < 0.0001$ for both CDH23 and PCDH15) (Figure 3.8c). The decrease in CDH23 hair bundle fluorescence after tip link and kinocilial link breakage was also observed with the cytoplasmic domain antibody of CDH23. Normalized C-cyto bundle fluorescence intensity decreased 2.9-fold, from 0.51 au in control to 0.18 au after EGTA treatment (Figure 3.9c,g). Co-staining with G19 again showed a decrease in normalized PCDH15 bundle fluorescence, from 0.33 au to 0.15 au to yield a 2.1-fold decrease after EGTA (Figure 3.9d,h).

Some hair bundles in the utricle appeared splayed after BAPTA treatment (Figure 3.7f, Figure 3.8b). This morphological change could be due to detachment of the kinocilial links that provide structural support to the bundle, as these links are also broken with calcium chelators (43). Hair bundles in the cochlea did not appear splayed after BAPTA, perhaps because the shorter cochlear bundle is structurally more stable (Figure 3.12f, Figure 3.13b). All stereocilia in cochlear bundles are relatively short, but in the utricle the tallest row of stereocilia is far taller than their shorter neighbors. Indeed, in the utricle the tallest row exhibited excessive charging and floppiness during SEM imaging, whereas cochlear bundles generally did not move under the electron beam. Perhaps the tall utricle hair bundles are structurally less stable than cochlear hair bundles, and more easily splay apart after BAPTA treatment.

In the chicken cochlea and the frog sacculus, CDH23 appears in a punctate staining pattern in the cell body after tip links are broken ((20), see also experiments in the next section of this chapter). The cuticular plate, which is part of the apical cell surface that anchors the hair bundle, is a dynamic trafficking region that continuously undergoes high rates of endocytosis (109, 110). The punctate staining pattern observed for CDH23 was reminiscent of endocytic vesicles, which prompted a closer examination of CDH23 and PCDH15 immunofluorescence under the cuticular plate. Colocalization analysis revealed that CDH23 and PCDH15 co-localized in this region after breaking tip links and kinocilial links, with a significant Pearson's correlation coefficient of 0.61 (Figure 3.10; r > 0.50 considered highly significant, according to (138, 139)). Co-localized puncta could represent CDH23 and PCDH15 molecules that were trafficked out of the

bundle upon BAPTA treatment, then bulk endocytosed at the cuticular plate. There

were also instances of CDH23 or PCDH15 puncta that were not co-localized (pink arrow

in Figure 3.10c), which could represent vesicles that contained only one of the two

proteins.

The prominence of CDH23 and PCDH15 antibody staining of kinocilial links in the

utricle, and the fact that BAPTA and EGTA also break kinocilial links, made it difficult to

draw conclusions about tip link-specific molecules based on immunohistochemistry. By

contrast, most cochlear hair cells do not contain a kinocilia; tall hair cells in the distal

region are more likely to contain a kinocilia, but I rarely examined these cells in my

experiments because the very basal region of the epithelium is often damaged (140).

There is also diversity in the age of hair cells in the utricle, with young hair cells

intermixed with mature hair cells. In addition, calcium chelation in the utricle led to

extensive cell extrusion after just 30 minutes in culture (see "Other experiments related

to tip link breakage"), so the health of utricle hair cells after EGTA treatment may be

compromised. For these reasons, the remainder of this chapter focuses on tip link

breakage in the cochlea, where kinocilial staining is limited and hair cells are all mature.

Antibody staining after tip link breakage in the cochlea

Tip link breakage in the cochlea resulted in loss of CEC15 immunoreactivity at

stereocilia tips, and a simultaneous increase in staining in the cell body below the

cuticular plate (Figure 3.11). A similar re-localization of CDH23 was previously reported

in the frog sacculus after breaking tip links (20). C2367 immunoreactivity in the hair

bundle also decreased after tip link breakage (Figure 3.12). Interestingly, G19

immunoreactivity did not appear to be reduced in cochlear bundles after breaking tip links, but there did appear to be an increase in cell body G19 immunoreactivity (Figure 3.12h). Normalized hair-bundle and cell body fluorescence intensity was quantified as described previously, with cell body ROIs positioned directly below the cuticular plate (Figure 3.13). CDH23 bundle fluorescence decreased from 1.00 ± 0.02 au to 0.50 ± 0.01 au after BAPTA treatment (n = 120 control, n = 95 BAPTA; $p < 0.0001$), while PCDH15 bundle fluorescence did not change (1.00 ± 0.03 au in control, n = 120; 1.00 ± 0.02 au in BAPTA, n = 95). PCDH15 fluorescence in the cell body did significantly increase after tip link breakage, from 1.00 ± 0.03 au to 1.52 ± 0.08 au (n = 115 in control, n = 94 in BAPTA; $p < 0.0001$), whereas CDH23 cell body fluorescence showed a modest but significant decrease after breaking tip links (1.00 ± 0.03 au in control, n = 115; 0.70 ± 0.03 au in BAPTA, n = 94; $p < 0.0001$).

To examine co-localization of tip link proteins in the cell body under the cuticular plate, YZ-reslices through individual hair cell bodies were selected and analyzed with Imaris co-localization software. BAPTA-treated hair cells had a significantly increased Pearson's coefficient for CDH23/PCDH15 co-localization, compared to untreated cells (0.063 ± 0.005 au in control, n = 12; 0.17 ± 0.01 au in BAPTA, n = 15; $p < 0.0001$) (Figure 3.14). Examples of co-localized puncta could be seen in the co-localization (CoLoc) channel and are highlighted with yellow arrows. There were also examples of non-co-localized puncta of CDH23 and PCDH15 (pink arrows). As in the utricle, this co-localization of CDH23 and PCDH15 could be tip link molecules that were bulk endocytosed at the cuticular plate after breaking tip links. It is particularly striking that

some of the PCDH15 spots appeared to span across the phalloidin-stained cuticular plate, which could represent vesicles that were in the process of endocytosing at the time of fixation (Figure 3.14a). Similarly, there was a higher density of these spots near the cuticular plate in front of the hair bundle with a decrease in density further down in the cell body, which may indicate that the spots originated in the cuticular plate region then spread throughout the cell.

Other experiments related to tip link breakage

In the experiments described above, the use of three separate antibodies against CDH23 helps to convince the researcher and the reader that the protein re-localized after tip link breakage. For PCDH15, only G19 was used, and this antibody showed somewhat limited staining at stereocilia tips in the cochlea. However, Goodyear and colleagues obtained excellent CDH23 and PCDH15 staining at each stereocilia tip in the chicken cochlea, using G19 antibody to detect PCDH15 (26). One major difference between these studies was the age of the animals: they used P2-P7 chickens, whereas my experiments were performed on E21/P0 chickens. To test if the age of the animal affects G19 antibody staining, I performed immunohistochemistry on P7 chickens obtained from a local chicken farm. G19 staining was substantially improved in these older animals (Figure 3.15, compare to Figure 3.5d). It is possible that E21/P0 chickens do not have PCDH15 in all of their tip links, or that the G19 epitope is partially masked in younger animals.

One early aspect of my thesis work involved culturing the utricle after breaking tip links. Through these experiments, I discovered that calcium chelation in the utricle

leads to dramatic hair cell extrusion, in as short as 30 minutes after a 1 minute EGTA treatment (Figure 3.16). Many factors were unsuccessfully tested to avoid cellular extrusion, including different extracellular calcium concentrations, temperature, transduction- and ATP-channel blockers to prevent calcium loading, and variations of the culture media (Table 3.1). I also observed that culturing after EGTA treatment resulted in hair cell extrusion in the frog sacculus (data not shown), but I did not encounter this problem in the chicken cochlea.

We hypothesized that the decrease in extracellular calcium could disrupt the tight junctions between hair cells in the utricle, allowing these damaged cells to then be pushed out of the sensory epithelium. In cultured epithelial cells, removing extracellular calcium disrupts tight junctions and causes the cells to rapidly dissociate. This effect occurs through PKA/PKC signaling and myosin light chain (MLC) activity, and can be blocked by PKA, PKC, and MLCK inhibitors (111-113). I tested inhibitors of this pathway on the utricle by pre-treating organs for 1 hour with H7, H89, and ML-7 to block PKA, PKC, and MLCK, respectively. Inhibitors were also included in the EGTA, wash, and culture steps. Unfortunately, these inhibitors did not prevent EGTA-induced hair cell extrusion (Table 3.1). The problem of cellular extrusion in the utricle complicates studies of tip link breakage, and makes studies of utricle tip link regeneration virtually impossible.

Discussion

Redistribution of CDH23 and PCDH15 after tip link breakage

Using three separate antibodies against CDH23 and one antibody against

PCDH15, I showed that these proteins redistributed after breakage of tip links and

kinocilial links in both the cochlea and utricle (see Table 3.2 for summary). For CDH23,

redistribution was observed in the utricle using the C-cyto antibody against the

cytoplasmic domain, and in the cochlea using the CEC15 and C2367 antibodies against

the extracellular domain. Interestingly, the C2367 extracellular domain antibody

showed a decrease in bundle staining in the cochlea, but also a slight decrease in cell

body staining after BAPTA treatment. This was in contradiction to the results with

CEC15 antibody, which showed a striking increase in the cell body after tip link

breakage. It is possible that the C2367 antibody had a decreased affinity for CDH23

when the protein was in intracellular compartments.

Although there was not always a complete loss of CDH23 fluorescent signal in

utricle and cochlear bundles after calcium chelation, there was always a substantial and

significant decrease. Interestingly, the CEC15 antibody consistently showed a nearly

complete loss of bundle staining, while the C2367 antibody always retained some tip

staining after tip link breakage. This could represent different pools of CDH23 with

different mobility, or may reflect CDH23 molecules that were in the bundle but were not

in the tip link. Alternatively, this result may be due to cross-reactivity of the antibody

with other bundle proteins. C2367 detected lower molecular weight bands that could

be splice forms of CDH23 or other bundle proteins. Unfortunately, there is no chicken knockout of CDH23, which would be the ultimate test of antibody specificity.

In the utricle, PCDH15 redistributed from the bundle to the cell body after BAPTA treatment. The G19 antibody used to detect PCDH15 strongly stained the kinocilial links, and some kinocilial staining remained after calcium chelation. This same antibody showed no decrease in bundle staining after tip link breakage in the cochlea, despite an increase in cell body staining. It could be that BAPTA treatment unmasked the antigenic site on PCDH15 such that G19 more efficiently detected this protein after treatment with BAPTA or when the protein was in intracellular compartments. Because transduction is mature in the early post-hatch chicken cochlea, it is likely that PCDH15 is present in the transduction complex. Yet G19 stained only some stereocilia tips at this age, and showed increased tip staining in older animals; this discrepancy was likely due to insufficient antibody labeling by G19. There is evidence that tip link proteins are glycosylated (13, 43), and perhaps G19 recognizes a sugar residue that is added to PCDH15 in older animals.

Alternatively, the increase in intracellular PCDH15 near the cuticular plate could have been due to trafficking of this protein from elsewhere in the cell. An interesting question is whether the CDH23 and PCDH15 under the cuticular plate after BAPTA treatment represents a pool of molecules that have come from the hair bundle or have been recruited from lower in the cell body. In comparative MS experiments, we have found that CDH23 and PCDH15 are highly enriched in the bundle compared to the cell body, suggesting that there are very few copies of these proteins that could be recruited

from elsewhere in the cell. To directly test the source of cell-body tip link proteins after

BAPTA treatment, live-cell labeling with C2367 and G19 could be used to tag only the

exposed extracellular domains of CDH23 and PCDH15. Antibodies would be added and

allowed to bind prior to tip link breakage. After washing out any unbound primary

antibody, one could then break the tip links with BAPTA, fix, and immediately add

secondary antibodies. Any intracellular staining would represent CDH23/PCDH15

proteins that were initially in the hair bundle before tip links were broken. I attempted

live-cell labeling with G19 and C2367 in the cochlea, but neither efficiently labeled tip

links (data not shown). This is perhaps not surprising, because G19 post-fix staining was

weak in E21 chicken cochlea, and C2367 post-fix staining was normally performed in

EGTA buffer to expose the antigenic site.

Co-localization of tip link proteins in the cell body

The most intriguing result was that CDH23 and PCDH15 co-localized in the cell

body after breaking tip links and kinocilial links. This was shown in both the utricle and

the cochlea, using an intracellular and extracellular CDH23 antibody, respectively. The

fact that this co-localization was seen just below the cuticular plate, a region of high

endocytosis, and was accompanied by a decrease in hair bundle staining of CDH23,

suggests that the co-localization could represent molecules that were trafficked out of

the hair bundle and endocytosed at the cuticular plate. Alternatively, as discussed

above, these proteins could be recruited from elsewhere in the cell. One experiment to

test if CDH23 and PCDH15 are in endocytic vesicles would be to measure co-localization

with endocytic markers such as WGA-FITC or cationic ferritin. WGA-FITC has been used

to label protein internalization from the apical surface of hair cells, and cationic ferritin labels vesicles of the apical surface endocytic pathway by TEM (109, 110). In one pilot experiment that I performed, ferritin staining was not bright enough to detect by confocal. Because G19 is a mouse monoclonal antibody and C2367 is made in goat, triple-labeling experiments using WGA-FITC would be very useful for determining if co-localized CDH23 and PCDH15 are in endocytic vesicles after BAPTA treatment.

If damaged tip link proteins are removed from the bundle after tip link breakage, this process must be fast, occurring in the time it takes to break the tip link, wash, and fix (~ 10 minutes). It is doubtful that simple diffusion would happen so quickly or so precisely, which implies that active transport may be involved. Myosin-VI (MYO6) is a minus-end directed hair-bundle motor that could bring damaged transduction components out of the bundle. MYO6 is normally localized to the stereocilia taper region, but initial immunohistochemistry experiments showed an increase in overall hair bundle staining for MYO6 after tip link breakage in the cochlea (data not shown). These results were quite variable, however, with a later experiment showing a less-dramatic increase in MYO6 staining. Future experiments involving more antibody staining and myosin inhibitors could address the role of active transport in removing damaged tip link components from the hair bundle.

Mechanism of tip link breakage

The experiments presented here shed light on the mechanism of tip link breakage in the chicken cochlea. Both BAPTA and EGTA treatment resulted in loss of tip links by SEM, whereas rough mechanical removal of the tectorial membrane did not

result in tip link loss. Furthermore, calcium chelation does not appear to break the tip link through an intermediate protease step, because pre-treatment with protease inhibitors did not prevent BAPTA-induced tip link breakage. However, it is possible that calcium chelation cleaves the tip link through activation of a protease that is not blocked by the inhibitors tested here. The action of a protease would have to be very fast, because BAPTA treatment results in tip link loss in as little as 50 milliseconds (14).

As has been suggested based on structural studies, it seems likely that removing calcium simply weakens the structural integrity of tip link molecules, causing them to unfold and be unable to withstand large displacement forces that are necessary to gate the transduction channel (40). The intriguing question that remains is whether CDH23 and PCDH15 dissociate from one another as a result of calcium chelation. Since it is not known how the N-termini of these proteins interact to form the tip link, it is hard to speculate on the precise effect of calcium chelation on this interaction. If the molecules simply unfold but stay connected, this extended tip link structure would now be long enough to span the distance between stereocilia at the taper region just above the cuticular plate, which is too great a distance for a properly folded tip link molecule to stretch. In this case, the tip link could be endocytosed as unfolded PCDH15 and CDH23 that are still connected at their N-termini.

From the work presented here, I conclude that CDH23 and PCDH15 redistribute when tip links and kinocilial links are broken by calcium chelators. Furthermore, calcium chelation caused these proteins to co-localize under the cuticular plate. Future work should focus on live-cell antibody labeling to more thoroughly determine if these co-

localized molecules are indeed originating from the hair bundle. It would be best to

perform these experiments on older animals, where G19 tip staining is more reliable,

and to develop better antibodies against PCDH15 for use in the chicken cochlea.

Discovering how CDH23 and PCDH15 interact in the tip link is essential to understanding

the mechanism and effect of tip link breakage by calcium chelation.

Experimental Procedures

Animals. Inner ear organs from E21-P0 *Gallus domesticus* chickens were

dissected in HEPES-buffered HBSS (Gibco) at room temperature, as described in Chapter

2. Cochlea were incubated in 50 μg/mL subtilisin protease (Sigma) for 20 minutes,

washed three times, and the tectorial membrane was removed using an eyelash and

forceps. In some experiments, the tectorial membrane was removed with forceps

without pre-treatment in subtilisin. To break tip links, organs were incubated in 5 mM

EGTA or BAPTA (BAPTA-tetrasodium, Invitrogen) in no calcium, no magnesium HEPES-

buffered HBSS for 5 minutes with gentle shaking, washed 3 times in calcium-containing

media, and immediately fixed for immunohistochemistry or SEM. For

immunohistochemistry experiments using C2367 and G19, a 15-gauge needle and

syringe was used to mechanically displace the hair bundles in the presence of calcium

chelators.

Scanning electron microscopy. Organs were fixed in 2% gluteraldehyde, 1%

tannic acid in 0.1 M cacodylate buffer (Electron Microscopy Sciences), in the dark at 4°C

for 3 hours - overnight, washed 3 times in PBS, and stored for less than 2 days at 4°C.

Organs were post-fixed in 1% osmium tetroxide (Electron Microscopy Sciences) in 0.1 M

cacodylate buffer for 15 minutes, followed by 4-5 washes in PBS. To preserve tip links,

organs were dehydrated in the following acetone series with sequential cooling, 15

minutes for each step: 30% at 4°C, 50% at -20°C, 70% at -35°C, 90% at -35°C, 100% at -

35°C, 100% at -35°C, 100% at 4°C. Samples were kept on ice and immediately critical

point dried in 100% cold ethanol. Organs were mounted in silver paint on carbon-

coated stubs, sputter coated in gold/palladium to yield ~ 10 nm coat, and imaged on an

FEI Sirion field emission scanning electron microscope with 5 kV accelerating voltage.

Immunohistochemistry. Organs were fixed in 4% PFA for 20 minutes, washed 3

times in PBS, and stored for less than 2 days at 4°C. At this point, organs stained with

CEC15 or C2367 were transferred to EGTA-IHC buffer containing 5 mM EGTA in calcium

and magnesium free HBSS for all remaining steps. Samples were permeabilized in 0.5%

TritonX-100 for 5 minutes and blocked with 3% normal serum, 2% BSA for 2-3 hours.

Organs were incubated with primary antibodies in blocking solution overnight at 4°C.

Organs were then washed 3 times and incubated with secondary antibodies in blocking

solution for 2 hours, followed by 3 washes. For C2367/G19 co-staining experiments,

organs were nutated during all antibody steps and washes, incubated in secondary

antibodies overnight at 4°C, extensively washed after the secondary antibody step, and

post-fixed in 4% PFA before mounting. Finally, organs were mounted in Vectashield on

#1 coverslips, with #1 + #0 spacers, sealed with VaLaP, and stored in the dark at 4°C until

imaging. For C2367/G19 co-staining in the utricle, an additional #0 spacer was added so

that the long hair bundles would stand upright for imaging.

Antibodies. Rabbit affinity-purified peptide antibody CEC15 was made against

the following sequence of mouse CDH23: (C)ATRPAPPDRERQ (Genemed Synthesis).

Goat affinity-purified antibody C2367 was made against the same sequence of mouse

CDH23, minus one amino acid: ATRPAPPDRER(C) (GenScript). Affinity purification of

these antibodies was performed as previously described (114). Briefly, 1.5 mg of

antigenic peptide was coupled to SulfoLink resin for 2 hours with rotating. Peptide-

SulfoLink resin was then washed and blocked overnight in 50 mM cysteine, washed in 1

M NaCl, and pre-eluted with 100 mM glycine, then 100 mM CAPS. 5 mL of rabbit or

goat serum was diluted in 45 mL 10 mM Tris and passed 4 times over the peptide-

SulfoLink purification column. The column was washed in 40 mL of 10 mM Tris, then 40

mL of 10 mM Tris + 500 mM NaCl. Bound antibodies were eluted from the column with

5 ml of 100 mM glycine pH 2.5, followed by 5 ml of 100 mM CAPS pH 11. Acid and base

eluted fractions were combined and concentrated to <200 µL in Centricon-30s filters in

a final buffer of PBS + 0.02% thimerosal, and stored in 50% glycerol at -20°C.

For immunohistochemistry, CEC15 antibody was used at 5 µg/mL, and C2367

was used at 8 µg/mL. Rabbit affinity purified polyclonal C-cyto antibody against mouse

CDH23 cytoplasmic domain (amino acids 3133-3291) was obtained from Dr. Uli Müller's

laboratory (Scripps Research Institute, La Jolla, CA) and was used at 1:500 (unknown

stock concentration). Mouse monoclonal G19 antibody against chicken PCDH15 was

used at 0.85 µg/mL for co-staining with C-cyto or 8.5 µg/mL for co-staining with C2367.

The following secondary antibodies were used at 1:500: donkey anti-rabbit-Alexa 555,

donkey anti-goat-Alexa 555, donkey anti-mouse-Alexa 647 (Invitrogen). All secondary

antibody incubations included Alexa 488-phalloidin at 1:200 (1 unit/mL) to visualize

filamentous actin in the stereocilia (Invitrogen). For immunoblot, C-cyto and C2367

were used at 1:200 and 4 µg/mL, respectively, and detected with either goat anti-rabbit-

HRP at 1:2500 or donkey anti-goat-HRP at 1:1000 (Jackson Labs). For peptide block of

CEC15, the antibody was incubated with 100x molar excess of the antigenic peptide for 1 hour at room temperature prior to the primary antibody incubation step.

Image acquisition, processing and analysis. Organs were imaged on an Olympus Fluoview 1000 confocal microscope, using a 60x/1.42 NA oil immersion Plan Apo objective, laser power of 5-10%, 4 µs/pixel scan speed, Kalman averaging of 3, and 0.2 µm z-steps. Z-stacks were deconvolved using softWoRx Suite (Applied Precision), and analyzed with Imaris 3D reconstruction software (Bitplane). 3D renderings allowed for XZ- or YZ-reslices through a field of hair cells, and the orthoslicer tool was used to isolate 2 µm sections through the entire image that were separately saved and exported as tiffs. Bundle and cell body ROIs were selected and quantified in ImageJ. For co-localization, the 3D crop tool was used to isolate individual hair cell bodies, and a CoLoc channel was built for each cell; threshold for CDH23 channel was set to include 80-90% of the data, and threshold for PCDH15 channel was set to include 100% of the data.

Western blots. Total inner ear protein and total protein from cochlear epithelial peels was collected as described in Chapter 2. 20 µg of each sample was incubated in sample buffer for 20 minutes at 65°C, and loaded onto 3-8% tris-acetate gradient gels (Invitrogen). Gels were run at 150 V for 1 hour on ice in tris-acetate buffer, then transferred onto PVDF membranes at 60 V for 90 minutes at 4°C, in tris-glycine transfer buffer + 10 % methanol. Blot were blocked in 5% liquid block (GE Healthcare) for 1 hour, probed with primary antibodies for 2 hours, washed, and probed with secondary antibodies for 30 minutes. HRP signal was detected using SuperSignal West Pico

Chemiluminescent reagents (Thermo Scientific) and the FujiFilm LAS 3000 Image

Reader.

Protease inhibitor treatment. Immediately prior to BAPTA treatment, cochlea

were pre-treated for 5 minutes in either calpain inhibitor type I (17 µg/mL or 34 µg/mL,

Roche) or protease inhibitor cocktail (1:100, Sigma) containing inhibitors with broad

specificity for serine, cysteine, and acid proteases, and aminopeptidases. For specific

inhibitor activity, please consult the spec sheet for product # P8340. Organs were then

treated with 5 mM EGTA + inhibitors for 5 minutes, washed in normal calcium buffer +

inhibitors, and fixed for SEM.

Immunohistochemistry in older animals. P7 chickens were obtained from

Skylane Farms (Woodburn, OR) and sacrificed by cervical dislocation on site, by the

farmers, to comply with their protocol. The skull was bisected, the brain removed, and

a small hole was opened in the temporal bone to allow fixative to reach the inner ear.

Half-skulls were immediately dropped into 4% PFA and stored on ice for the 30 minute

car ride through the country back to OHSU, then stored at 4°C overnight. Organs were

thoroughly washed, dissected, and stained as above, with the tectorial membrane left

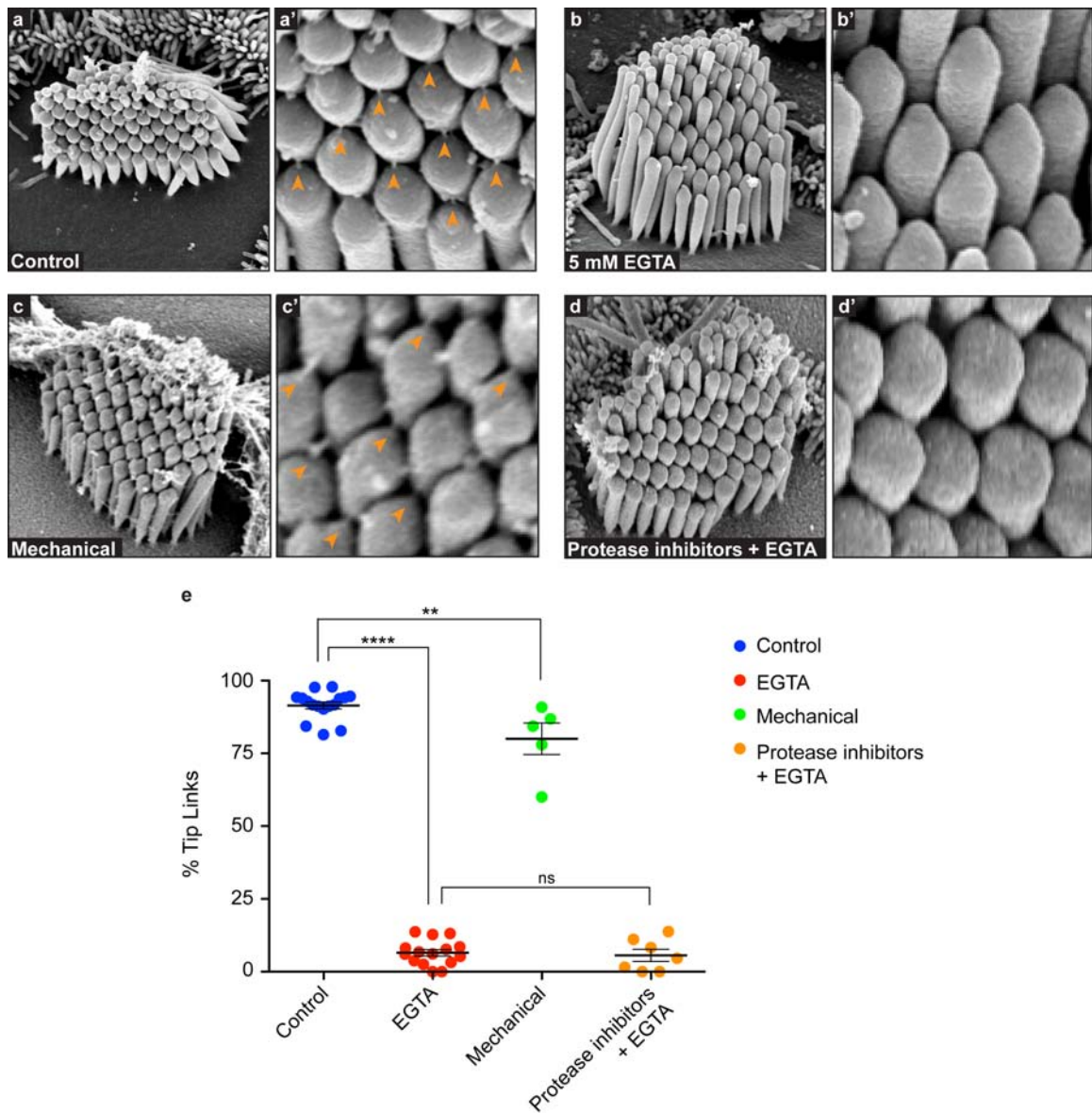on; G19 was used at 1:500 for this experiment.

Figure 3.1 – Tip link breakage in the chicken cochlea.

(a) Control hair bundles had many tip links at their stereocilia tips (orange arrows). (b) Hair bundles treated with 5 mM EGTA for 5 minutes showed a significant reduction in the number of tip links. (c) Mechanical removal of the tectorial membrane, without subtilisin protease, retained tip links in the bundle (orange arrows). (d) Pre-treatment with protease inhibitors + 5 mM EGTA resulted in tip link loss. (e) Tip links were quantified by dividing the number of tip links in a bundle by the number of observable tip link positions (**** $p < 0.0001$, ** $p < 0.005$, ns = not significant).
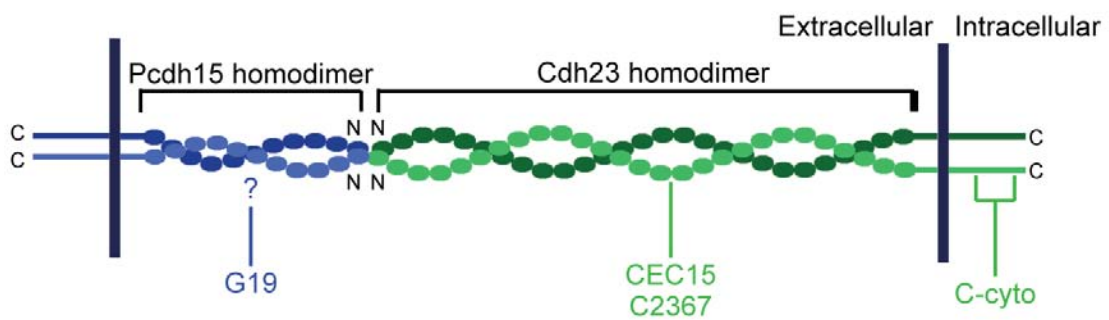
Figure 3.2 – Diagram of tip link antibodies.

Cartoon depicting antibodies used to detect CDH23 in green, and PCDH15 in blue. Monoclonal G19 antibody against chicken PCDH15 recognizes an extracellular epitope of unknown identity. Peptide antibodies CEC15 and C2367 against CDH23 recognize the extracellular EC15/16 interdomain of the chicken and mouse sequence, respectively. CDH23 antibody C-cyto recognizes a portion of the intracellular domain, including exon 68.
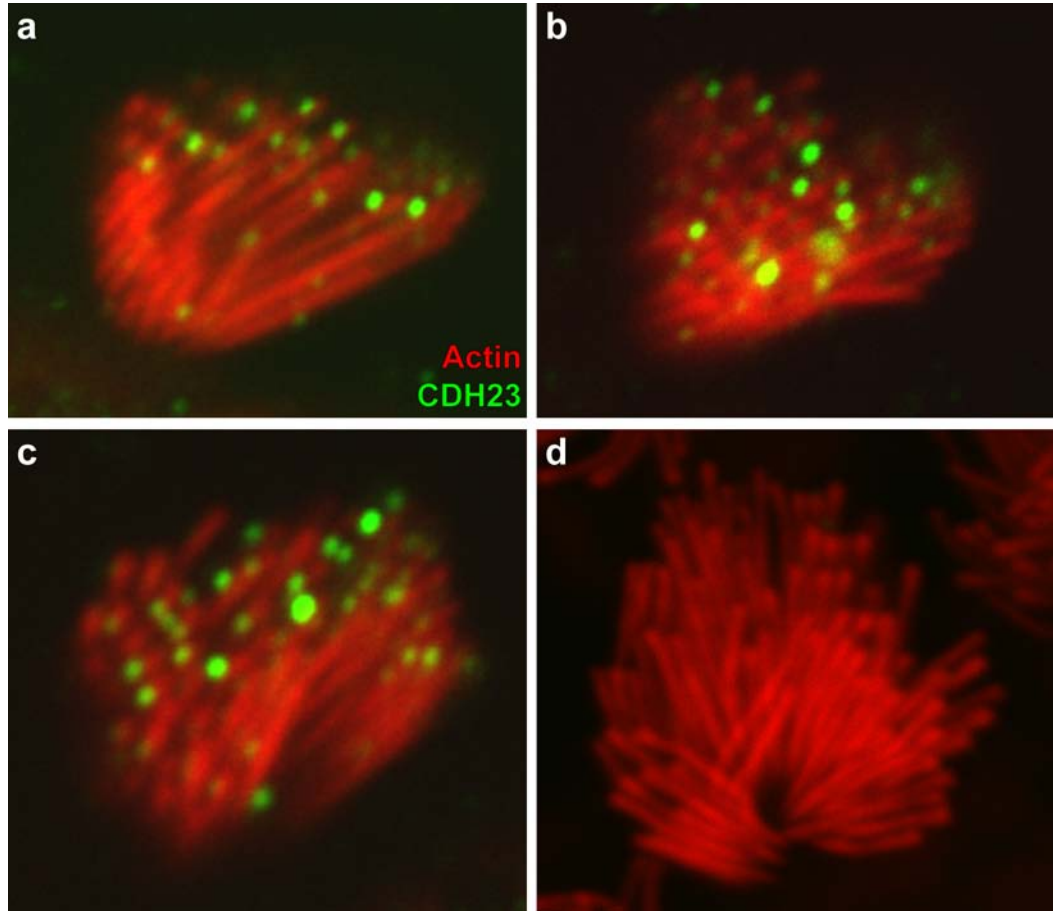
Figure 3.3 – CEC15 antibody staining in the cochlea.

CEC15 antibody against CDH23 localizes to stereocilia tips of chicken cochlear hair bundles. (a-c) three examples of chicken cochlear hair cells stained with CEC15 (d) pre-incubation with the antigenic peptide results in loss of staining. For all panels, CDH23 detected by CEC15 is in green and actin detected by phalloidin is in red.
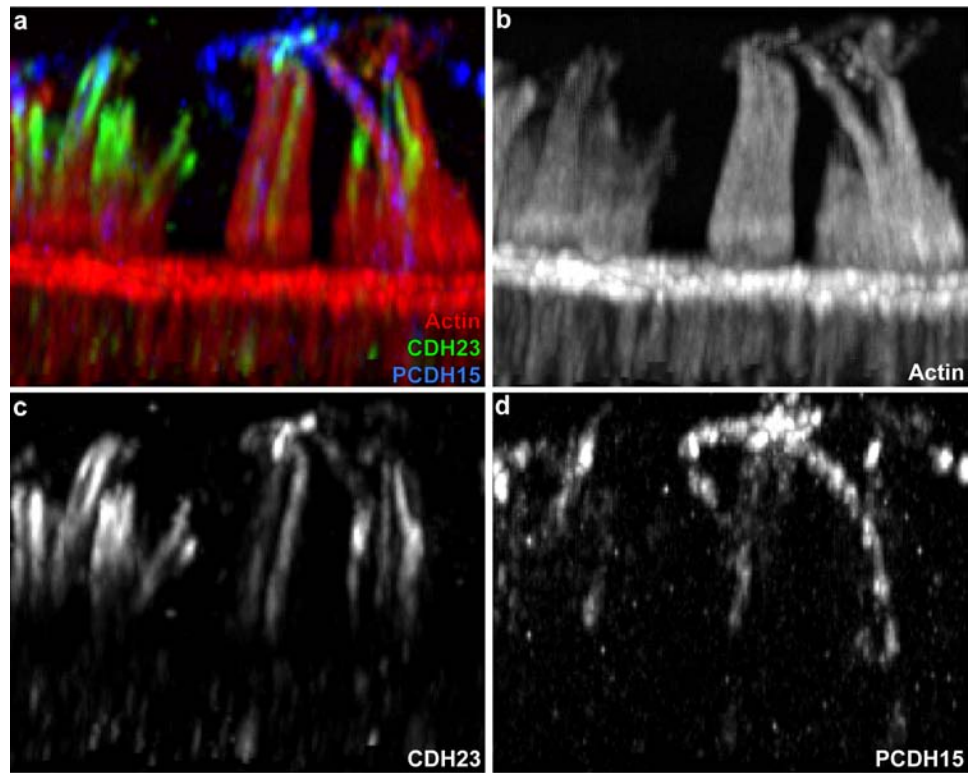
Figure 3.4 – C-cyto and G19 antibody staining in the utricle.

C-cyto antibody against CDH23 and G19 antibody against PCDH15 prominently stain kinocilial links and some tip links in the utricle. Reconstructed 3D XZ-reslice through a population of hair cells. (a) C-cyto in green, G19 in blue, phalloidin in red. (b) Phalloidin channel (c) C-cyto channel (d) G19 channel. Bright red horizontal belt in (a) shows the cuticular plate, with hair bundles extending upward.
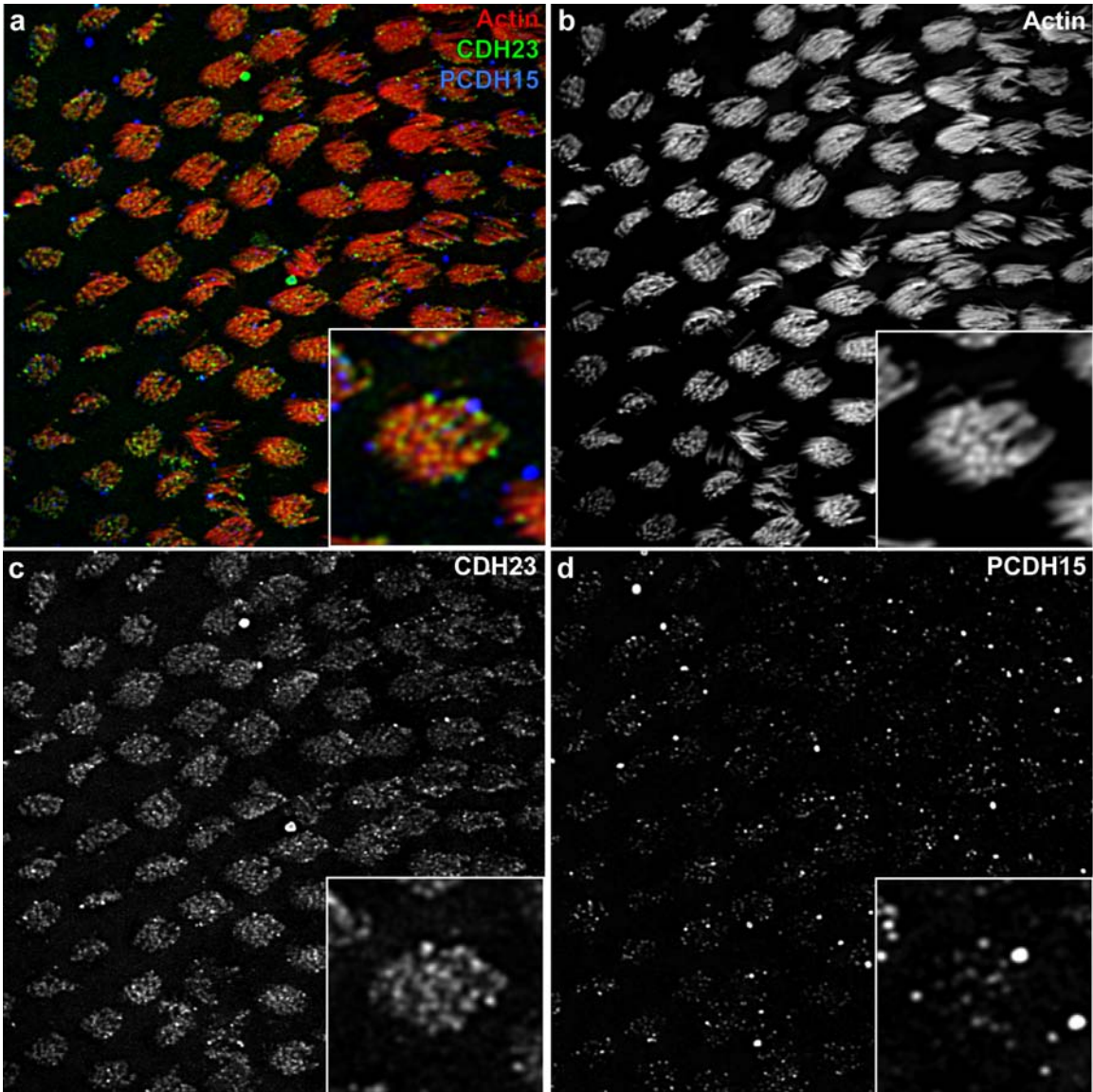
Figure 3.5 – C2367 and G19 antibody staining in the cochlea.

C2367 antibody against CDH23 stains stereocilia tips in the cochlea, with some accompanying tip staining for PCDH15 with G19 antibody. (a) C2367 in green, G19 in blue, phalloidin in red. (b) Phalloidin channel (c) C2367 channel (d) G19 channel. Boxed section is a zoomed-in image of one hair bundle.
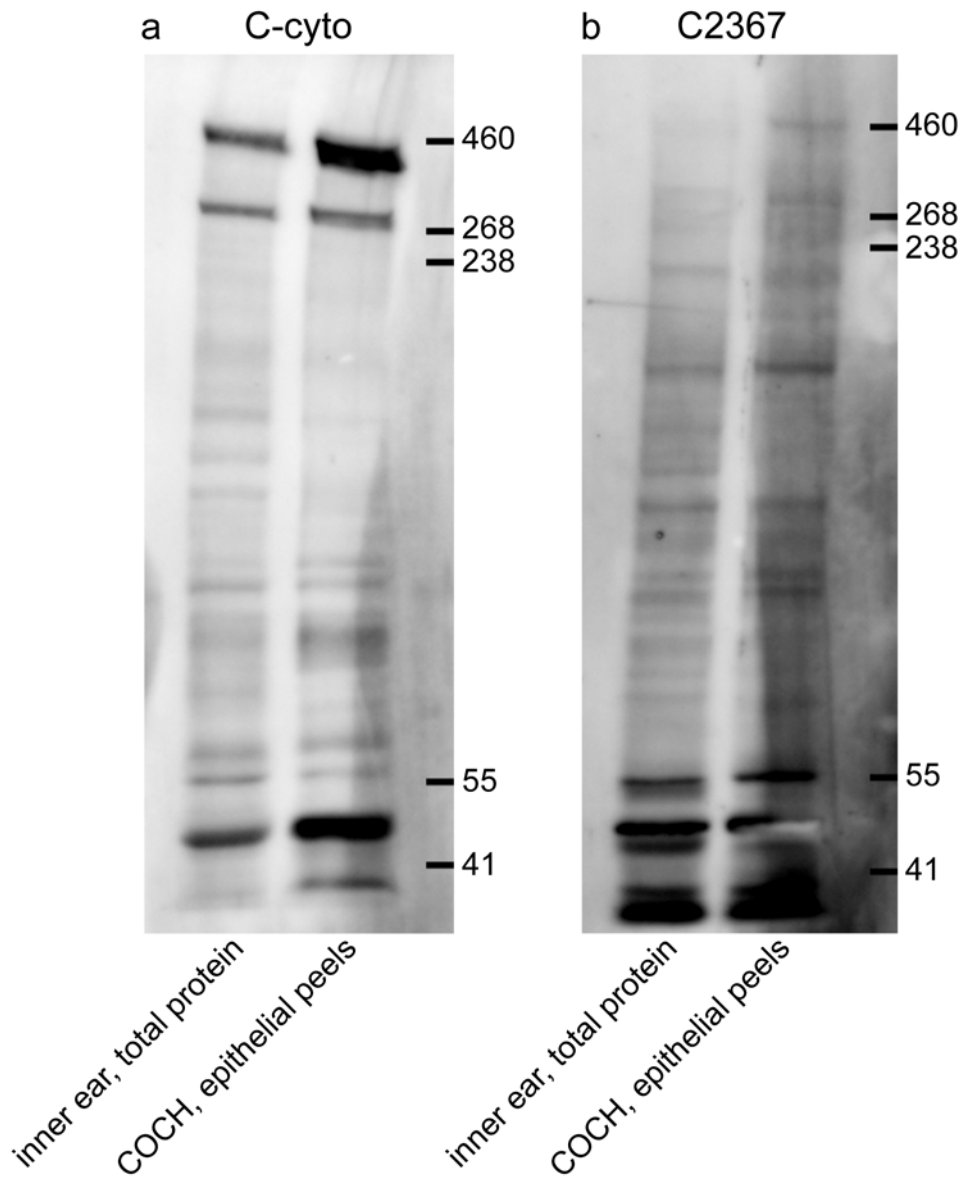
Figure 3.6 – Immunoblot detection of CDH23 in chicken inner ears.

(a) C-cyto antibody recognizes full-length CDH23 (370 kDa) from total inner ear protein, with stronger detection in cochlear epithelial peels. (b) C2367 antibody recognizes full-length CDH23 in cochlear epithelial peels, and also cross-reacts with lower molecular weight bands.
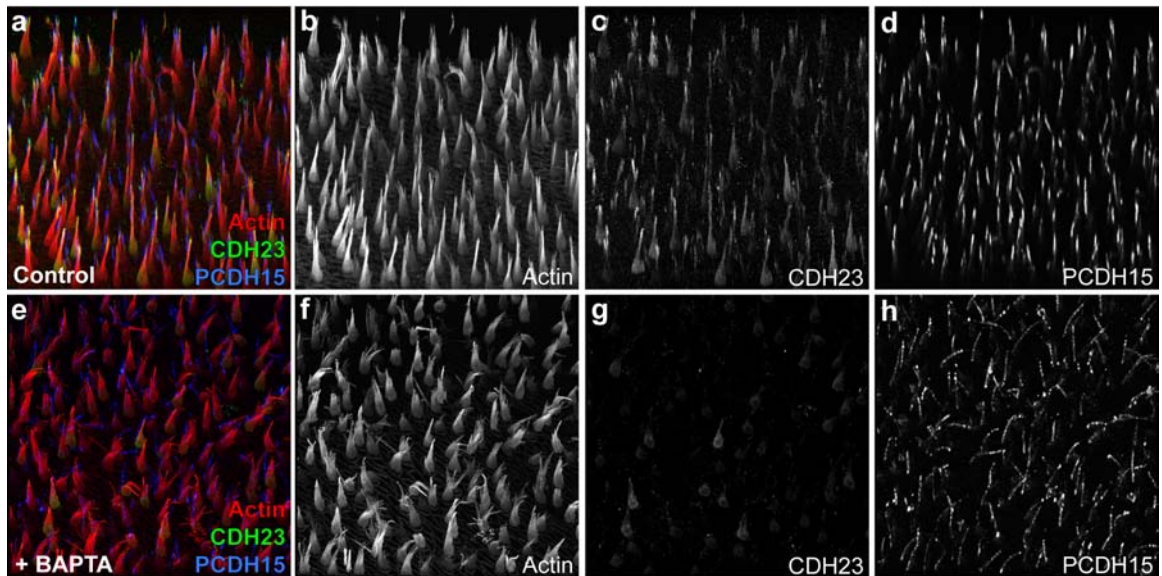
Figure 3.7 – C2367 and G19 staining after BAPTA treatment in the utricle.

Decrease in CDH23 and PCDH15 bundle fluorescence after breaking tip links and kinocilial links in the utricle. (a-d) In control hair bundles, CDH23 and PCDH15 staining is strong, and this staining decreases after treatment with 5 mM BAPTA for 5 minutes (e-h); 3D reconstruction of a population of hair cells. (a, e) CDH23 detected with C2367 in green, PCDH15 detected with G19 in blue, and phalloidin to detect actin in red.
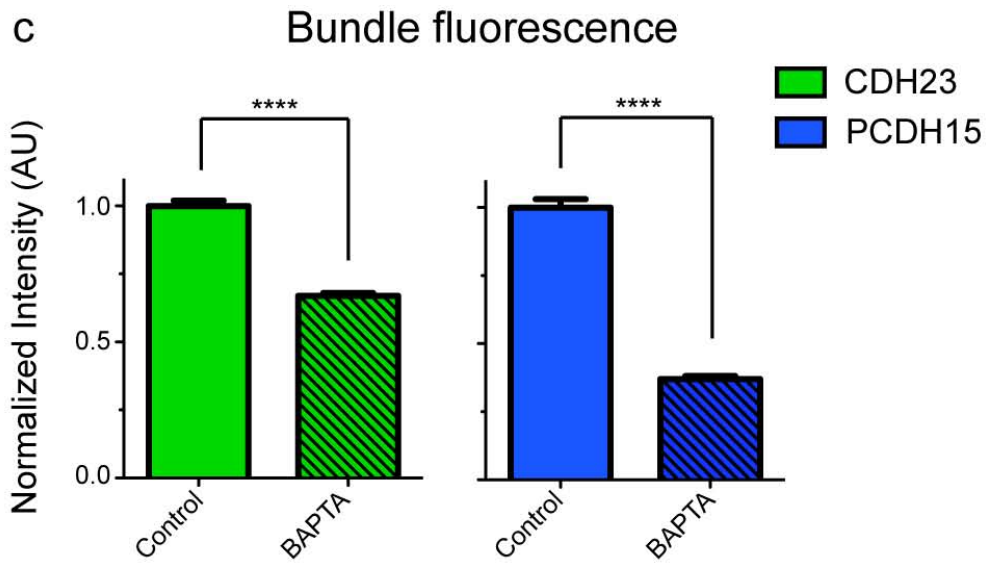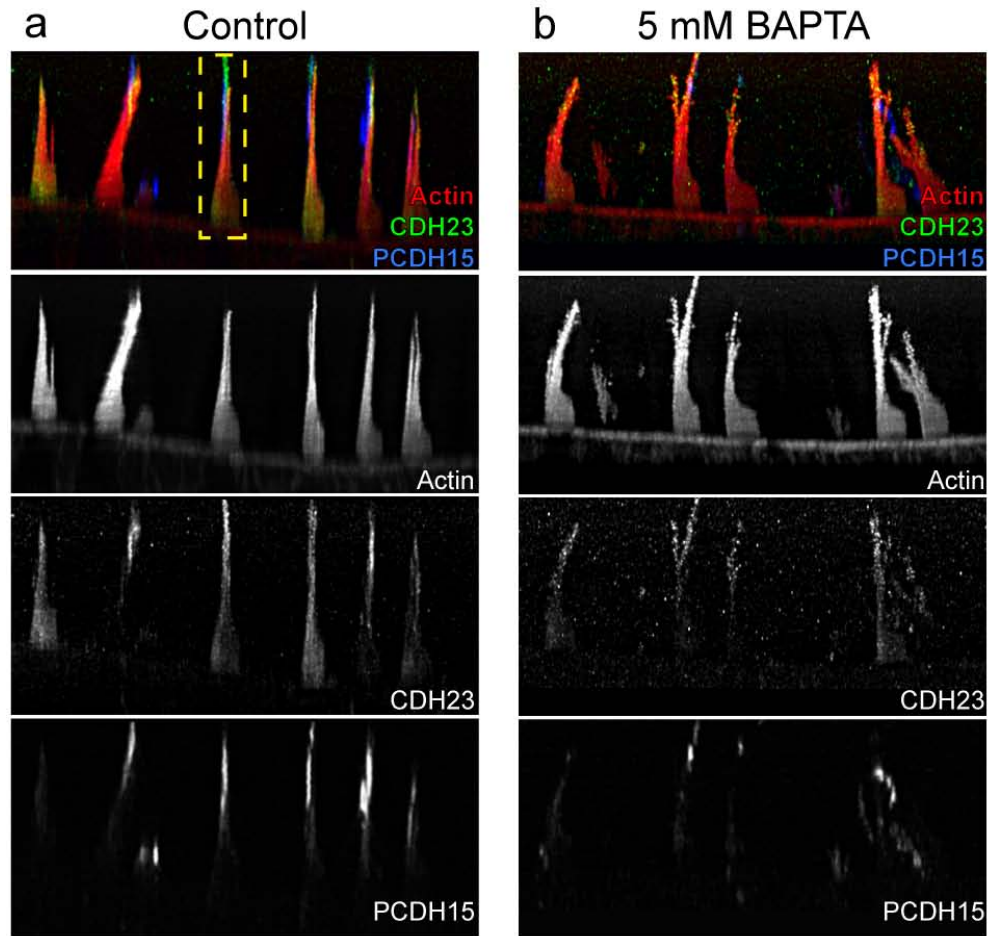
Figure 3.8 – C2367 and G19 bundle fluorescence decreases after BAPTA treatment in the utricle.

Significant decrease in both CDH23 and PCDH15 bundle staining after breaking tip links and kinocilial links. (a) Control hair bundles had more C2367 and G19 bundle fluorescence compared to hair cells treated with 5 mM BAPTA for 5 minutes (b). (c) Fluorescence was quantified by isolating individual bundles and analyzing mean fluorescence intensity of CDH23 and PCDH15 channel, normalized to phalloidin, then normalized to mean control values for either CDH23 or PCDH15 (n = 178 in control, n = 157 in BAPTA, **** $p < 0.0001$). Example of a bundle ROI in yellow box in a. (a, b) CDH23 detected with C2367 in green, PCDH15 detected with G19 in blue, and phalloidin to detect actin in red.
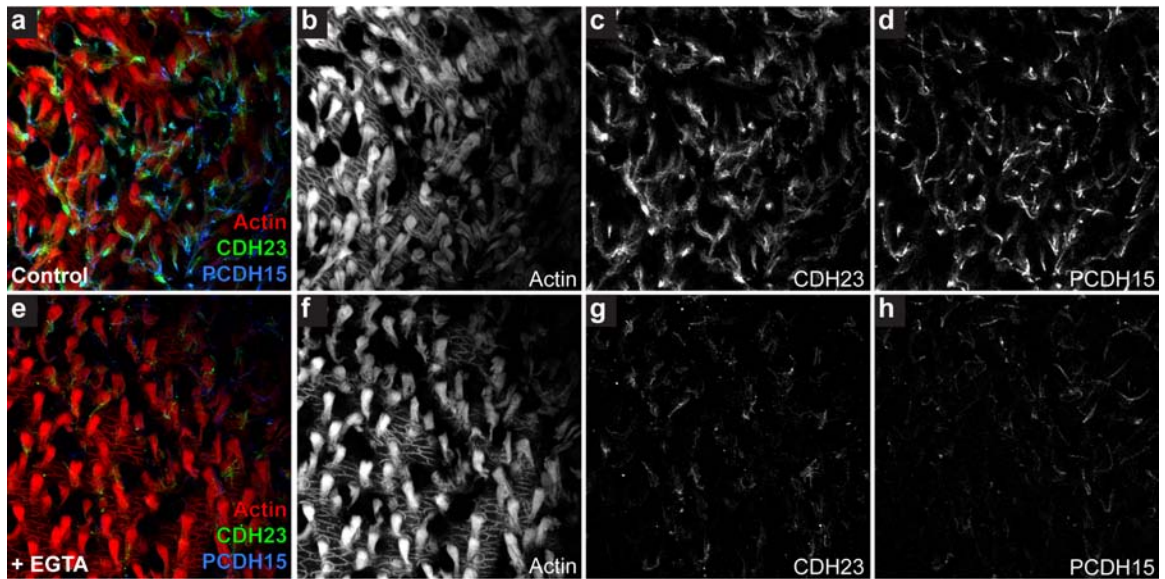
Figure 3.9 – CDH23 and PCDH15 bundle staining decreases after EGTA treatment in the utricle.

(a-d) In control conditions, CDH23 antibodies (C-cyto) and PCDH15 antibodies (G19) both stain the hair bundle. This staining decreases after treatment with 5 mM EGTA for 5 minutes (e-h). Fluorescence intensity of panel c normalized to panel b = 0.51, and panel g normalized to panel f = 0.18, to yield a 2.9-fold decrease in C-cyto bundle fluorescence. Fluorescence intensity of panel d normalized to panel b = 0.33, and panel h normalized to panel f = 0.15, to yield a 2.1-fold decrease in G19 bundle fluorescence. (a, e) CDH23 detected with C-cyto in green, PCDH15 detected with G19 in blue, and phalloidin to detect actin in red.
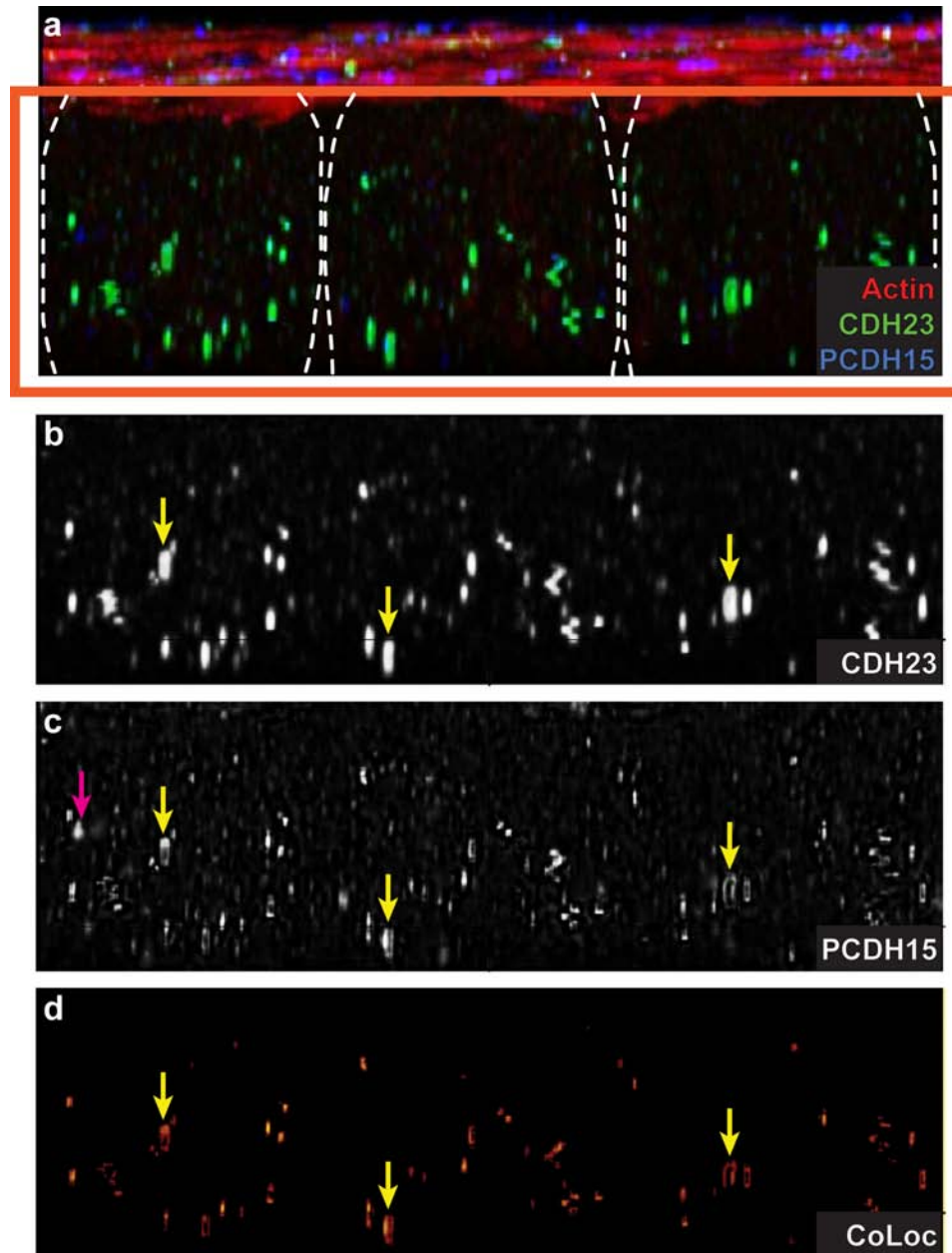
Figure 3.10 – Co-localization of CDH23 intracellular epitope and PCDH15 extracellular epitope in the cell body after EGTA treatment in the utricle.

(a) Cuticular plate (red) and cell body region of utricle epithelium after 5 mM EGTA; white dotted outlines represent three hair cell bodies, orange rectangle shows the area that was selected for co-localization analysis in panels b-d. (b) CDH23 channel (c) PCDH15 channel (d) CoLoc channel resulting from Imaris co-localization analysis, giving a Pearson's correlation coefficient of 0.61. Yellow arrows show co-localized puncta, pink arrow shows an example of a CDH23 punctum that does not co-localize with CDH23. (a) CDH23 detected with C-cyto in green, PCDH15 detected with G19 in blue, and phalloidin to detect actin in red.
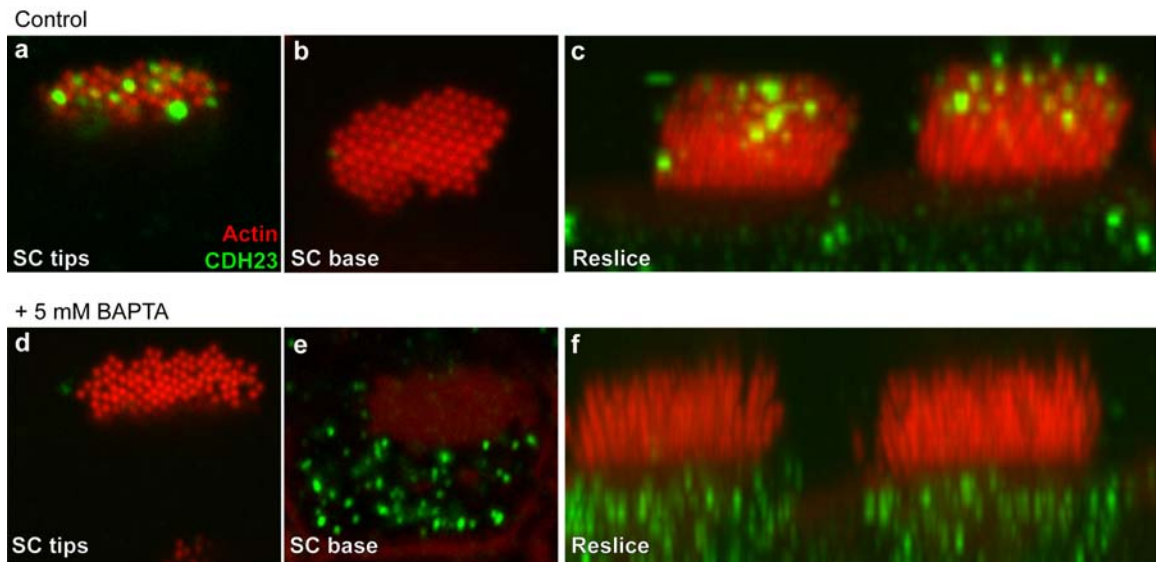
Figure 3.11 – CDH23 redistributes to the cell body after breaking tip links in the cochlea.

CDH23 tip staining disappears after BAPTA treatment in the cochlea, with a simultaneous increase in the cell body. (a) CEC15 staining at the tips of the stereocilia in control conditions. (b) CEC15 does not stain the stereocilia base in control conditions. (c) XZ-reslice through two hair cells shows staining localized to the tip region. (d) Tip link breakage results in a loss of tip staining, and an increase in staining in the cell body below the cuticular plate (e). (f) XZ-reslice highlights the decrease in tip staining and strong increase in cell body staining. For all panels, CEC15 in green, phalloidin in red.
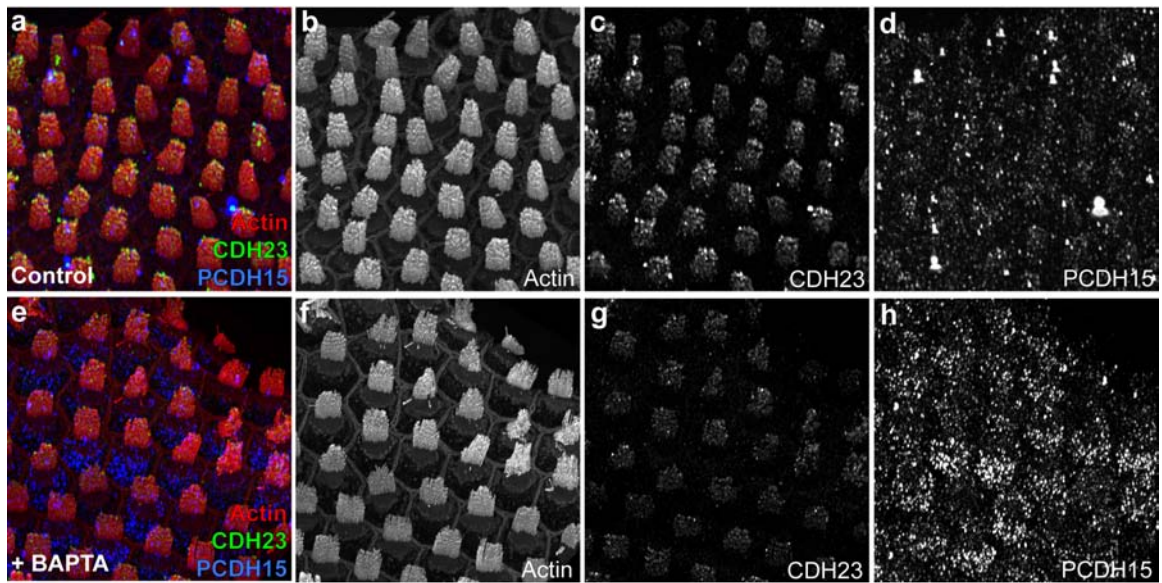
Figure 3.12 – C2367 and G19 bundle after tip link breakage in the cochlea.

(a-d) Strong staining with C2367 in control hair bundles, with G19 staining also present in the bundle. (e-h) Treatment with 5 mM BAPTA to break the tip links resulted in a decrease in CDH23 bundle staining. No obvious decrease in PCDH15 bundle staining was observed, but an obvious increase in cell body staining could be seen (e, h). 3D reconstruction of a population of hair cells. (a, e) CDH23 detected with C2367 in green, PCDH15 detected with G19 in blue, and phalloidin to detect actin in red.
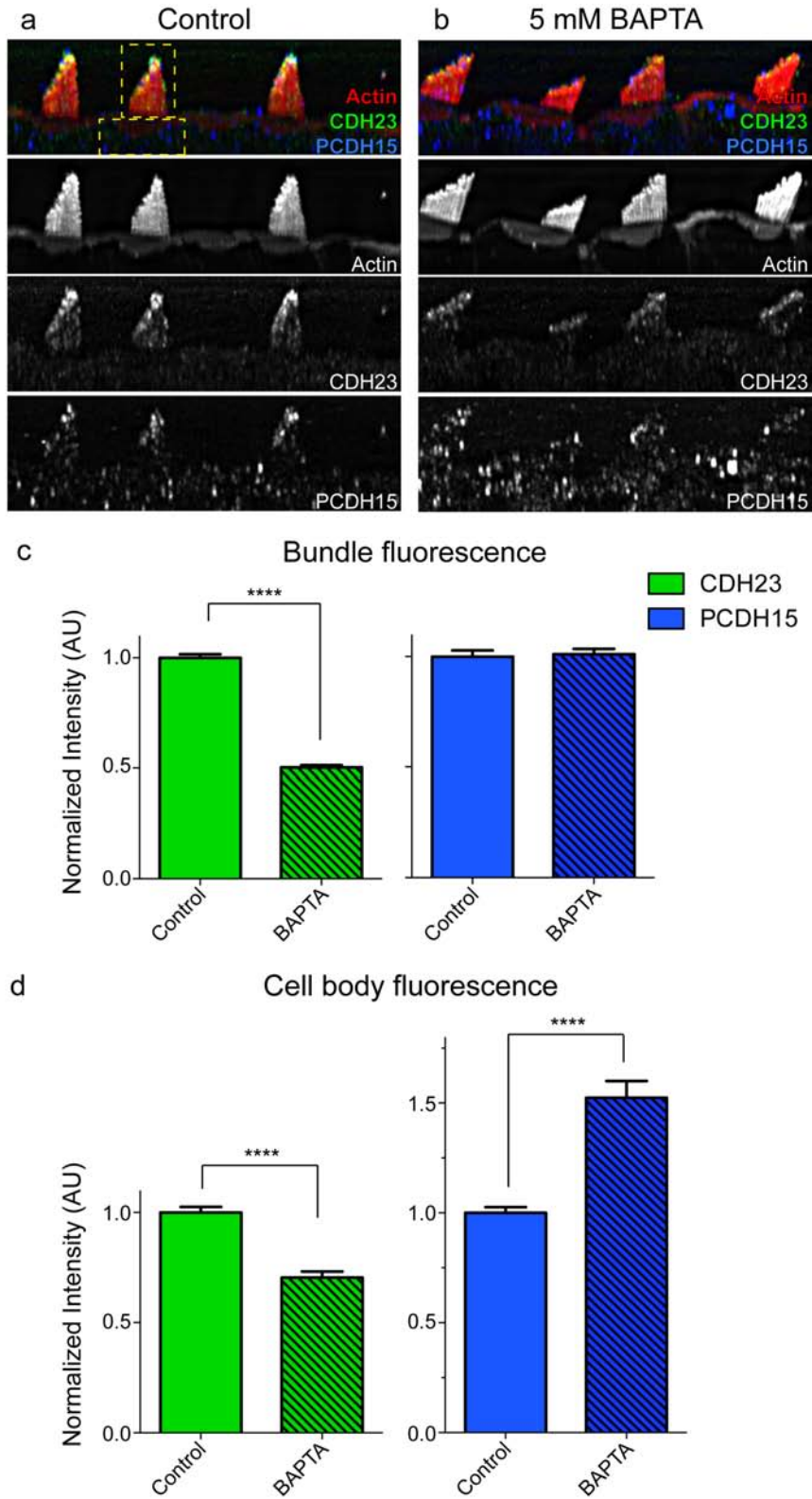
Figure 3.13 – Changes in C2367 and G19 fluorescence in the hair bundle and cell body after tip link breakage in the cochlea.

(a) Image of a single YZ-reslice through control hair bundles, with examples of bundle and cell body ROIs in yellow boxes. (b) Treatment with BAPTA to break the tip links caused a marked decrease in CDH23 bundle fluorescence, and an increase in PCDH15 cell body fluorescence. (c) Fluorescence was quantified by isolating individual bundle or cell body ROIs and analyzing mean fluorescence intensity of CDH23 and PCDH15 channel, normalized to phalloidin, then normalized to mean control values for either CDH23 or PCDH15 (bundle control n = 120, BAPTA n = 95; cell body control n = 115, BAPTA n = 94; **** $p < 0.0001$). (a, b) CDH23 detected with C2367 in green, PCDH15 detected with G19 in blue, and phalloidin to detect actin in red.
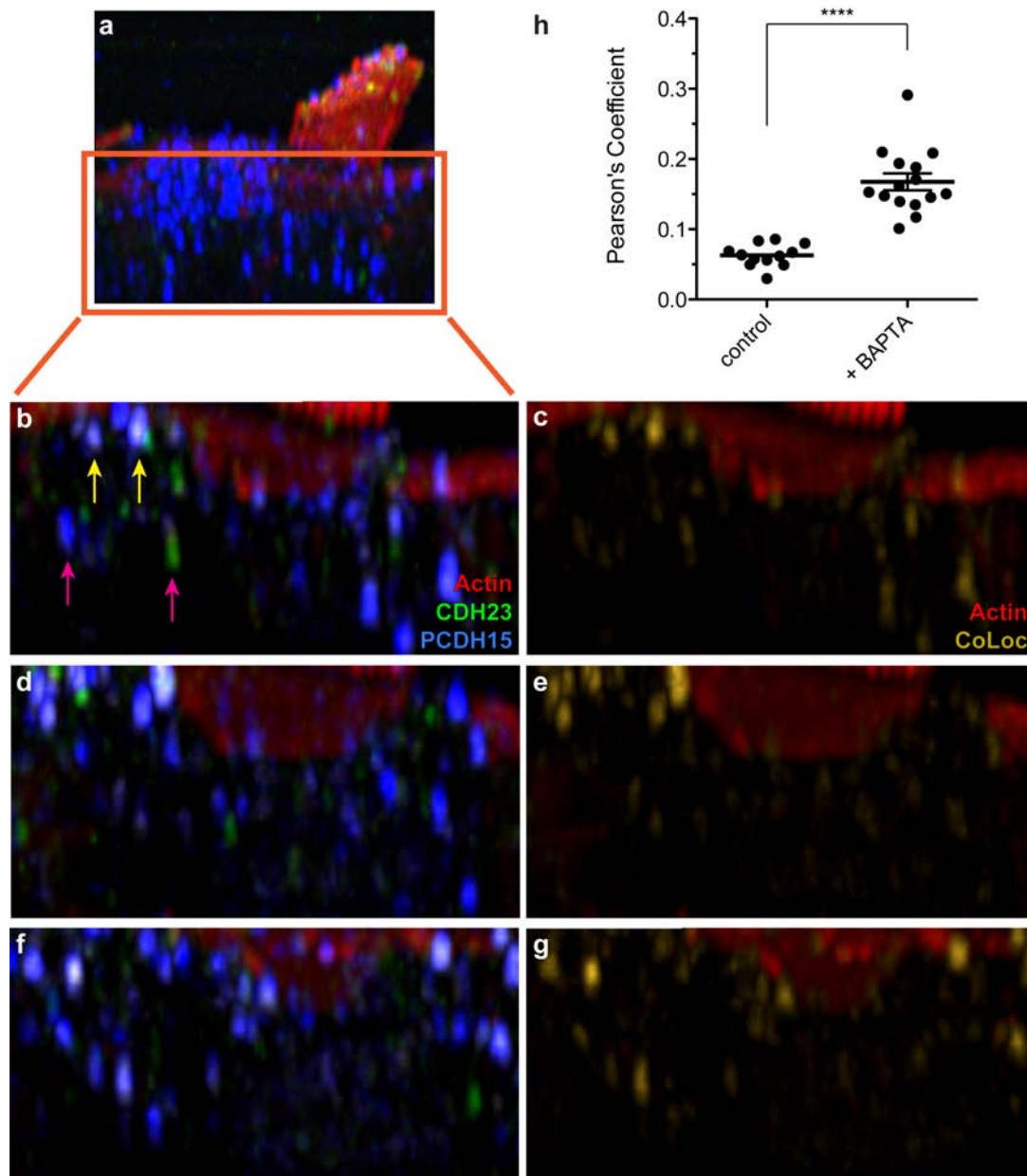
Figure 3.14 – CDH23 and PCDH15 co-localize in the cell body when tip links are broken in the cochlea.

(a) 3D reconstructed image of one hair cell used for analysis, with orange box indicating cropped cell body area. (b, d, f) Examples of individual XZ-reslices showing C2367 fluorescence in green, G19 fluorescence in blue, and phalloidin in red. Yellow arrows indicate co-localized puncta, pink arrows indicate non-co-localized puncta. (c, e, g) Corresponding Imaris CoLoc channel in yellow, with phalloidin counterstain in red. (h) Significant increase in Pearson's co-localization coefficient for CDH23 and PCDH15 after BAPTA treatment (n = 12 in control, n = 15 in BAPTA, **** p < 0.0001).
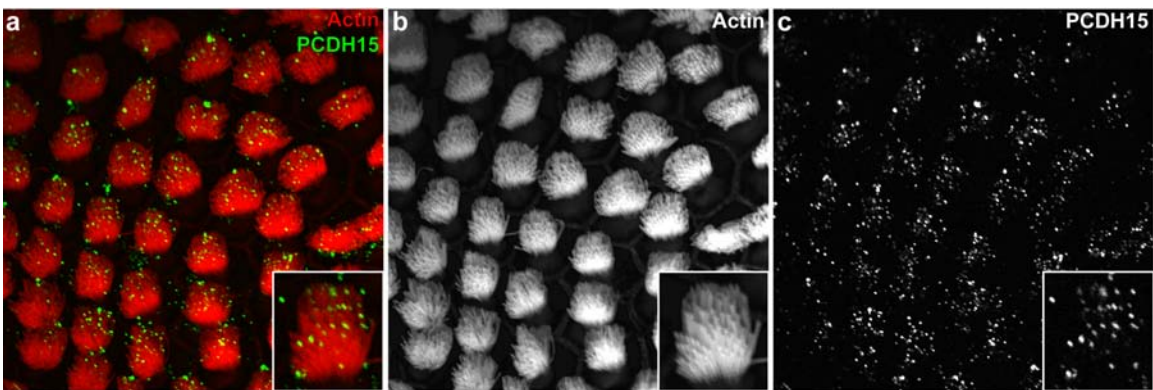
Figure 3.15 – G19 antibody staining in P7 chicken cochlea.

Improved G19 detection of PCDH15 at stereocilia tips in older animals, compared to E21/P0 cochlea (Figure 3.5d). G19 in green, phalloidin in red.
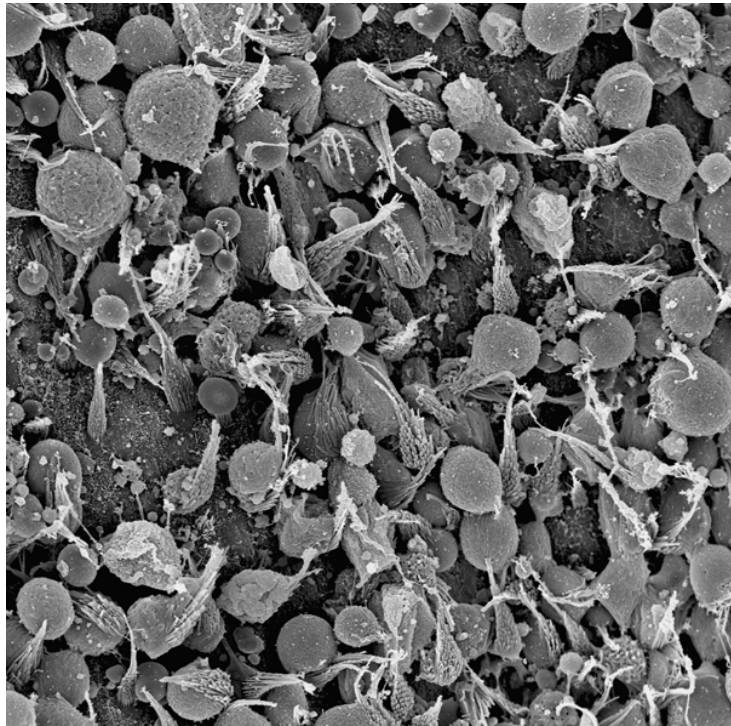
Figure 3.16 – Utricle hair-cell extrusion in EGTA-treated cultures.

SEM shows excessive hair cell extrusion in the utricle after 5 mM EGTA treatment for 1 minute, followed by 6 hours in culture.

Dissect	[Ca]	Break tip links	Culture
Chick Standard Saline	4 mM	5 mM EGTA in chick No Ca Saline, 1 min	M199 + HEPES
Chick Standard Saline	4 mM	5 mM BAPTA in chick No Ca Saline, 1 min	M199 + HEPES
Chick Standard Saline, on ice	4 mM	5 mM EGTA in chick No Ca Saline, 1 min	M199 + HEPES

Chick Standard Saline
  + 1.4 mM Amiloride + 100 uM PPADS
	4 mM	5 mM EGTA in chick No Ca Saline, 1 min
		    + channel blockers
			M199 + HEPES
			    + channel blockers

Chick Standard Saline
   + 100 uM DHS + 100 uM PPADS
	4 mM	5 mM EGTA in chick No Ca Saline, 1 min
		    + channel blockers
			M199 + HEPES
			    + channel blockers

Hepes-buffered Hanks (HBHBSS)	1.26 mM	5 mM EGTA in HBHBSS, 1 min	M199 + HEPES
Hepes-buffered Hanks (HBHBSS)	1.26 mM	5 mM EGTA in HBHBSS, 1 min	HBHBSS + 5% FBS
Low Ca chick saline	100 uM	5 mM EGTA in chick No Ca Saline, 1 min	M199 + HEPES
Low Ca chick saline	100 uM	5 mM EGTA in chick No Ca Saline, 1 min	Low Ca M199 + HEPES
Chick Standard Saline	4 mM	260 nM Ca-buffered chick saline, 1 min	M199 + HEPES + 5% FBS
Chick Standard Saline	4 mM	200 nM Ca-buffered chick saline, 1 min	M199 + HEPES + 5% FBS
Chick Standard Saline	4 mM	100 nM Ca-buffered chick saline, 1 min	M199 + HEPES + 5% FBS
Chick Standard Saline	4 mM	100 nM Ca-buffered chick saline, 1 min	M199 + HEPES + 10% FBS
Chick Standard Saline*	4 mM	5 mM EGTA in HBHBSS, 1 min	HBHBSS + 5% FBS

Chick Standard Saline*ξ
  + 100 uM H7 + 20 uM H89 + 15 uM ML-7
	4 mM	5 mM EGTA in HBHBSS, 1 min
		    + inhitibors
			HBHBSS + 5% FBS
			    + inhibitors

* extrusion after 30 mins in culture

ξ pre-treated with inhibitors for 1 hr at 37°C

Table 3.1 – Summary of factors tested to prevent EGTA-induced hair-cell extrusion in the utricle.

Antibody	Antigen	Utricle	Cochlea	Control staining	Post-BAPTA staining
CEC15 ♪	CDH23 extracellular		X	Distinct tip staining	Complete loss of bundle staining, increase in staining below the cuticular plate
C-cyto ♬	CDH23 intracellular	X		Stains tip links and kinocilial links	Decrease in bundle staining, co-localizes with G19 in cell body
C2367	CDH23 extracellular	X	X	Stains tip links and kinocilial links	Decrease in bundle staining, co-localizes with G19 in cell body in cochlea
G19	PCDH15 extracellular	X	X	Stains tip links and kinocilial links, enhanced staining of cochlear tip links in older animals	Utricle - decrease in bundle staining; Cochlea - no change in bundle staining, but increase in cell body staining; co-localizes with C-cyto in cell bodies in utricle, and C2367 in cell bodies in cochlea

♪ staining is sensitive to subtilisin treatment, antibody is only stable for a few months when stored at -20°C in 50% glycerol

♬ excellent for western blot detection of full-length CDH23

Table 3.2 – Summary of antibodies and results.

Chapter 4 – Monitoring intracellular calcium dynamics in a population of hair cells with Fluo4-AM

Kateri J. Spinelli and Peter G. Gillespie

Abstract

Tip links that are broken by calcium chelators can reform to restore proper transduction. Little is known about the molecular mechanism of tip link regeneration, but this process does depend on changes in intracellular calcium. Here I describe a technique for loading hair cells in the chicken cochlea with the cell-permeable calcium indicator Fluo4-AM. Breaking tip links and blocking the transduction channel both decreased the hair bundle and cell body Fluo-4 signal, whereas blocking voltage gated calcium channels selectively decreased cell body Fluo-4. Mechanical stimulation of the bundle with a fluid-jet caused a rapid increase in Fluo-4 signal in the bundle, indicating that the dye responded to calcium entry through functional transduction channels. Individual cells that were observed by live-cell imaging could be found in SEM, allowing for a correlative analysis of Fluo-4 signal and bundle morphology. This new way of imaging intracellular calcium in a population of hair cells should allow the study of calcium dynamics during tip link regeneration.

Introduction

Inner ear hair cells are highly specialized sensory cells that require intracellular calcium for graded neurotransmitter release, synaptic transmission, and adaptation of the mechanotransduction channel (1, 115). Calcium also plays a role in repairing damage to the sensory hair bundle, specifically damage to the tip link. Tip links are extracellular filaments that connect adjacent stereocilia; one tip link per stereocilia tip is believed to gate the transduction channel. Tip links are broken by chelation of extracellular calcium, which results in rapid loss of mechanotransduction, and both tip links and transduction can recover over 3-12 hours in culture (42, 54). Previous work in our lab showed that addition of the calcium ionophore ionomycin during regeneration blocked the return of tip links, indicating that lower intracellular calcium is necessary for tip link regeneration (42).

When tip links are broken, a number of physiological changes involving calcium occur within the cell. Under control conditions, tension on the gating elements of the transduction channel results in a 10-50% open probability at rest, depending on the extracellular calcium concentration; this creates a substantial inward current that is partially carried by calcium (8, 56, 57, 116). Indeed, loading hair cells with a calcium indicator dye reveals a "tip blush" of calcium at the stereocilia tips, which is the presumed site of transduction channels (117). This inward current also depolarizes the hair cell to a membrane potential of -60 to -40 mV, which in turn should open a small fraction of voltage-gated calcium channels in the basolateral membrane (55-57) (Figure

4.1). When tip links break and transduction channels close, there is presumably a two-step effect on intracellular calcium: first hair-bundle calcium decreases as a direct result of transduction channel closure; second the cell hyperpolarizes, closing voltage-gated calcium channels to decrease cell body calcium (Figure 4.1). This decrease in hair bundle and cell body calcium is likely important for regeneration of tip links, since keeping intracellular calcium high with ionomycin blocks regeneration (42).

Typical hair cell calcium imaging experiments use whole-cell patch clamp to deliver a calcium dye through the pipette (8, 118). This is a powerful technique for pairing electrophysiological recordings with measurements of intracellular calcium dynamics. However, this approach labels only one cell at a time, and in the cochlea it requires damaging surrounding hair cells to gain access to the cell of interest. To study a population of cells is therefore time-consuming, because one must individually patch clamp each cell, and requires technical training on the difficult method of recording from hair cells. Furthermore, tip link breakage by calcium chelators is not reversible; monitoring the calcium environment in the same cell before and after breaking tip links consumes one organ for every cell studied.

A handful of previous studies have reported the use of cell-permeable calcium indicators in hair cells. To examine defects in the hair bundle calcium pump, Bortollozzi and colleagues used a cell-permeable calcium indicator to monitor clearance rates in the hair bundle after uncaging of intracellular calcium (119, 120). Another group reported loading of hair cells with a cell-permeable calcium dye in a semi-intact mouse cochlear preparation, citing modest changes in cell body fluorescence in response to stimulation

of the stapes as an indicator of mechanotransduction (121). However, none of these studies specifically compared hair bundle fluorescence to morphological state of the bundle, the presence of tip links, and transduction. One study even showed that imaging hair cells loaded with a UV-activated cell-permeable calcium indicator induced outer hair cell death, presumably due to phototoxicity and calcium loading of the cells (122). Other reports in isolated cells loaded with a cell-permeable dye showed fluorescence in the cell body but no fluorescence in the hair bundle, which was likely due to damage to the tip links that would have resulted in transduction channel closure (117, 123).

To examine intracellular calcium simultaneously in a population of hair cells, I optimized a protocol to load hair cells with the cell-permeable calcium indicator Fluo4-AM (F4-AM). This minimally invasive protocol labeled most hair cells in the chicken cochlea while maintaining excellent tissue and bundle morphology. Control experiments verified that the Fluo-4 (F4) signal in the hair bundle was due to calcium entry through functional transduction channels. This method should be particularly useful for studying calcium dynamics during tip link regeneration, where the epithelium must be kept intact for 3-12 hours in culture and all hair cells in the epithelium can be monitored in parallel.

Results

Loading chicken cochlear hair cells with F4-AM

F4 is a high-affinity calcium dye that shows a >100-fold increase in fluorescence when bound to calcium. With a K_d of 350 nM, similar to the buffering capacity of BAPTA (136 nM), F4 is sensitive enough to detect and report low concentrations of free intracellular calcium. Modification of the dye with an acetoxymethyl (AM) ester moiety allows this dye to cross the cell membrane, where endogenous esterases cleave the AM group to liberate the active dye. F4-AM is virtually non-fluorescent, ensuring that the indicator detects calcium only when F4 is activated intracellularly.

To load hair cells with F4-AM, early post-hatch chicken cochleae (P0) were removed from the skull and acutely dissected at room temperature, with removal of the tectorial membrane after incubation with subtilisin protease. To slow adaptation and increase the open probability of the transduction channel, low calcium media (0.5 mM) were used throughout these experiments (8, 56, 57, 116, 124). Compared to organs dissected and imaged in normal calcium saline (1.26 mM), low calcium medium resulted in an increased level of hair bundle F4 signal (data not shown). Importantly, 0.5 mM calcium is closer to that of the endolymph that bathes the hair bundle *in vivo* (20 – 50 µM).

Careful preparation of the F4-AM solution was necessary to achieve efficient loading of hair cells. The dye was first dissolved in high quality, anhydrous dimethylsulfoxide (DMSO) at a concentration of 10 mM, then diluted 1:1 in the

dispersing agent Pluronic F-127, and added to the media at a final concentration of 10 µM (Figure 4.2). To ensure that the dye was completely dissolved, vortex and sonication steps were included between each dilution (117). In addition to normal loading into the cytoplasm, F4-AM can enter the cell through endocytosis and can also incorporate into intracellular compartments; both mechanisms are enhanced at physiological temperatures. To minimize subcellular compartmentalization, loading, wash steps, and imaging were performed at room temperature.

Cochlear epithelia were incubated with 10 µM F4-AM for 15 minutes, then washed 3 times for 15 minutes total to allow complete de-esterification of the dye (Figure 4.2). Organs were either mounted upside down on an inverted confocal microscope to image the bundles near the objective, or right side up on an upright confocal microscope for fluid jet stimulation. An electrophysiology harp was used to hold the epithelium in place. Most hair cells in the epithelium took up the dye and had bright F4 signal in the cell body (Figure 4.3a). Hair bundle F4 fluorescence was also observed in many cells, albeit at lower intensity; over-saturation of the cell body signal was necessary to detect the hair bundle signal (Figure 4.3b). A tip blush of calcium was sometimes seen at the stereocilia tips, indicating that the F4 signal could be due to calcium entry through functional transduction channels (4 out of 7 cells analyzed). Hair cells retained the dye for up to 2 hours after loading, if kept at rest in the dark. Once the organ was placed on the microscope stage for imaging, the F4 signal was maintained for 30-45 minutes, depending on how much damage the harp introduced to the fragile epithelium. Because dissecting and loading conditions vary from day to day, all

experiments described below had a corresponding control organ that was dissected and loaded in parallel, and imaged with identical microscope acquisition parameters.

F4 signal appeared uniform along the length of epithelium, but was not directly analyzed. For simplicity, the mid-apical region was chosen, which contains a mix of tall and short hair cells. No obvious differences in F4 signal or response to drugs were observed between hair cell types. Hair bundles in this region are optimally oriented for fluid-jet displacement, with the axis of sensitivity perpendicular to the neural edge and facing the basal end where the fluid-jet pipette was placed.

Testing the source of F4 hair bundle calcium

A number of experiments were performed to determine if F4 signal in the hair bundle was due to entry of calcium through mechanotransduction channels. First, the cochlea was pre-treated with 5 mM EGTA to break tip links and close transduction channels that are open at rest. Breaking tip links significantly decreased both hair bundle and cell body F4 signal, from 0.43 ± 0.02 arbitrary units (au) to 0.184 ± 0.004 au in the hair bundle, and from 1.75 ± 0.07 au to 0.84 ± 0.04 au in the cell body (Figure 4.4; $p < 0.0001$ for both regions). A similar decrease in hair bundle F4 signal was observed when EGTA was applied to the hair bundle during continuous calcium imaging (data not shown). As described above, this decrease in cell body calcium is likely due to the two-step process that results in closure of voltage-gated calcium channels (Figure 4.1). There was some remaining F4 signal in EGTA-treated cell bodies, which could be seen in a punctate staining pattern and likely represented dye that was trapped in intracellular compartments. Much of the punctate staining was concentrated under the cuticular

plate, which is an active region of endocytosis and also contains a high density of mitochondria that have been shown to take up calcium dyes (8, 109). To quantify cytoplasmic F4 signals and avoid confusion with dye trapped in intracellular compartments, all cell body fluorescence measurements were taken from the lower half of the cell (Figure S-4.1).

For both hair bundle and cell body F4 signal, the spread of the data in control conditions was greater than after EGTA treatment. This diversity in F4 signal likely reflects differences in the physiological state of the hair cells. While many control cells in a single epithelium had roughly the same F4 bundle intensity (also see Figure 4.5a), some cells' F4 bundle and cell body signal were comparable to EGTA-treated cells. It is likely that these cells' tip links had broken during dissection. There were also a few control cells with substantially elevated F4 signal in both the bundle and cell body, which could indicate dying hair cells that had become calcium-loaded.

To examine the ultrastructure of the hair bundle and overall epithelium, F4 imaged organs were fixed and processed for SEM. Using landmarks observed during live-cell imaging, the same cells could be found in the electron microscope. Indeed, cells with very strong F4 signal in the bundle and cell body were extruding from the epithelium, an indication of cell death (Figure 4.5a,b). Regions of the epithelium that had mid-level F4 signal in the bundle and cell body had organized stereocilia and tip links by SEM (Figure 4.5c,d). Splayed and damaged bundles with few tip links correlated with bundles that had low levels of F4 during live-cell imaging (Figure 4.5e,f). Therefore in live-cell experiments, hair cells could be distinguished based on bundle and cell body

calcium signals – dead or dying cells with very bright F4, healthy cells with tip links

corresponding to mid-level F4 bundle signal, and cells with damaged bundles or tip links

corresponding to low F4 bundle signal. The majority of cells in the epithelium had mid-

level F4 signal, demonstrating that most cells were healthy and had organized bundles

and tip links. These data also show that hair bundle F4 signal directly correlated with

the presence of tip links, further supporting the hypothesis that bundle F4 signal is due

to calcium entry through functional transduction channels.

I used channel blockers to test the influence of calcium entry through the

transduction channel or through voltage-gated calcium channels in the basolateral

membrane. Organs pre-treated with 100 µM tubocurare, an open-channel transduction

blocker, had decreased bundle and cell body F4 signal compared to untreated organs

(Figure 4.6; control bundle fluorescence = 1.66 ± 0.06 au, tubocurare bundle

fluorescence = 0.50 ± 0.02 au, control cell body fluorescence = 6.8 ± 0.3 au, tubocurare

cell body fluorescence = 2.8 ± 0.1 au; p < 0.0001 for both bundle and cell body) (125).

As with breaking the tip link, the decrease in cell-body calcium was likely due to

hyperpolarization of the cell and closing of voltage-gated calcium channels. In chicken

auditory hair cells, L-type calcium channels are the predominant subtype, and they can

be blocked by dihydropyridines including nimodipine (126, 127). To directly test the

role of voltage-gated calcium channels on cell body F4 signal, nimodipine was added

during live-cell imaging. Addition of 10 µM nimodipine caused a decrease in cell body

F4 signal over time, with no effect on bundle F4 signal (Figure 4.7; for t=0 minutes,

bundle fluorescence = 230 ± 21 au and cell body fluorescence = 802 ± 39 au; for t=35

minutes, bundle fluorescence = 215 ± 26 au and cell body fluorescence = 665 ± 47 au; p

< 0.05 for cell body fluorescence between t=0 minutes and t=35 minutes). This provides

evidence that F4 signal in the hair bundle represents a separate calcium source from

that of F4 in the cell body.

The final test of the source of F4 bundle signal was to mechanically activate

transduction channels while simultaneously measuring F4 fluorescence in the bundle.

To stimulate the hair bundle using a fluid jet, a glass pipette with a 10-12 µm diameter

tip was bent at a 30° angle, mounted on a micromanipulator on the microscope stage,

and positioned underneath the objective (Figure 4.8a,b). The bend in the pipette was

essential to ensure that the tip was oriented parallel to the epithelium, to allow

stimulation of the bundles without disrupting the cell bodies and underlying epithelium.

(Figure 4.8c). Hair bundles in the middle of the mid-apical region were chosen, as these

bundles face the basal end of the epithelium and will be maximally stimulated by the

fluid jet (see also Figure 4.3a). Cells with modest F4 bundle fluorescence were selected,

because these are likely healthy cells with intact tip links (Figure 4.5). To normalize the

F4 signal and to account for movement of the hair bundle, the membrane-permeable

cell fill CellTracker Red (CT-Red) was loaded after F4-AM loading and wash steps (Figure

4.8d,e).

Continuous imaging of a single hair bundle ROI before, during, and after

stimulating the bundle with a fluid jet showed that normalized F4 fluorescence (ΔG/R)

increased during fluid jet stimulation, with a rapid onset and slower decay (Figure 4.8f).

The gradual return of F4 signal to baseline between stimulations reflects the activity of

the calcium pump PMCA2a, which pumps calcium out of the bundle, as well as mitochondria and ER sequestration of calcium and diffusion to the cell body. Fluid-jet stimulation caused a marked increase in calcium in 2 hair bundles of hair cells loaded with F4-AM, and 1 hair bundle of a hair cell loaded with a lower affinity indicator Fluo5ff-AM (data not shown). Increases in F4 were always timed with the fluid jet stimulation, and varied in intensity from 1.2 to 2.0 (normalized **Δ**G/R) for Fluo5ff-AM. A decrease in the spike maximum at stimulus onset was always observed with repeated stimulations (Figure 4.8f), and could represent saturation of the dye, breaking of tip links during fluid jet steps, or incomplete adaptation of the transduction channel. These results demonstrate that mechanically stimulating the hair bundle with a fluid jet increases hair bundle F4 signal, reflecting calcium entry into the bundle when transduction channels open.

Discussion

Here I present a novel method for labeling hair cells with the cell-permeable calcium indicator F4-AM. Several lines of evidence indicate that F4 fluorescence in the hair bundle is a measure of calcium entry through functional mechanotransduction channels. First, by correlating live-cell imaging and SEM, I showed that hair bundles with moderate F4 signal at rest have ordered stereocilia and tip links, whereas bundles with low F4 signal are damaged and those with very bright F4 represent dead or dying hair cells. Second, bundle F4 fluorescence significantly decreased when tip links were broken, due to inactivation of the transduction channel. Cell body fluorescence also decreased, likely due to hyperpolarization of the cell and subsequent closure of voltage-gated calcium channels. Third, blocking the transduction channel with tubocurare resulted in a similar decrease in hair bundle and cell body F4 signal, again reflecting the expected physiological changes. Fourth, the voltage-gated calcium channel blocker nimodipine selectively decreased cell body F4 signal without affecting bundle F4 signal. Finally, direct mechanical activation of the transduction channel by fluid jet stimulation resulted in increased F4 signal in the bundle that precisely followed the mechanical stimulation.

Combined, these data demonstrate that F4-AM loading of hair cells can be used as a tool to investigate intracellular calcium dynamics simultaneously in many hair cells in the epithelium, with the ability to distinguish cell body calcium from hair bundle calcium entering through the mechanotransduction channel. This technique

circumvents the technical expertise required for patch clamp recordings of hair cells, and provides an alternative way to assess intracellular calcium. Given that hair cells with very bright F4 can be seen extruding from the epithelium by SEM, this technique also could be used to quickly estimate the health of hair cells in the epithelium. For labs that do not routinely perform patch clamp experiments or examine tip links by SEM, this technique could be combined with FM1-43 labeling to identify hair cells that have intact tip links and active transduction channels (128).

One complication of loading hair cells with an AM calcium indicator is the partitioning of the dye into intracellular compartments. Indeed, in many cells, I saw a punctate pattern of F4 fluorescence under the cuticular plate, which likely represents labeling of the mitochondrial belt and dye uptake by endocytosis (8, 109). Endocytic uptake could potentially be reduced by decreasing the F4-AM loading concentration to 5 μM, although this might sacrifice the ability to detect F4 in the bundle, which was at lower fluorescence levels compared to the cell body. Another modification would be to decrease the extracellular calcium to 50-100 μM to further increase the open probability of the mechanotransduction channel at rest, thus allowing more calcium into the bundle (8, 56). This would also more closely mimic *in vivo* conditions of the endolymph that bathes the hair bundle, which contains 20-50 μM calcium.

Among the many cellular processes that involve intracellular calcium, F4-AM loading would be particularly useful for examining the role of calcium in tip link regeneration. Regeneration of broken tip links occurs over 3-12 hours in culture, and hair cell health must be maintained during this time. F4-AM loading and calcium

imaging is minimally invasive, and many organs examined in this study were still healthy at the end of the experiment. In preliminary experiments I found that continuous live-cell imaging over 3 hours on the microscope caused hair cell extrusion, which was likely due to phototoxicity or damage introduced from the electrophysiology harp that holds the tissue in place. In contrast, epithelium that were quickly imaged and then removed from the microscope and cultured for 3 hours had no obvious signs of hair cell extrusion or damage to the epithelium (data not shown). It is likely possible to perform calcium imaging, break the tip links and culture the epithelium to induce tip link regeneration, then re-load the cells with F4-AM to examine intracellular calcium. This technique could be used to investigate the time course over which calcium returns to the bundle and cell body during tip link regeneration, which would provide valuable information on the role of calcium in this process. One could potentially track the same cells through all phases (pre-EGTA, EGTA treated, and regenerating), and process the organ for SEM to determine the state of tip links on the same bundles investigated by live-cell imaging.

In conclusion, I present a minimally invasive technique for examining intracellular calcium in hair cells of the chicken cochlea. This protocol for loading hair cells can be used as an alternative to the more difficult and time-consuming method of calcium imaging coupled with electrophysiology. Moreover, the ability to simultaneously monitor all cells in the epithelium, and to find the same cells by SEM, potentially makes this technique an excellent tool for studying the role of calcium in tip link regeneration.

Experimental Procedures

Tissue and dye preparation: P0 *Gallus domesticus* chickens were dissected as described in chapter 3, including removal of the tectorial membrane with subtilisin protease. Low calcium saline was used at room temperature for all dissecting, loading, and imaging steps and contained the following (in mM): 87 NaCl, 0.5 KCl, 0.5 CaCl$_2$, 1.25 NaH$_2$PO$_4$, 2 ascorbate, 2 creatine, 6 Na-pyruvate, 75 sucrose, 25 D-glucose, 10 HEPES (pH 7.4, 310-320 mOsm). Fluo4-AM dye was prepared as described in Figure 4.2, using the following reagents: Fluo4-AM (Invitrogen, F14201), DMSO (Invitrogen, C6667), Pluronic F-127, 20% solution in DMSO (Invitrogen P3000MP). It was essential that all dye reagents were brought to room temperature before beginning, and all preparation and loading steps were carried out at room temperature in foil-wrapped tubes to protect the fluorescence of the dye. DMSO stocks could be stored frozen and used for 3 days. To allow for dye normalization in fluid jet experiments, cell-permeable CellTracker Red CMTPX (Invitrogen C34552) was added to the organs for 15 minutes following the Fluo4-AM loading.

Drugs. 50 mM stock solutions of (+)-tubocurarine chloride (Sigma) were stored at -20°C and diluted to 100 µM in extracellular solution a few hours before use. 500 mM stock solutions of nimodipine (Calbiochem) in DMSO were stored at -20°C and diluted to 10 µM in extracellular solution immediately prior to use. Organs were incubated in calcium chelators and returned to normal calcium solution prior to F4-AM loading, and tubocurare was added prior to F4-AM loading and was included in all washing and

imaging solutions. For nimodipine treatment during live-cell imaging, 25 mL of

nimodipine solution was exchanged into the microscope chamber (5 mL dish) over 10

minutes.

Image acquisition and analysis. For measuring control, EGTA, and tubocurare F4

calcium signals, organs were imaged on an inverted Zeiss LSM710 confocal microscope

(40xW/1.1 NA objective), bundles facing down. For the nimodipine time-lapse and fluid

jet experiments, an upright Olympus FV-1000 confocal microscope was used (60xW/1.0

NA or 40xW/0.8 NA dipping objectives). Dental floss attached to an electrophysiology

harp was used to pin the organ down at the lagena and basal ends. Images were

acquired using 1.0 - 2.0 μm z-steps through the hair bundles and cell bodies. Z-stacks

were processed with Imaris 3D software, where individual 2 μm XZ- or YZ-reslice images

were taken through the field of hair cells. Fiji software was used to select and quantify

hair bundle and cell body ROIs. In some experiments, organs were immediately placed

into SEM fixative following imaging, fixed overnight at 4°C, and processed for SEM.

Fluid jet stimulation. Borosilicate glass pipettes with long, thin shafts were

pulled and broken to give 10-12 μm diameter tips. An open flame was used to bend the

pipette along the shaft to a 30° angle, which allowed the pipette to be lowered close

enough to the tissue without bumping the sidewall at the basal end of the cochlea.

Pipettes were filled with dissection solution. A Pico-Spritzer III was attached to the

pipette, which was subsequently mounted on a micromanipulator on the microscope

stage and positioned underneath the objective. Olympus FV-1000 software was used to

deliver 10 second, 0.2 psi pulses; an in-line manometer was used to accurately measure

pressure in mm Hg. By isolating a single hair bundle region of interest (ROI) of 12 x 20

pixels, two-color images were acquired at 70 milliseconds per frame. Data was analyzed

using IgorPro software, and **Δ**G/R was calculated by normalizing F4 to CT-Red, then

normalizing to the average response from the first 40 seconds of imaging.
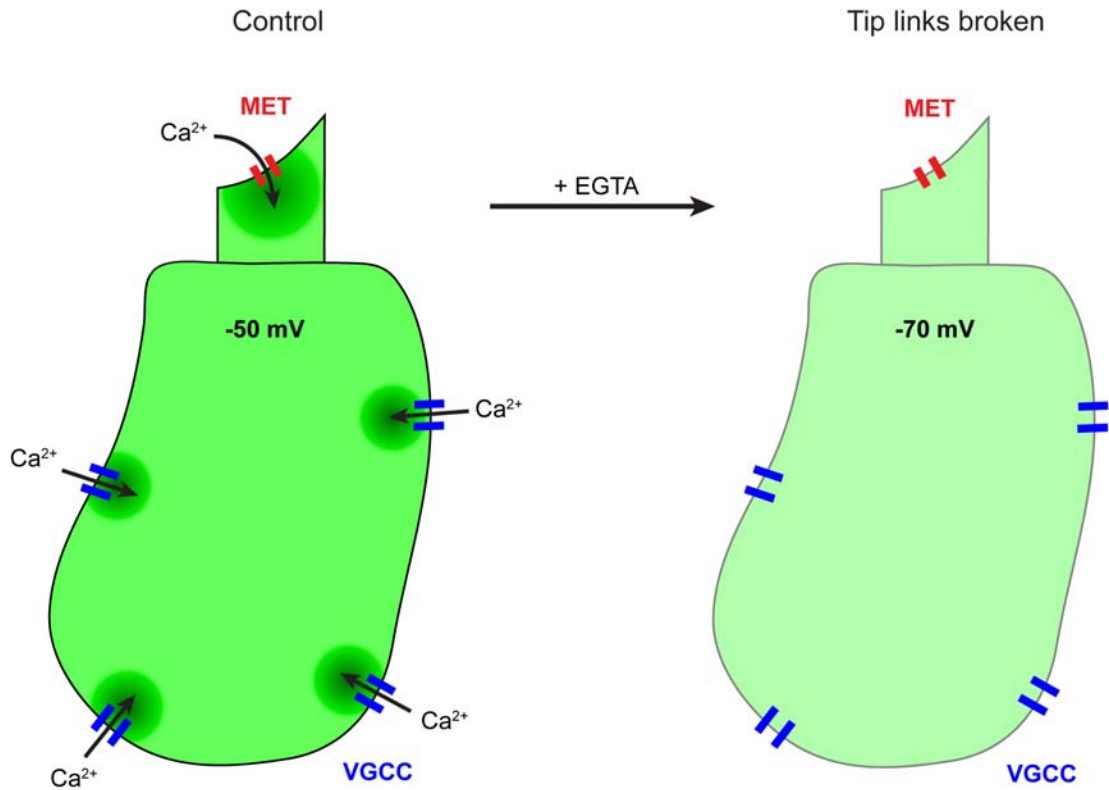
Figure 4.1 – Expected physiological changes in the hair cell when tip links are broken.

In control conditions, calcium enters the cell through mechanoelectrical transduction (MET) channels that are open at rest. Inward transduction current depolarizes the cell to open voltage gated calcium channels (VGCC). After breaking tip links with EGTA, the transduction channel closes, which leads to hyperpolarization of the cell and closure of voltage-gated calcium channels.
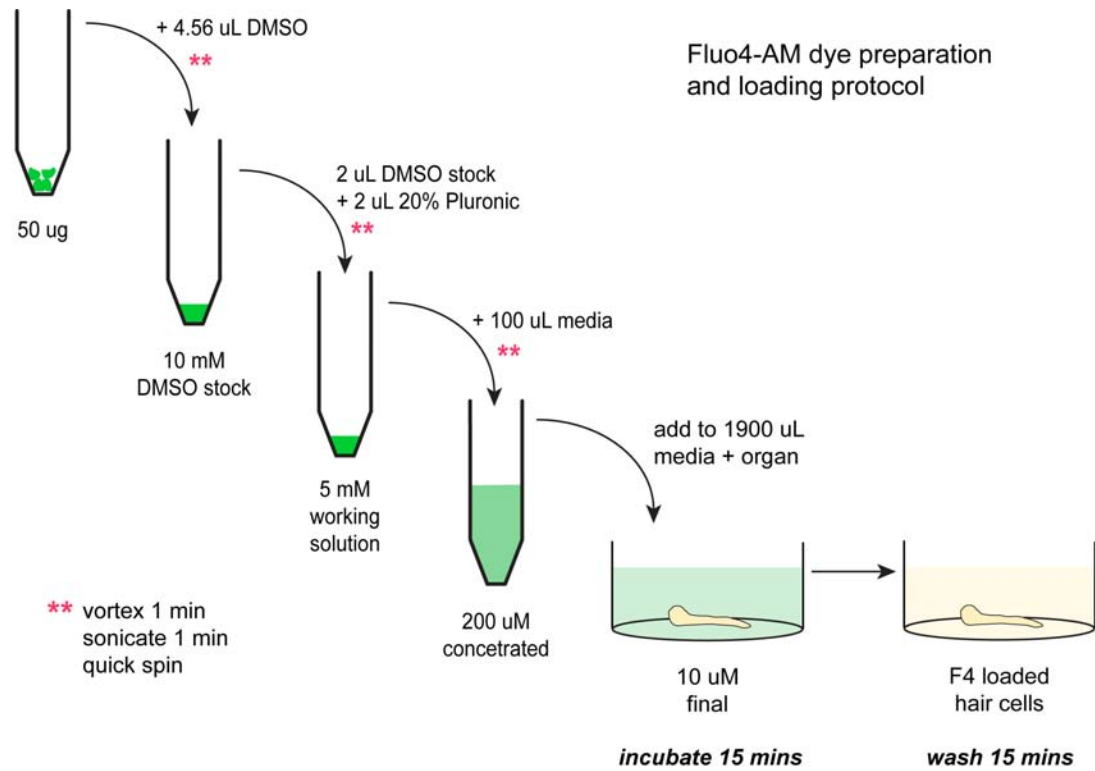
Figure 4.2 – Fluo4-AM dye preparation and loading protocol.

Between each of the steps highlighted with ** dye solution is rigorously vortexed for 1 minute, bath sonicated for 1 minute, and spun down.
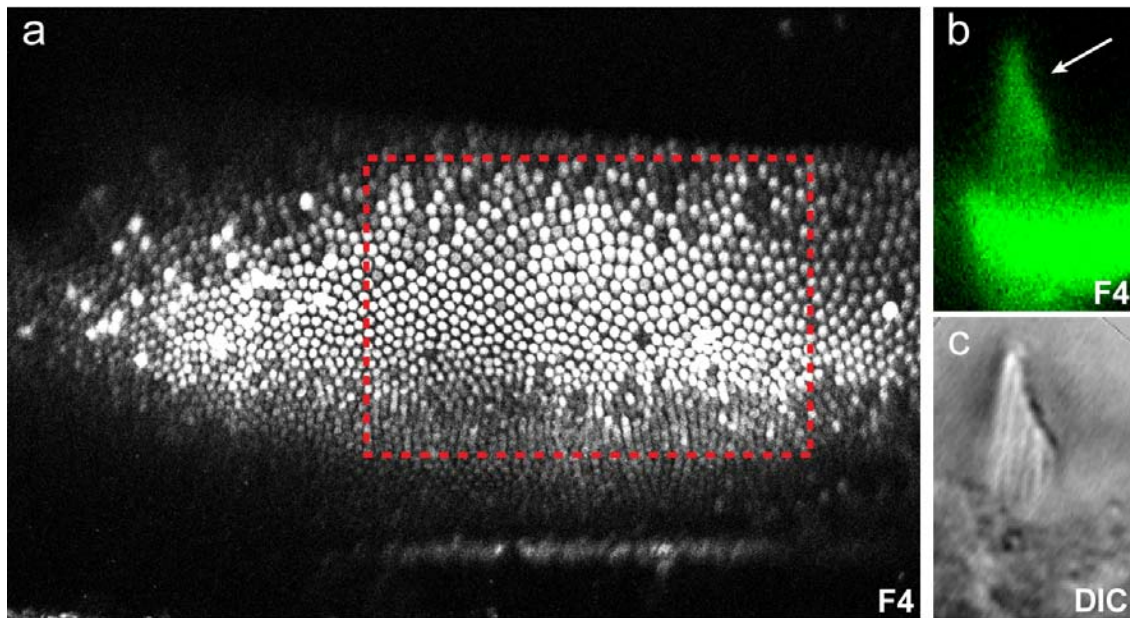
Figure 4.3 – Fluo4 imaging of cochlear hair cells.

Confocal imaging of cochlear hair cells loaded with Fluo-4 AM calcium indicator. (a) 10x view of the cochlear epithelium shows that hair cells selectively load with F4 dye. (b-c) Side view of a single hair bundle loaded with F4 (b), with corresponding DIC image (c). Arrow in b indicates a tip blush of calcium entering through mechanotransduction channels. Red box in (a) indicates the mid-apical region of the epithelium, which was used for all experiments.

Figure 4.4 – Breaking the tip links decreases bundle and cell body calcium.

(a-d) Control hair cells have F4 signal in the bundle (b) and cell body (d). (e-h) Hair cells pre-treated with 5 mM EGTA to break tip links have decreased F4 signal in the bundle (f) and cell body (h). (i, j) To quantify F4 fluorescence, individual bundle and cell body ROIs were selected using Imaris and Fiji software, and integrated density of F4 channel was calculated (Figure S1). (a, c, e, g) Corresponding DIC images. (AU = arbitrary units; control bundles n = 72, EGTA bundles n = 65, control cell bodies n = 79, EGTA cell bodies n = 76; **** p < 0.0001).
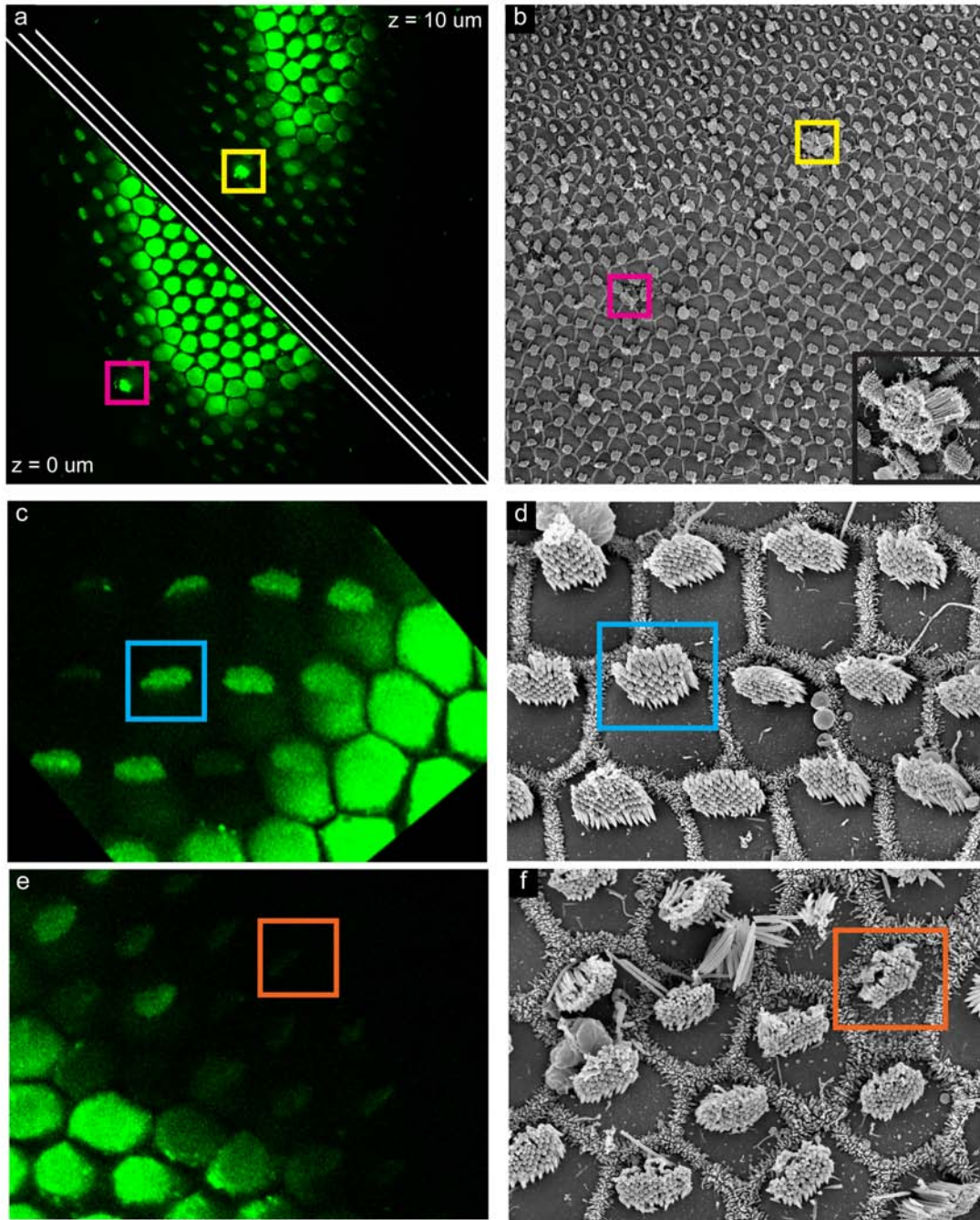
Figure 4.5 – Live-cell calcium imaging correlates with SEM ultrastructure.

Fluo4-imaged organs (a,c,e) were fixed and processed for SEM (b,d,f). (a, b) Cells with very bright F4 (yellow and pink boxes) could be seen extruding from the epithelium in SEM. (c) Bundles with average F4 signal have ordered stereocilia and tip links (d), and bundles with very low F4 signal (e) have damaged bundles (f). (a) Shows the same epithelium at two separate z-planes; for all panels, colored boxes highlight corresponding cells in live-cell and SEM images.
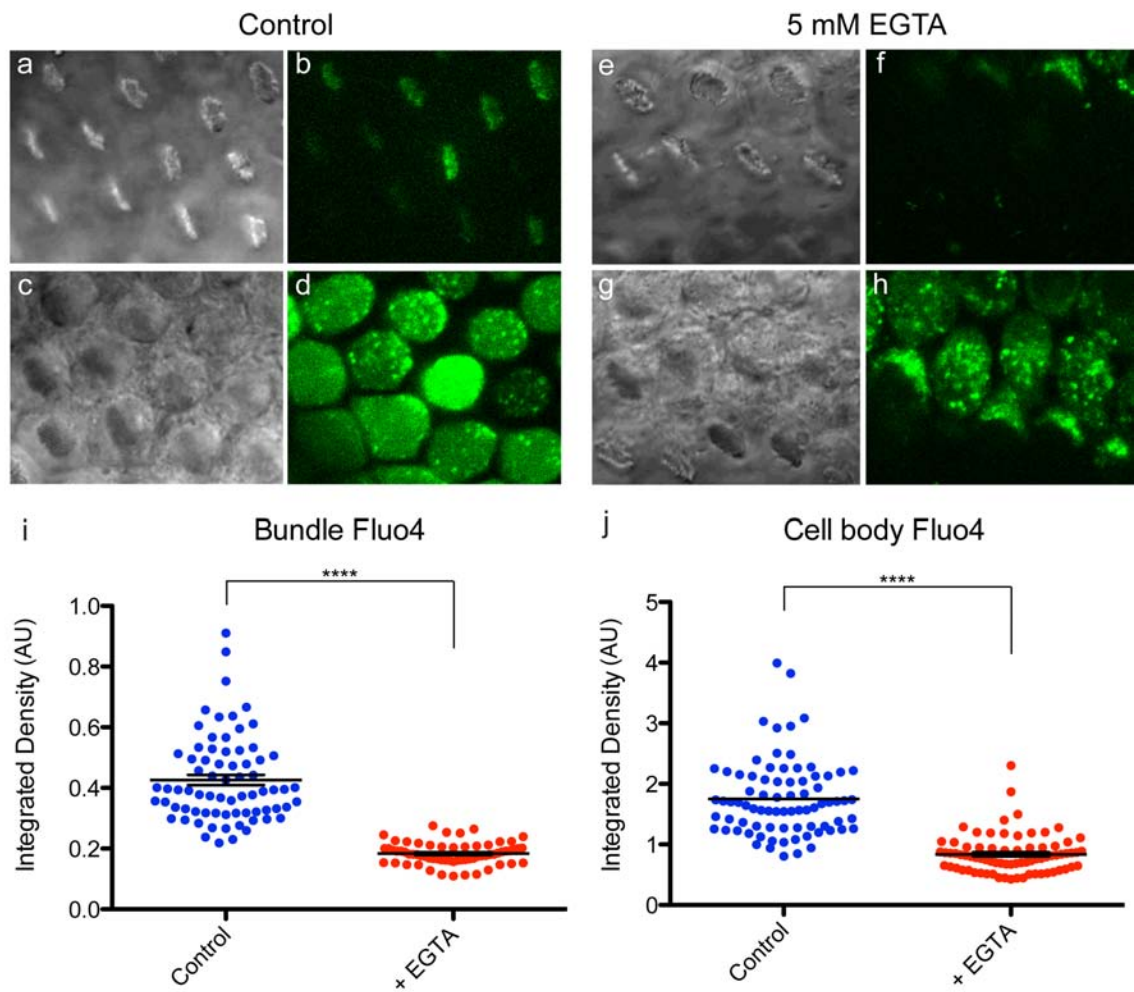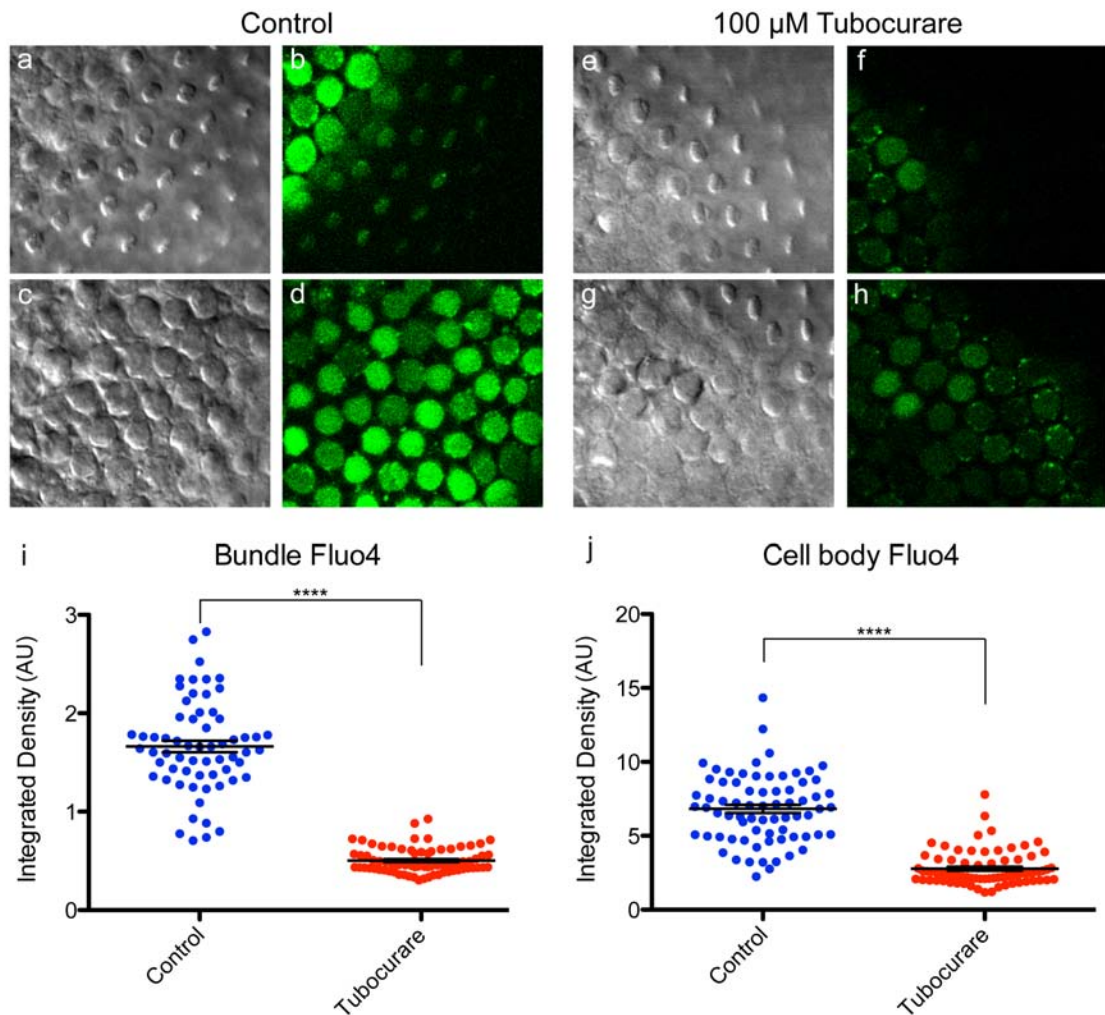
Figure 4.6 – Blocking the transduction channel decreases bundle and cell body calcium.

(a-d) Control hair cells have F4 signal in the bundle (b) and cell body (d). (e-h) Hair cells incubated with 100 μM tubocurare to block the transduction channel have decreased F4 signal in the bundle (f) and cell body (h). (i-j) F4 fluorescence was quantified as in Figures 4.1 and S1. (a, c, e, g) Corresponding DIC images. (AU = arbitrary units; control bundles n = 63, tubocurare bundles n = 73, control cell bodies n = 72, tubocurare cell bodies n = 77; **** $p < 0.0001$).
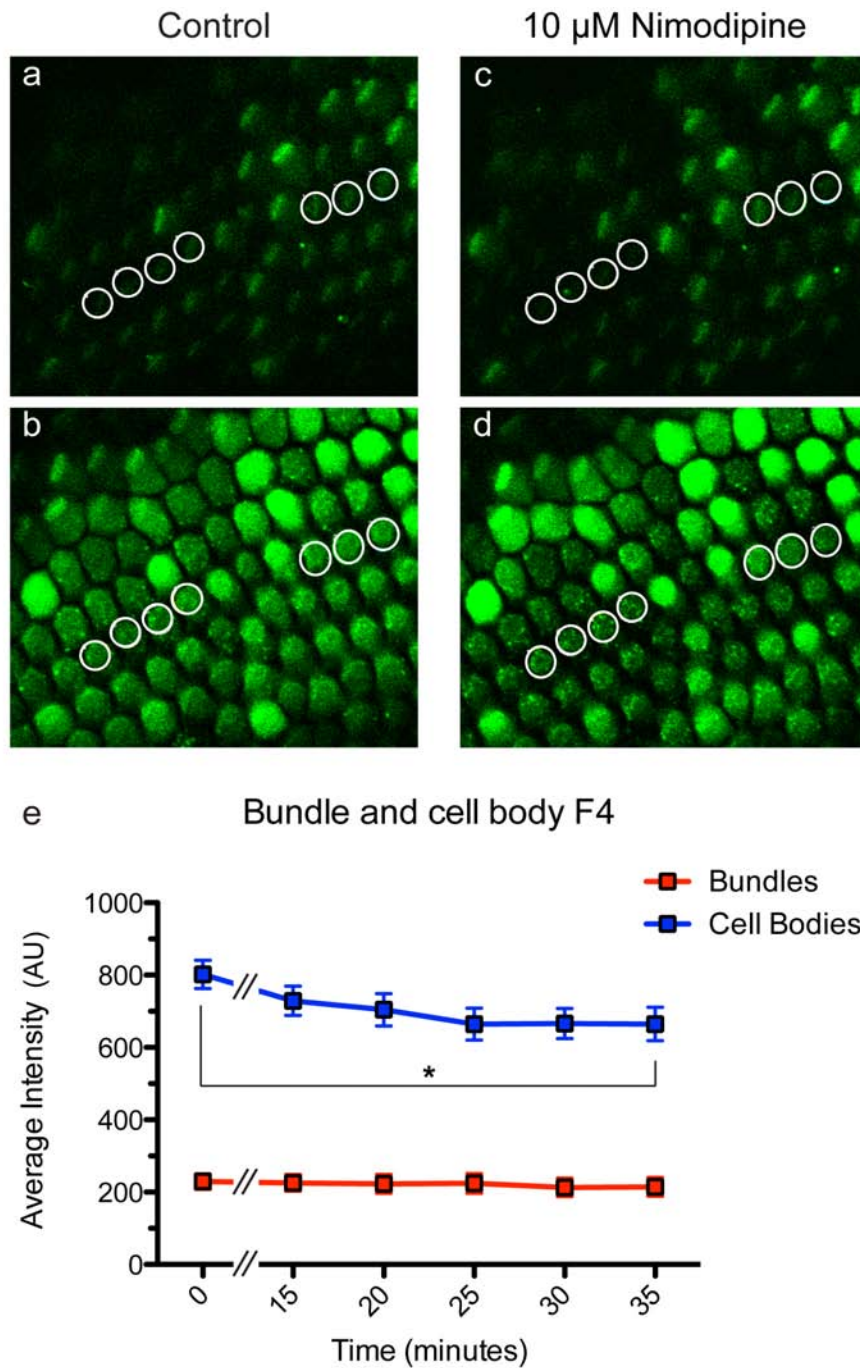
Figure 4.7 – Blocking voltage gated calcium channels decreases cell body calcium.

Bundles (a) and cell bodies (b) before application of nimodipine, and after 35 minutes of 10 µM nimodipine (c, d). Average intensity of individual ROIs (white circles) was tracked over time before (time = 0) and after bath application of nimodipine. (e) Selective decrease in F4 fluorescence for cell body ROIs, with no significant change in bundle ROIs (AU = arbitrary units; bundles n = 7, cell bodies n = 7; * $p < 0.05$ for cell bodies at t=0 compared to t=35)
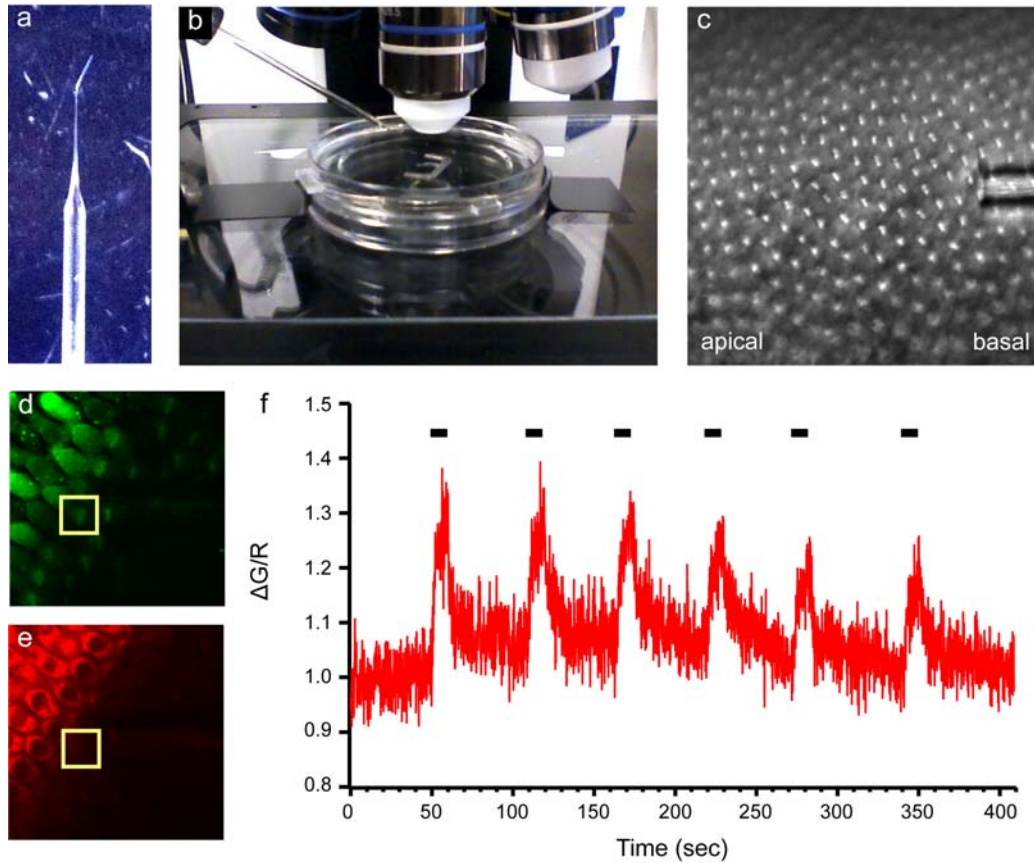
Figure 4.8 – Fluid-jet stimulation of the hair bundle increases F4 calcium signal.

(a) Pipette with a 30° bend, attached to a Pico Spritzer III, was positioned under the objective parallel to the bottom of the dish (b). (c) The pipette tip was brought close to the hair bundles, and the dish was rotated to orient the bundles for optimal response to fluid jet displacement. (e) CT-Red was used as a cell fill to normalize the F4 fluorescence signal (d). A single hair bundle ROI (yellow box) was continually monitored during the fluid jet pulses. (f) Fluid jet deflection of the hair bundle with a 0.2 psi pulse for 10 seconds causes an increase in F4 calcium signal, which was timed with the stimulus (black bars).
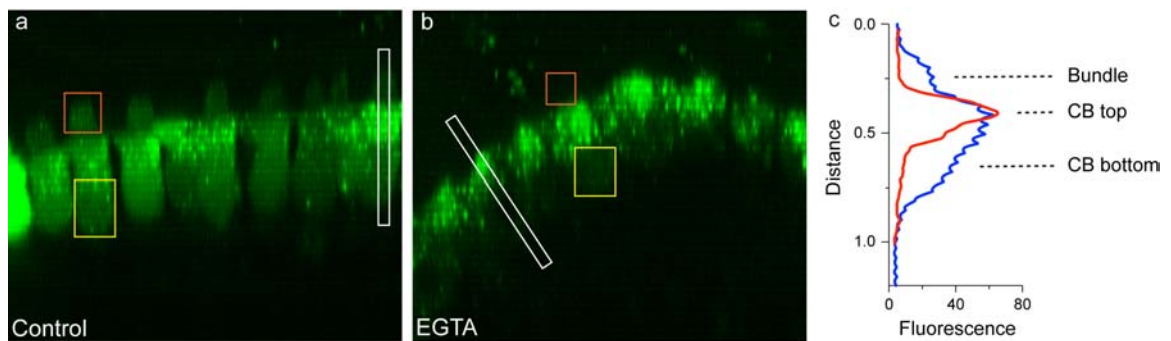
Figure S-4.1 – Quantification of Fluo4 fluorescence.

YZ-reslice images of control (a) and EGTA-treated (b) hair cells. To quantify fluorescence as reported in Figure 4.4 and 4.6, hair bundle ROIs (orange square) or cell body ROIs in the bottom half of the cell (yellow rectangle) were selected and integrated density was calculated (mean gray value X area). (c) Representative line scan profiles for the ROIs indicated by white rectangles in (a) and (b). Control hair cell (blue trace) has fluorescence in the bundle, top half of the cell body (CB top) and bottom half of the cell body (CB bottom). EGTA-treated hair cell (red trace) has fluorescence concentrated in the top half of the cell, where the dye is trapped in intracellular compartments, but lacks hair bundle and cytoplasmic CB bottom F4 signal.

Chapter 5 – Conclusions and future directions

General summary

The work presented in this thesis provides new information on the function of chicken inner ear hair cells at the molecular level, from energy metabolism to tip link damage. Chapter 2 describes differences in metabolic pathways between the auditory and vestibular organs. By probing the molecular composition of each epithelium at the protein and mRNA level, we report that the utricle predominantly relies on the oxidative phosphorylation pathway whereas the cochlea prefers glycolytic energy production. In Chapter 3, I characterized a specific type of damage to the hair bundle – breaking the tip link. Using immunohistochemistry, I show that tip link breakage caused redistribution and intracellular co-localization of tip link proteins CDH23 and PCDH15. Hair cells can regenerate broken tip links over a few hours in culture, a process that has been shown to depend on changes in intracellular calcium. Chapter 4 describes a new method of studying intracellular calcium by loading hair cells with F4-AM and shows that hair bundle F4 signal is dependent on calcium entry through functional transduction channels. This technique is potentially suitable for studying the role of calcium in tip link regeneration.

Chapter 2 conclusions and future directions

In chapter 2 we report striking differences in energy metabolism pathways between auditory and vestibular organs. In the cochlea, every step in the glycolytic pathway is upregulated relative to the utricle, most at both the transcript and protein

level, and glycolytic rate is 4 times higher than in the utricle. We believe this preference

for glycolysis could be regulated through the transcription factor hypoxia-inducible

factor α (HIF1-A; Figure 5.1). This protein is stabilized by low oxygen tension, which is

consistent with the lack of blood vessel infiltration in the cochlea. Transcripts for a

number of anti-angiogenesis factors are upregulated in the cochlea, suggesting that this

organ actively inhibits vascularization, thus developing a reliance on glycolytic energy

production. This organ-specific inhibition of angiogenesis is likely a mechanism to

protect the cochlea from heart-beat induced mechanical stimulations, which could

activate hair cells and dampen the sensitivity of the system (Figure 5.1).

Another potential advantage of reduced vascularization and decreased reliance

on oxidative phosphorylation in the cochlea is protection from oxygen deprivation. By

monitoring ATP levels and enzymes involved in energy production under ischemic

conditions, Thalmann and colleagues showed that the cochlea is more resistant to

oxygen depletion than the vestibular organs and the stria (9, 129). The stria is the most

sensitive to ischemia, showing a 70% drop in ATP levels in the first 30 seconds of

ischemia (9, 129, 130). This organ is highly vascularized, implying a heavy reliance on

oxygen from the blood (10, 131). The stria, called the tegmentum vasculosum in the

chicken, requires significant energy to fuel ion pumps that maintain the ionic

environment of the endolymph and create the endocochlear potential. Indeed, many

deafness mutations link to ion transporter proteins in the stria (132, 133). It would be

interesting to characterize the stria using our quantitative MS methods paired with

microarrays to more thoroughly investigate energy metabolism pathways in this organ.

During our comparative MS analysis, we noticed a number of interesting

differences in hair-cell specific molecules, including hair-bundle myosin motors.

Myosin-1c (MYO1C) was detected only in the utricle, whereas a separate isoform,

myosin-1h (MYO1H), was detected in the cochlea. Myosin-III isoforms also differed

between organs – myosin-IIIa (MYO3A) was detected in the cochlea, and myosin-IIIb

(MYO3B) was detected in the utricle. We verified these expression differences using

immunohistochemistry and confirmed that the myosin motors were detected in the hair

bundle (Figure 5.2). MYO1C is the presumed hair-cell adaptation motor and has been

linked to hearing loss in humans, and MYO3A corresponds to deafness mutation

DFNB30 and has been shown to regulate actin dynamics in the hair bundle (135, 136).

The other newly-identified myosins, MYO1H and MYO3B, have not been characterized

in hair cells, but given the tissue-specific isoform differences discovered here, these

proteins could potentially play a role in adaptation and actin dynamics, respectively.

Future experiments should investigate the roles of MYO1H in cochlear hair bundles and

MYO3B in vestibular hair bundles. These data also emphasize that our techniques and

analyses are sensitive enough to measure changes in low abundance, hair-bundle

specific molecules.

Chapter 3 conclusions and future directions

The analysis of tip links in chapter 3 deepens our understanding of the

mechanism of tip link breakage and provides new information on controversial antibody

staining for CDH23 and PCDH15 after breaking tip links. Immunohistochemistry

revealed that CDH23 bundle staining decreases after BAPTA treatment, which is in

agreement with published results in chicken and frog. Furthermore, CDH23 and

PCDH15 co-localized in the cell body under the cuticular plate, a finding that has not yet

been reported in the literature. As discussed in chapter 3, future experiments using live-

cell antibody labeling and experiments to test the role of endocytosis would further our

understanding of the fate of these proteins following tip link breakage.

As with all immunohistochemistry data, we are limited by antibody efficiency.

Hair cells are particularly difficult for antibody labeling, because many of the bundle

proteins are unique and do not have verified, commercially available antibodies. Ideally,

GFP-tagged versions of CDH23 and PCDH15 could be used to monitor these proteins

after tip link breakage. Both proteins are over 150 kDa, and such large constructs are

difficult to transfect into cells. Transfection itself is challenging in hair cells, with the

most reliable method (gene gun transfection) yielding only a few positive cells per

organ. Alas we must rely on antibody labeling. Verifying each antibody using multiple

assays and verifying a finding with multiple antibodies, as I have done here for CDH23,

becomes essential.

An intriguing question is whether broken tip links dissociate from the

transduction complex. If the interaction remains intact, then the transduction channel

may also be internalized. Because we do not know the identity of the channel, or the

nature of the tip link/channel interaction, it is not yet possible to determine whether the

channel itself changes location after BAPTA treatment. If broken tip links detach from

the channel, it is possible that the channel or channel-interacting proteins serve as a

molecular place-holder for the tip link to reconnect to during regeneration.

Chapter 4 conclusions and future directions

Chapter 4 of this thesis presents a method for loading hair cells with F4-AM to study intracellular calcium dynamics. These experiments convincingly show that the hair bundle F4 signal can be used to monitor calcium entering the bundle through functional transduction channels. Most of the hair cells in the epithelium loaded with F4-AM, making this a powerful technique for studying intracellular calcium in many cells at the same time. Perhaps even more powerful is the ability to link F4 bundle signal with ultrastructural SEM analysis of the stereocilia. Potentially one could directly correlate calcium in individual stereocilia with the presence or absence of tip links in that stereocilia. Imaging F4 in a single stereocilia would likely require super-resolution techniques such as structured illumination microscopy (SIM), which in the chicken cochlea increases resolution of the phalloidin-stained bundle by two-fold (data not shown).

The decrease in intracellular calcium that accompanies tip link breakage is important for regeneration of the tip link (42). Chapter 3 showed that tip link proteins re-localize to the cell body upon tip link breakage, where they could act in coordination with decreased calcium to trigger tip link regeneration. One way to induce the physiological changes in the hair cell without breaking the original tip link is to block the transduction channel. Indeed, the open channel blocker tubocurare elicited changes in bundle and cell body calcium similar to what was observed when tip links were broken (Figure 4.6). To test if the physiological changes associated with turning off the transduction current are sufficient to trigger tip link regeneration, cochlear epithelia

were cultured in the presence of tubocurare. In this experiment, the original tip links

remain intact, eliminating the possibility of broken tip link components signaling to the

cell body.

Hair cells that are undergoing tip link regeneration manifest unique, angled links

at stereocilia tips, which increase in the bundle during early time points of regeneration

(42). I used the presence of these angled links as an assay to determine whether

blocking the transduction channel could mimic regeneration. Cochlea that were

cultured for 3.5 hours in tubocurare had significantly more angled links compared to

control, approaching the number of angled links seen in regenerating cultures (Figure

5.3; Table 5.1). As expected, there was no difference in the number of tip links between

control and tubocurare cultures. This finding shows that extended block of the

transduction channel is sufficient to induce the formation of angled links. This implies

that cellular changes associated with transduction channel closure, rather than

internalization of CDH23 and PCDH15, triggers tip link regeneration.

These data are based on the presence of angled links as an assay for hair cells

undergoing tip link regeneration. However, by itself, this assay is not ideal for

demonstrating whether a particular cell is underdoing regeneration, because many cells

had no angled links in the bundle at 3.5 hours of regeneration (Figure 5.2d). Angled

links were more prominent in short hair cells in the mid and mid-basal regions of the

epithelium. Although there are hair cells at other locations of the epithelium that are

likely undergoing tip link regeneration, unfortunately there is no other way to measure

regeneration by SEM aside from the presence of angled links. To further study the

mechanism of tip link regeneration, including the role of calcium, future experiments should aim at developing other assays for hair cells that are undergoing tip link regeneration.

The results from these experiments open the possibility of pharmacologically teasing apart how calcium in different intracellular domains contributes to tip link regeneration. An interesting experiment would be to load hair cells with BAPTA-AM to chelate intracellular calcium without changing the membrane voltage, and determine if this treatment induces tip link regeneration. Another interesting experiment would be to culture organs in the presence of nimodipine to selectively block cell body calcium. With all culturing experiments that rely on pharmacology, the health of the culture must be considered. In the experiments presented here, tubocurare was chosen because it has been shown to successfully block the transduction channel in culture without compromising organ health (134).

Concluding remarks

New tools that emerge from this thesis include quantitative MS paired with gene microarrays, which enhances our ability to deeply investigate the molecular composition of whole organs. The discovery that entire groups of functionally related molecules differ between inner ear organs and cause a dramatic biological switch in energy metabolism may speak to the evolutionary reasons for differences in vascularization. This discovery may also inform how we dissect and culture these epithelia in the future, and could spark new hypotheses regarding ischemia and reactive oxygen species in the cochlea. The characterization of two new tip link antibodies for detecting CDH23 opens

the door to further analysis of this protein in mature, cochlear chicken hair bundles. By

describing the intracellular co-localization of CDH23 and PCDH15 after tip link breakage,

we are one step closer to understanding the molecular mechanisms of tip link breakage

and regeneration. Finally, the new method of calcium imaging by loading cochlear hair

cells with F4-AM opens the door to studying intracellular calcium in the cells native

environment, potentially at the level of individual stereocilia. Thus, this thesis provides

practical methods for probing specific molecular questions in the hair cell, from

individual stereocilia to the entire inner ear landscape.
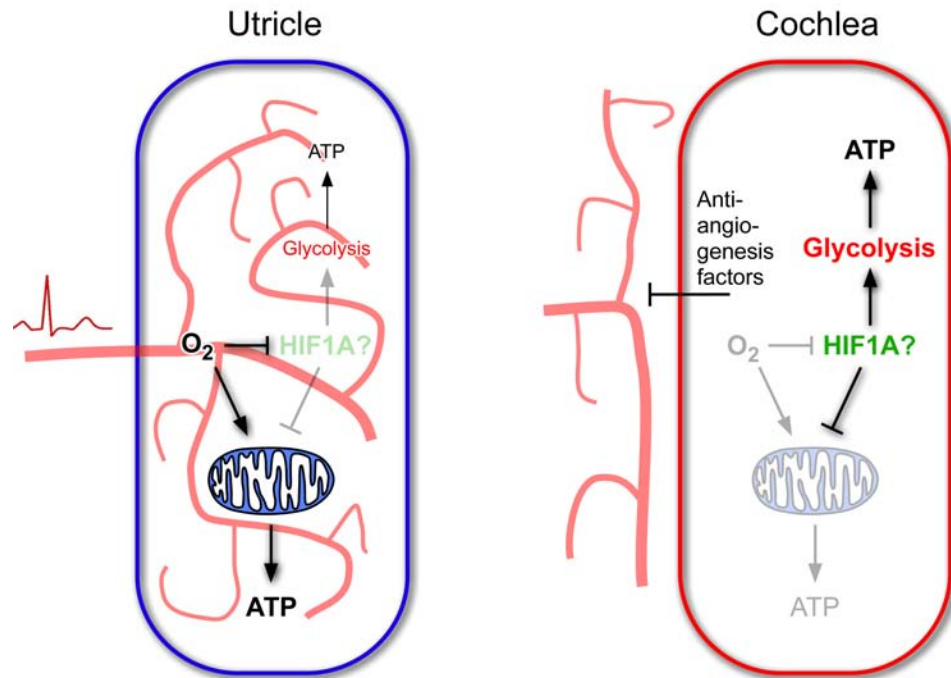
Figure 5.1 – Summary of energy metabolism in the utricle and cochlea.

Proposed mechanism for enhancement of glycolysis and suppression of oxidative phosphorylation in cochlea. In the utricle (left), a ready supply of O_2 presumably degrades hypoxia-inducible factor α (HIF1A), a protein associated with oxygen-independent energy production (i.e., glycolysis), maintaining normal oxygen-involving energy-producing reactions (i.e., oxidative phosphorylation). By contrast, in the cochlea (right), a bevy of antiangiogenesis factors preventing blood-vessel infiltration are expressed. In response, O_2 levels diminish, and HIF1A is presumably stabilized. In turn, HIF1A increases levels of glycolytic enzymes, thereby increasing glycolysis rates. HIF1A also degrades mitochondria (responsible for oxygen-dependent energy production). Because sound stimuli activate hair cells through vibration of the underlying ECM, the absence of blood vessels in the cochlea prevents disruption of cochlear sensitivity by the heartbeat.
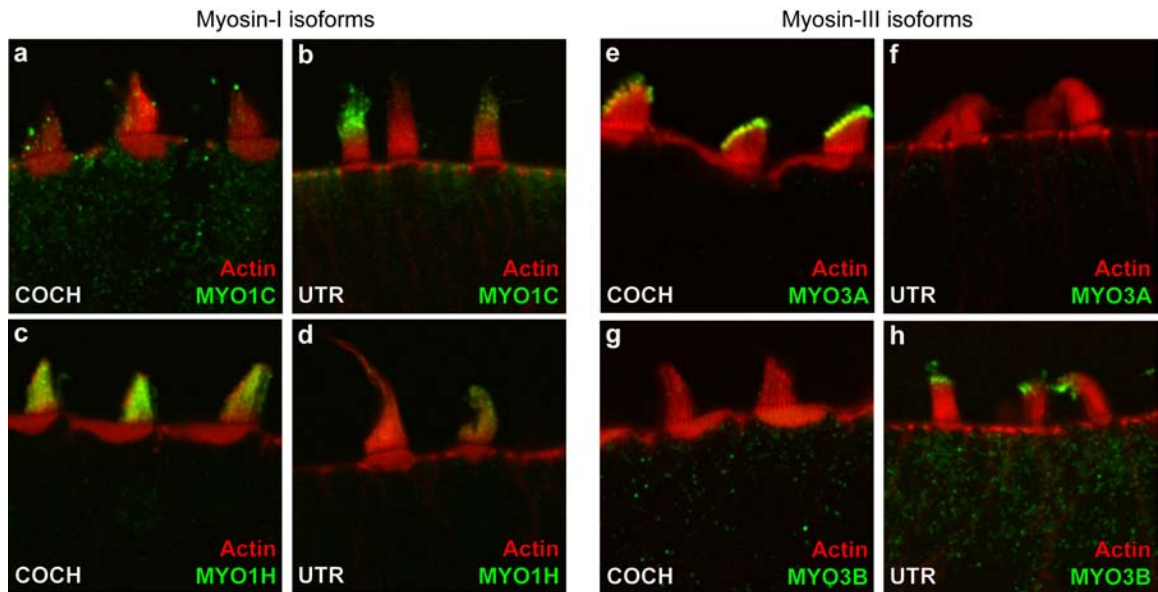
Figure 5.2 – Differential expression of myosin motors in cochlea and utricle.

Immunohistochemistry for myosin-I (a-d) and myosin-III (e-h) isoforms reflects MS data and shows that the proteins localize to the hair bundle. (a) MYO1C antibody shows minimal staining in the cochlea, and stains stereocilia tips in the utricle (b). (c) MYO1H antibody shows strong staining throughout the bundle in cochlea, and weak staining of some bundles in the utricle (d). (e) MYO3A antibody specifically localizes to stereocilia tips in the cochlea, and shows not staining in the utricle (f). (g) MYO3B antibody shows no hair bundle staining in the cochlea, and stains stereocilia tips in the utricle.
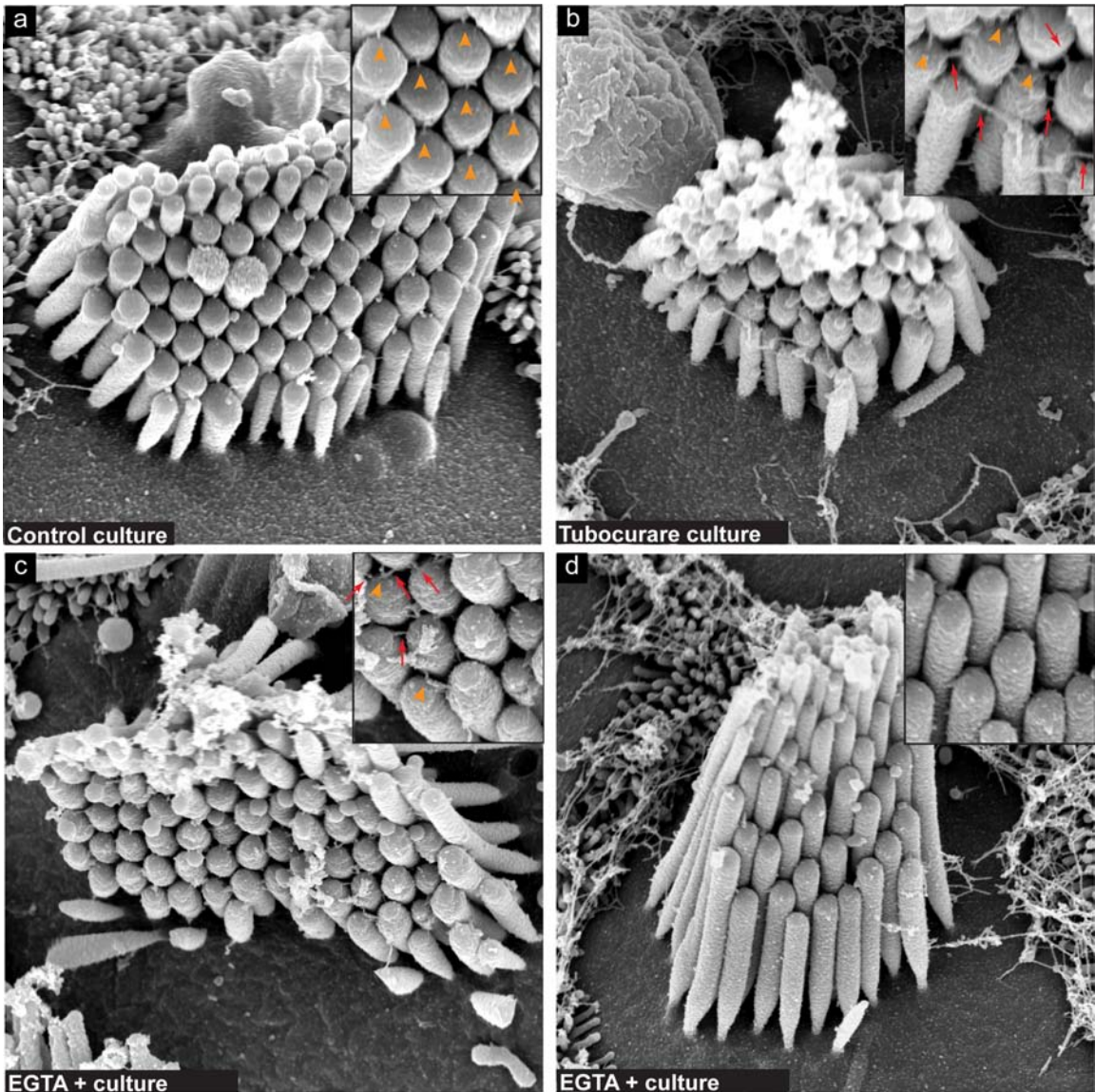
Figure 5.3 – Prolonged transduction channel block induces the formation of angled links.

(a) Hair cells in control cultures have many tip links at stereocilia tips (orange arrowheads). (b) Hair cells that were cultured in the presence of 100 μM tubocurare to block the transduction channel had both tip links and angled links (red arrows). (c) Hair cells that were treated with 5 mM EGTA to break the tip link, then cultured in normal calcium to induce tip link regeneration sometimes had angled links and tip links in the bundle. Shown here is a hair cell from the mid-basal region. (d) Hair cells in the apical region of tip-link regenerating epithelia often had very few tip links or angled links.

Culture condition	% Tip links	Angled links/tip links
Control	85.9 ± 1.6	0.14 ± 0.03
100 µM tubocurare	81.7 ± 5.6	0.41 ± 0.08
5 mM EGTA + culture in normal calcium	18.8 ± 5.9	0.87 ± 0.29

Table 5.1 – Tip links and angled links in culture.

Supplemental Methods

Immunohistochemistry. Organs were dissected, fixed, and processed for immunohistochemistry as described in chapter 3. For vibratome sectioning, organs were embedded in 4% UltraPure LMP agarose (Invitrogen) at 4°C for 30 minutes, then sectioned into 50 μm sections on a vibratome. Rabbit anti-rat MYO1C antibody was made against the C-terminal 30 kDa rat MYO1C tail domain and has been previously characterized by our lab (Dumont 2002). Rabbit anti-chicken MYO1H antibody was made against the 15 kDa tail region of chicken MYO1H. Rabbit anti-mouse MYO3B antibody was made against amino acids 12-35 of chicken MYO3B. Affinity purification of MYO1H and MYO3B antibodies was performed as described in chapter 3 by Barb Rainish, a technician in the lab. Rabbit anti-xenopus MYO3A/QHF antibody was provided by Dr. Beth Burnside (University of California, Berkeley) and is against the C-terminal 22 amino acids of *Xenopus laevis* MYO3A. Antibodies were used at the following concentrations: MYO1C 1:150, MYO1H 1:200, MYO3A 1:500, MYO3B 1:250. Specificity of all antibodies was confirmed by western blot of inner ear tissue.

Cochlear cultures. Cochlea were dissected as described in chapter 3, except that the tectorial membrane was detached from the side wall with an eyelash, rather than treated with subtilisin and completely removed. Removal of the tectorial membrane prior to culturing caused the hair bundles to flop over, causing difficulties with tip link imaging and quantitation ((42), data not show). To break tip links, 5 mM EGTA was

added to the cochlea for 5 minutes, with gentle agitation, followed by wash steps in

normal calcium media. Organs were cultured for 3.5 hours at 37°C in HBSS

supplemented with 5% FBS and 10 mM HEPES; tubocurare cultures also contained 100

µM (+)-tubocurarine chloride (Sigma). After culturing, organs were incubated in 50

µg/mL subtilisin for 15 minutes, the tectorial membrane was removed, and organs were

fixed and processed for SEM.

References

1. Gillespie PG, Muller U (2009) Mechanotransduction by hair cells: models, molecules, and mechanisms. *Cell* 139:33–44.

2. Fettiplace R, Hackney CM (2006) The sensory and motor roles of auditory hair cells. *Nat Rev Neurosci* 7:19–29.

3. Joliot M, Ribary U, Llinas R (1994) Human oscillatory brain activity near 40 Hz coexists with cognitive temporal binding. *Proc Natl Acad Sci U S A* 91:11748–11751.

4. Kozlov AS, Baumgart J, Risler T, Versteegh CP, Hudspeth AJ (2011) Forces between clustered stereocilia minimize friction in the ear on a subnanometre scale. *Nature* 474:376–379.

5. Eatock RA, Fay RR (2010) *Vertebrate Hair Cells (Springer Handbook of Auditory Research)* (Springer,

6. Yamoah EN, Lumpkin EA, Dumont RA, Smith PJ, Hudspeth AJ, Gillespie PG (1998) Plasma membrane Ca^{2+}-ATPase extrudes Ca^{2+} from hair cell stereocilia. *J Neurosci* 18:610–624.

7. Shin JB, Streijger F, Beynon A, Peters T, Gadzala L, McMillen D, Bystrom C, Van der Zee CE, Wallimann T, Gillespie PG (2007) Hair bundles are specialized for ATP delivery via creatine kinase. *Neuron* 53:371–386.

8. Beurg M, Nam JH, Chen Q, Fettiplace R (2010) Calcium balance and mechanotransduction in rat cochlear hair cells. *J Neurophysiol* 104:18–34.

9.   Thalmann R (1971) Metabolic Features of auditory and vestibular systems. *Laryngoscope* 81:1245–1260.

10.   Schmidt RS (1964) Blood supply of the pigeon inner ear. *J Comp Neurol* 123:187–203.

11.   Spinelli KJ, Gillespie PG (2009) Bottoms up: transduction channels at tip link bases. *Nat Neurosci* 12:529–530.

12.   Tsuprun V, Goodyear RJ, Richardson GP (2004) The structure of tip links and kinocilial links in avian sensory hair bundles. *Biophys J* 87:4106–4112.

13.   Kachar B, Parakkal M, Kurc M, Zhao Y, Gillespie PG (2000) High-resolution structure of hair-cell tip links. *Proc Natl Acad Sci USA* 97:13336–13341.

14.   Assad JA, Shepherd GMG, Corey DP (1991) Tip-link integrity and mechanical transduction in vertebrate hair cells. *Neuron* 7:985–994.

15.   Duncan RK, Dyce OH, Saunders JC (1998) Low calcium abolishes tip links and alters relative stereocilia motion in chick cochlear hair cells. *Hear Res* 124:69–77.

16.   Furness DN, Mahendrasingam S, Ohashi M, Fettiplace R, Hackney CM (2008) The dimensions and composition of stereociliary rootlets in mammalian cochlear hair cells: comparison between high- and low-frequency cells and evidence for a connection to the lateral membrane. *J Neurosci* 28:6342–6353.

17.   Marquis RE, Hudspeth AJ (1997) Effects of extracellular Ca2+ concentration on hair-bundle stiffness and gating-spring integrity in hair cells. *Proc Natl Acad Sci USA* 94:11923–11928.

18. Michel V, Goodyear RJ, Weil D, Marcotti W, Perfettini I, Wolfrum U, Kros CJ, Richardson GP, Petit C (2005) Cadherin 23 is a component of the transient lateral links in the developing hair bundles of cochlear sensory cells. *Dev Biol* 280:281–294.

19. Goodyear R, Richardson G (1999) The ankle-link antigen: an epitope sensitive to calcium chelation associated with the hair-cell surface and the calycal processes of photoreceptors. *J Neurosci* 19:3761–3772.

20. Siemens J, Lillo C, Dumont RA, Reynolds A, Williams DS, Gillespie PG, Müller U (2004) Cadherin 23 is a component of the tip link in hair-cell stereocilia. *Nature 428*:950–955.

21. Sollner C, Rauch GJ, Siemens J, Geisler R, Schuster SC, Muller U, Nicolson T (2004) Mutations in cadherin 23 affect tip links in zebrafish sensory hair cells. *Nature* 428:955–959.

22. Senften M, Schwander M, Kazmierczak P, Lillo C, Shin JB, Hasson T, Geleoc GS, Gillespie PG, Williams D, Holt JR *et al.* (2006) Physical and functional interaction between protocadherin 15 and myosin VIIa in mechanosensory hair cells. *J Neurosci* 26:2060–2071.

23. Kazmierczak P, Sakaguchi H, Tokita J, Wilson-Kubalek EM, Milligan RA, Muller U, Kachar B (2007) Cadherin 23 and protocadherin 15 interact to form tip-link filaments in sensory hair cells. *Nature* 449:87–91.

24. Ahmed ZM, Goodyear R, Riazuddin S, Lagziel A, Legan PK, Behra M, Burgess SM, Lilley KS, Wilcox ER, Riazuddin S *et al.* (2006) The tip-link

antigen, a protein associated with the transduction complex of sensory hair cells, is protocadherin-15. *J Neurosci* 26:7022–7034.

25. Schwander M, Xiong W, Tokita J, Lelli A, Elledge HM, Kazmierczak P, Sczaniecka A, Kolatkar A, Wiltshire T, Kuhn P *et al.* (2009) A mouse model for nonsyndromic deafness (DFNB12) links hearing loss to defects in tip links of mechanosensory hair cells. *Proc Natl Acad Sci U S A* 106:5252– 5257.

26. Goodyear RJ, Forge A, Legan PK, Richardson GP (2010) Asymmetric distribution of cadherin 23 and protocadherin 15 in the kinocilial links of avian sensory hair cells. *J Comp Neurol* 518:4288–4297.

27. Alagramam KN, Goodyear RJ, Geng R, Furness DN, van Aken AF, Marcotti W, Kros CJ, Richardson GP (2011) Mutations in protocadherin 15 and cadherin 23 affect tip links and mechanotransduction in mammalian sensory hair cells. *PLoS One* 6:e19183.

28. Bolz H, von Brederlow B, Ramirez A, Bryda EC, Kutsche K, Nothwang HG, Seeliger M, Cabrera M, Vila MC, Molina OP *et al.* (2001) Mutation of CDH23, encoding a new member of the cadherin gene family, causes Usher syndrome type 1D. *Nat Genet* 27:108–12.

29. Bork JM, Peters LM, Riazuddin S, Bernstein SL, Ahmed ZM, Ness SL, Polomeno R, Ramesh A, Schloss M, Srisailpathy CR *et al.* (2001) Usher syndrome 1D and nonsyndromic autosomal recessive deafness DFNB12 are caused by allelic mutations of the novel cadherin-like gene CDH23. *Am J Hum Genet* 68:26–37.

30. Ahmed ZM, Riazuddin S, Bernstein SL, Ahmed Z, Khan S, Griffith AJ, Morell RJ, Friedman TB, Wilcox ER (2001) Mutations of the protocadherin gene PCDH15 cause Usher syndrome type 1F. *Am J Hum Genet* 69:25–34.

31. Ahmed ZM, Riazuddin S, Riazuddin S, Wilcox ER (2003) The molecular genetics of Usher syndrome. *Clin Genet* 63:431–444.

32. Alagramam KN, Yuan H, Kuehn MH, Murcia CL, Wayne S, Srisailpathy CR, Lowry RB, Knaus R, Van Laer L, Bernier FP *et al.* (2001) Mutations in the novel protocadherin PCDH15 cause Usher syndrome type 1F. *Hum Mol Genet* 10:1709–1718.

33. Di Palma F, Holme RH, Bryda EC, Belyantseva IA, Pellegrino R, Kachar B, Steel KP, Noben-Trauth K (2001) Mutations in Cdh23, encoding a new type of cadherin, cause stereocilia disorganization in waltzer, the mouse model for Usher syndrome type 1D. *Nat Genet* 27:103–17.

34. Richardson GP, de Monvel JB, Petit C (2011) How the genetics of deafness illuminates auditory physiology. *Annu Rev Physiol* 73:311–334.

35. Goodyear RJ, Marcotti W, Kros CJ, Richardson GP (2005) Development and properties of stereociliary link types in hair cells of the mouse cochlea. *J Comp Neurol* 485:75–85.

36. Waguespack J, Salles FT, Kachar B, Ricci AJ (2007) Stepwise morphological and functional maturation of mechanotransduction in rat outer hair cells. *J Neurosci* 27:13890–13902.

37. Si F, Brodie H, Gillespie PG, Vazquez AE, Yamoah EN (2003) Developmental assembly of transduction apparatus in chick basilar papilla. *J Neurosci* 23:10815–10826.

38. Pickles JO, von Perger M, Rouse GW, Brix J (1991) The development of links between stereocilia in hair cells of the chick basilar papilla. *Hearing Res* 54:153–163.

39. Nayak GD, Ratnayaka HS, Goodyear RJ, Richardson GP (2007) Development of the hair bundle and mechanotransduction. *Int J Dev Biol* 51:597–608.

40. Sotomayor M, Weihofen WA, Gaudet R, Corey DP (2010) Structural determinants of cadherin-23 function in hearing and deafness. *Neuron* 66:85–100.

41. Elledge HM, Kazmierczak P, Clark P, Joseph JS, Kolatkar A, Kuhn P, Muller U (2010) Structure of the N terminus of cadherin 23 reveals a new adhesion mechanism for a subset of cadherin superfamily members. *Proc Natl Acad Sci U S A* 107:10708–10712.

42. Zhao Y, Yamoah EN, Gillespie PG (1996) Regeneration of broken tip links and restoration of mechanical transduction in hair cells. *Proc Natl Acad Sci USA* 93:15469–15474.

43. Goodyear RJ, Richardson GP (2003) A novel antigen sensitive to calcium chelation that is associated with the tip links and kinocilial links of sensory hair bundles. *J Neurosci* 23:4878–4887.

44. Henderson D, Bielefeld EC, Harris KC, Hu BH (2006) The role of oxidative stress in noise-induced hearing loss. *Ear Hear* 27:1–19.

45. Adler HJ, Kenealy JF, Dedio RM, Saunders JC (1992) Threshold shift, hair cell loss, and hair bundle stiffness following exposure to 120 and 125 dB pure tones in the neonatal chick. *Acta Otolaryngol* 112:444–454.

46. Gao WY, Ding DL, Zheng XY, Ruan FM, Liu YJ (1992) A comparison of changes in the stereocilia between temporary and permanent hearing losses in acoustic trauma. *Hear Res* 62:27–41.

47. Canlon B (1988) The effect of acoustic trauma on the tectorial membrane, stereocilia, and hearing sensitivity: possible mechanisms underlying damage, recovery, and protection. *Scand Audiol Suppl* 27:1–45.

48. Pickles JO, Osborne MP, Comis SD (1987) The vulnerability of tip links between stereocilia in hair cells of the chick basilar papilla. *Hearing Res* 25:173–187.

49. Takumida M, Fredelius L, Bagger-Sjoback D, Harada Y, Wersall J (1989) Effect of acoustic overstimulation on the glycocalyx and the ciliary interconnections in the organ of Corti: high resolution scanning electron microscopic investigation. *J Laryngol Otol* 103:1125–1129.

50. Kurian R, Krupp NL, Saunders JC (2003) Tip link loss and recovery on chick short hair cells following intense exposure to sound. *Hear Res* 181:40–50.

51. Husbands JM, Steinberg SA, Kurian R, Saunders JC (1999) Tip-link integrity on chick tall hair cell stereocilia following intense sound exposure. *Hear Res* 135:135–145.

52. Mills JH, Gilbert RM, Adkins WY (1979) Temporary threshold shifts in humans exposed to octave bands of noise for 16 to 24 hours. *J Acoust Soc Am* 65:1238–1248.

53. Mills JH, Osguthorpe JD, Burdick CK, Patterson JH, Mozo B (1983) Temporary threshold shifts produced by exposure to low-frequency noises. *J Acoust Soc Am* 73:918–923.

54. Lelli A, Kazmierczak P, Kawashima Y, Muller U, Holt JR (2010) Development and regeneration of sensory transduction in auditory hair cells requires functional interaction between cadherin-23 and protocadherin-15. *J Neurosci* 30:11259–11269.

55. Fettiplace R, Fuchs PA (1999) Mechanisms of hair cell tuning. *Annu Rev Physiol* 61:809–834.

56. Farris HE, Wells GB, Ricci AJ (2006) Steady-state adaptation of mechanotransduction modulates the resting potential of auditory hair cells, providing an assay for endolymph [Ca2+]. *J Neurosci* 26:12526–12536.

57. Johnson SL, Beurg M, Marcotti W, Fettiplace R (2011) Prestin-driven cochlear amplification is not limited by the outer hair cell membrane time constant. *Neuron* 70:1143–1154.

58. Choudhary C, Mann M (2010) Decoding signalling networks by mass spectrometry-based proteomics. *Nat Rev Mol Cell Biol* 11:427–439.

59. Domon B, Aebersold R (2010) Options and considerations when selecting a quantitative proteomics strategy. *Nat Biotechnol* 28:710–721.

60. Ong SE, Blagoev B, Kratchmarova I, Kristensen DB, Steen H, Pandey A, Mann M (2002) Stable isotope labeling by amino acids in cell culture, SILAC, as a simple and accurate approach to expression proteomics. *Mol Cell Proteomics* 1:376–386.

61. Gygi SP, Rist B, Gerber SA, Turecek F, Gelb MH, Aebersold R (1999) Quantitative analysis of complex protein mixtures using isotope-coded affinity tags. *Nat Biotechnol* 17:994–999.

62. Ross PL, Huang YN, Marchese JN, Williamson B, Parker K, Hattan S, Khainovski N, Pillai S, Dey S, Daniels S *et al.* (2004) Multiplexed protein quantitation in Saccharomyces cerevisiae using amine-reactive isobaric tagging reagents. *Mol Cell Proteomics* 3:1154–1169.

63. Turck CW, Falick AM, Kowalak JA, Lane WS, Lilley KS, Phinney BS, Weintraub ST, Witkowska HE, Yates NA (2007) The Association of Biomolecular Resource Facilities Proteomics Research Group 2006 study: relative protein quantitation. *Mol Cell Proteomics* 6:1291–1298.

64. Liu H, Sadygov RG, Yates JRr (2004) A model for random sampling and estimation of relative protein abundance in shotgun proteomics. *Anal Chem* 76:4193–4201.

65. Lundgren DH, Hwang SI, Wu L, Han DK (2010) Role of spectral counting in quantitative proteomics. *Expert Rev Proteomics* 7:39–53.

66. Griffin NM, Yu J, Long F, Oh P, Shore S, Li Y, Koziol JA, Schnitzer JE (2010) Label-free, normalized quantification of complex mass spectrometry data for proteomic analysis. *Nat Biotechnol* 28:83–89.

67. Wilmarth PA, Riviere MA, David LL (2009) Techniques for accurate protein identification in shotgun proteomic studies of human, mouse, bovine, and chicken lenses. *J Ocul Biol Dis Infor* 2:223–234.

68. Fei SS, Wilmarth PA, Hitzemann RJ, McWeeney SK, Belknap JK, David LL (2011) Protein database and quantitative analysis considerations when integrating genetics and proteomics to compare mouse strains. *J Proteome Res* 10:2905–2912.

69. Fermin CD, Cohen GM (1984) Developmental gradients in the embryonic chick's basilar papilla. *Acta Otolaryngol* 97:39–51.

70. Goodyear RJ, Gates R, Lukashkin AN, Richardson GP (1999) Hair-cell numbers continue to increase in the utricular macula of the early posthatch chick. *J Neurocytol* 28:851–861.

71. Rebillard G, Rubel EW (1981) Electrophysiological study of the maturation of auditory responses from the inner ear of the chick. *Brain Res* 229:15–23.

72. Jones SM, Jones TA (2000) Ontogeny of vestibular compound action potentials in the domestic chicken. *J Assoc Res Otolaryngol* 1:232–242.

73. Tilney LG, Tilney MS, DeRosier DJ (1992) Actin filaments, stereocilia, and hair cells: how cells count and measure. *Ann Rev Cell Biol* 8:257–274.

74. Hillier LW, Miller W, Birney E, Warren W, Hardison RC, Ponting CP, Bork P, Burt DW, Groenen MA, Delany ME *et al.* (2004) Sequence and comparative analysis of the chicken genome provide unique perspectives on vertebrate evolution. *Nature* 432:695–716.

75. Shin JB, Longo-Guess CM, Gagnon LH, Saylor KW, Dumont RA, Spinelli KJ, Pagana JM, Wilmarth PA, David LL, Gillespie PG *et al.* (2010) The R109H variant of fascin-2, a developmentally regulated actin crosslinker in hair-cell stereocilia, underlies early-onset hearing loss of DBA/2J mice. *J Neurosci* 30:9683–9694.

76. Pavelka N, Fournier ML, Swanson SK, Pelizzola M, Ricciardi-Castagnoli P, Florens L, Washburn MP (2008) Statistical similarities between transcriptomics and quantitative shotgun proteomics data. *Mol Cell Proteomics* 7:631–644.

77. Tusher VG, Tibshirani R, Chu G (2001) Significance analysis of microarrays applied to the ionizing radiation response. *Proc Natl Acad Sci U S A* 98:5116–5121.

78. Fulton AB (1982) How crowded is the cytoplasm? *Cell* 30:345–347.

79. Srivastava DK, Bernhard SA (1986) Enzyme-enzyme interactions and the regulation of metabolic reaction pathways. *Curr Top Cell Regul* 28:1–68.

80. Oberholtzer JC, Buettger C, Summers MC, Matschinsky FM (1988) The 28-kDa calbindin-D is a major calcium-binding protein in the basilar papilla of the chick. *Proc Natl Acad Sci U S A* 85:3387–3390.

81. Hackney CM, Mahendrasingam S, Jones EM, Fettiplace R (2003) The distribution of calcium buffering proteins in the turtle cochlea. *J Neurosci* 23:4577–4589.

82. Hackney CM, Mahendrasingam S, Penn A, Fettiplace R (2005) The concentrations of calcium buffering proteins in mammalian cochlear hair cells. *J Neurosci* 25:7867–7875.

83. Gygi SP, Rochon Y, Franza BR, Aebersold R (1999) Correlation between protein and mRNA abundance in yeast. *Mol Cell Biol* 19:1720–1730.

84. Ideker T, Thorsson V, Ranish JA, Christmas R, Buhler J, Eng JK, Bumgarner R, Goodlett DR, Aebersold R, Hood L (2001) Integrated genomic and proteomic analyses of a systematically perturbed metabolic network. *Science* 292:929–934.

85. Tian Q, Stepaniants SB, Mao M, Weng L, Feetham MC, Doyle MJ, Yi EC, Dai H, Thorsson V, Eng J *et al.* (2004) Integrated genomic and proteomic analyses of gene expression in mwammalian cells. *Mol Cell Proteomics* 3:960–969.

86. Mijalski T, Harder A, Halder T, Kersten M, Horsch M, Strom TM, Liebscher HV, Lottspeich F, de Angelis MH, Beckers J (2005) Identification of coexpressed gene clusters in a comparative analysis of transcriptome and proteome in mouse tissues. *Proc Natl Acad Sci U S A* 102:8621–8626.

87. Irmler M, Hartl D, Schmidt T, Schuchhardt J, Lach C, Meyer HE, Hrabe de Angelis M, Klose J, Beckers J (2008) An approach to handling and interpretation of ambiguous data in transcriptome and proteome comparisons. *Proteomics* 8:1165–1169.

88. Wu Z, Irizarry RA, Gentleman R, Murillo, F.M., Spencer F (2004) A model based background adjustment for oligonucleotide expression arrays. *Journal of the American Statistical Association* 99:909–917.

89. Bolstad BM, Irizarry RA, Astrand M, Speed TP (2003) A comparison of normalization methods for high density oligonucleotide array data based on variance and bias. *Bioinformatics* 19:185–193.

90. Schwanhausser B, Busse D, Li N, Dittmar G, Schuchhardt J, Wolf J, Chen W, Selbach M (2011) Global quantification of mammalian gene expression control. *Nature* 473:337–342.

91. Semenza GL (2010) HIF-1: upstream and downstream of cancer metabolism. *Curr Opin Genet Dev* 20:51–56.

92. Papandreou I, Cairns RA, Fontana L, Lim AL, Denko NC (2006) HIF-1 mediates adaptation to hypoxia by actively downregulating mitochondrial oxygen consumption. *Cell Metab* 3:187–197.

93. Zhang H, Bosch-Marce M, Shimoda LA, Tan YS, Baek JH, Wesley JB, Gonzalez FJ, Semenza GL (2008) Mitochondrial autophagy is an HIF-1-dependent adaptive metabolic response to hypoxia. *J Biol Chem* 283:10892–10903.

94. Ashcroft SJ, Weerasinghe LC, Bassett JM, Randle PJ (1972) The pentose cycle and insulin release in mouse pancreatic islets. *Biochem J* 126:525–532.

95. Qi JH, Ebrahem Q, Moore N, Murphy G, Claesson-Welsh L, Bond M, Baker A, Anand-Apte B (2003) A novel function for tissue inhibitor of

metalloproteinases-3 (TIMP3): inhibition of angiogenesis by blockage of VEGF binding to VEGF receptor-2. *Nat Med* 9:407–415.

96. Adams JC (2001) Thrombospondins: multifunctional regulators of cell interactions. *Annu Rev Cell Dev Biol* 17:25–51.

97. Qin J, Chen X, Yu-Lee LY, Tsai MJ, Tsai SY (2010) Nuclear receptor COUP-TFII controls pancreatic islet tumor angiogenesis by regulating vascular endothelial growth factor/vascular endothelial growth factor receptor-2 signaling. *Cancer Res* 70:8812–8821.

98. Seckinger A, Meissner T, Moreaux J, Goldschmidt H, Fuhler GM, Benner A, Hundemer M, Reme T, Shaughnessy JDJ, Barlogie B *et al.* (2009) Bone morphogenic protein 6: a member of a novel class of prognostic factors expressed by normal and malignant plasma cells inhibiting proliferation and angiogenesis. *Oncogene* 28:3866–3879.

99. Hu J, Dong A, Fernandez-Ruiz V, Shan J, Kawa M, Martinez-Anso E, Prieto J, Qian C (2009) Blockade of Wnt signaling inhibits angiogenesis and tumor growth in hepatocellular carcinoma. *Cancer Res* 69:6951–6959.

100. Picotti P, Bodenmiller B, Mueller LN, Domon B, Aebersold R (2009) Full dynamic range proteome analysis of S. cerevisiae by targeted proteomics. *Cell* 138:795–806.

101. Vander Heiden MG, Cantley LC, Thompson CB (2009) Understanding the Warburg effect: the metabolic requirements of cell proliferation. *Science* 324:1029–1033.

102. Fang M, Shen Z, Huang S, Zhao L, Chen S, Mak TW, Wang X (2010) The ER UDPase ENTPD5 promotes protein N-glycosylation, the Warburg effect, and proliferation in the PTEN pathway. *Cell* 143:711–724.

103. Schirle M, Heurtier MA, Kuster B (2003) Profiling core proteomes of human cell lines by one-dimensional PAGE and liquid chromatography-tandem mass spectrometry. *Mol Cell Proteomics* 2:1297–1305.

104. Keller A, Nesvizhskii AI, Kolker E, Aebersold R (2002) Empirical statistical model to estimate the accuracy of peptide identifications made by MS/MS and database search. *Anal Chem* 74:5383–5392.

105. Elias JE, Gygi SP (2007) Target-decoy search strategy for increased confidence in large-scale protein identifications by mass spectrometry. *Nat Methods* 4:207–214.

106. Team RDC (2011) R: A language and environment for statistical computing.

107. Osborne MP, Comis SD (1990) Action of elastase, collagenase and other enzymes upon linkages between stereocilia in the guinea pig cochlea. *Acta Otolaryngol(Stockh)* 110:37–45.

108. Auer M, Koster AJ, Ziese U, Bajaj C, Volkmann N, Wang da N, Hudspeth AJ (2008) Three-dimensional architecture of hair-bundle linkages revealed by electron-microscopic tomography. *J Assoc Res Otolaryngol* 9:215–224.

109. Griesinger CB, Richards CD, Ashmore JF (2004) Apical endocytosis in outer hair cells of the mammalian cochlea. *Eur J Neurosci* 20:41–50.

110. Richardson GP, Forge A, Kros CJ, Fleming J, Brown SD, Steel KP (1997) Myosin VIIA is required for aminoglycoside accumulation in cochlear hair cells. *J Neurosci* 17:9506–919.

111. Klingler C, Kniesel U, Bamforth SD, Wolburg H, Engelhardt B, Risau W (2000) Disruption of epithelial tight junctions is prevented by cyclic nucleotide-dependent protein kinase inhibitors. *Histochem Cell Biol* 113:349–361.

112. Citi S (1992) Protein kinase inhibitors prevent junction dissociation induced by low extracellular calcium in MDCK epithelial cells. *J Cell Biol* 117:169–178.

113. Ma TY, Tran D, Hoa N, Nguyen D, Merryfield M, Tarnawski A (2000) Mechanism of extracellular calcium regulation of intestinal epithelial tight junction permeability: role of cytoskeletal involvement. *Microsc Res Tech* 51:156–168.

114. Dumont RA, Lins U, Filoteo AG, Penniston JT, Kachar B, Gillespie PG (2001) Plasma membrane Ca^{2+}-ATPase isoform 2a is the PMCA of hair bundles. *J Neurosci* 21:5066–5078.

115. Glowatzki E, Grant L, Fuchs P (2008) Hair cell afferent synapses. *Curr Opin Neurobiol* 18:389–395.

116. Crawford AC, Evans MG, Fettiplace R (1991) The actions of calcium on the mechano-electrical transducer current of turtle hair cells. *J Physiol (Lond)* 434:369–398.

117. Lumpkin EA, Hudspeth AJ (1995) Detection of Ca^{2+} entry through mechanosensitive channels localizes the site of mechanoelectrical transduction in hair cells. *Proc Natl Acad Sci USA* 92:10297–10301.

118. Beurg M, Fettiplace R, Nam JH, Ricci AJ (2009) Localization of inner hair cell mechanotransducer channels using high-speed calcium imaging. *Nat Neurosci* 12:553–558.

119. Bortolozzi M, Brini M, Parkinson N, Crispino G, Scimemi P, De Siati RD, Di Leva F, Parker A, Ortolano S, Arslan E *et al.* (2010) The novel PMCA2 pump mutation Tommy impairs cytosolic calcium clearance in hair cells and links to deafness in mice. *J Biol Chem* 285:37693–37703.

120. Ficarella R, Di Leva F, Bortolozzi M, Ortolano S, Donaudy F, Petrillo M, Melchionda S, Lelli A, Domi T, Fedrizzi L *et al.* (2007) A functional study of plasma-membrane calcium-pump isoform 2 mutants causing digenic deafness. *Proc Natl Acad Sci U S A* 104:1516–1521.

121. Yuan T, Gao SS, Saggau P, Oghalai JS (2010) Calcium imaging of inner ear hair cells within the cochlear epithelium of mice using two-photon microscopy. *J Biomed Opt* 15:016002.

122. Frolenkov GI (2009) Ion imaging in the cochlear hair cells. *Methods Mol Biol* 493:381–399.

123. Raybould NP, Jagger DJ, Kanjhan R, Greenwood D, Laslo P, Hoya N, Soeller C, Cannell MB, Housley GD (2007) TRPC-like conductance mediates restoration of intracellular Ca2+ in cochlear outer hair cells in the guinea pig and rat. *J Physiol* 579:101–113.

124. Lumpkin EA, Marquis RE, Hudspeth AJ (1997) The selectivity of the hair cell's mechanoelectrical-transduction channel promotes Ca^{2+} flux at low Ca^{2+} concentrations. *Proc Natl Acad Sci USA* 94:10997–11002.

125. Farris HE, LeBlanc CL, Goswami J, Ricci AJ (2004) Probing the pore of the auditory hair cell mechanotransducer channel in turtle. *J Physiol* 558:769–792.

126. Fuchs PA, Evans MG, Murrow BW (1990) Calcium currents in hair cells isolated from the cochlea of the chick. *J Physiol* 429:553–568.

127. Zidanic M, Fuchs PA (1995) Kinetic analysis of barium currents in chick cochlear hair cells. *Biophys J* 68:1323–1336.

128. Meyers JR, MacDonald RB, Duggan A, Lenzi D, Standaert DG, Corwin JT, Corey DP (2003) Lighting up the senses: FM1-43 loading of sensory cells through nonselective ion channels. *J Neurosci* 23:4054–4065.

129. Thalmann R, Miyoshi T, Thalmann I (1972) The influence of ischemia upon the energy reserves of inner ear tissues. *Laryngoscope* 82:2249–2272.

130. Matschinsky FM, Thalmann R (1967) Quantitative histochemistry of microscopic structures of the cochlea. II. Ischemic alterations of levels of glycolytic intermediates and cofactors in the organ of corti and stria vascularis. *Ann Otol Rhinol Laryngol* 76:638–646.

131. Hossler FE, Olson KR, Musil G, McKamey MI (2002) Ultrastructure and blood supply of the tegmentum vasculosum in the cochlea of the duckling. *Hear Res* 164:155–165.

132. Zdebik AA, Wangemann P, Jentsch TJ (2009) Potassium ion movement in the inner ear: insights from genetic disease and mouse models. *Physiology (Bethesda)* 24:307–316.

133. Nickel R, Forge A (2008) Gap junctions and connexins in the inner ear: their roles in homeostasis and deafness. *Curr Opin Otolaryngol Head Neck Surg* 16:452–457.

134. Alharazneh A, Luk L, Huth M, Monfared A, Steyger PS, Cheng AG, Ricci AJ (2011) Functional hair cell mechanotransducer channels are required for aminoglycoside ototoxicity. *PLoS One* 6:e22347.

135. Holt JR, Gillespie SK, Provance DW, Shah K, Shokat KM, Corey DP, Mercer JA, Gillespie PG (2002) A chemical-genetic strategy implicates myosin-1c in adaptation by hair cells. *Cell* 108(3):371-81.

136. Salles FT, Merritt RC, Manor U, Dougherty GW, Sousa AD, Moore JE, Yengo CM, Dose AC, Kachar B (2009) Myosin IIIa boosts elongation of stereocilia by transporting espin 1 to the plus ends of actin fillaments. *Nat Cell Biol* 11(4):443-50.

137. Wang GL, Jiang BH, Rue EA, Semenza GL (1995) Hypoxia-inducible factor 1 is a basic-helix-loop-helix-PAS heterodimer regulated by cellular O2 tension. *Proc Natl Acad Sci* 92(12):5510-4.

138. Manders EM, Stap J, Brakenhoff GJ, Van Driel R Aten JA (1992) Dynamics of three-dimensional replication patters during S-phase, analysed by double labelling of DNA and confocal microscopy. *Journal of Cell Science* (103):857-862.

139. Costes SV, Daelemans D, Cho EH, Dobbin Z, Pavlakis G, Lockett S (2004) Automatic and quantitative measurement of protein-protein colocalization in live cells. *Biophysical Journal* (86):3993-4003.

140. Tanaka K, Smith CA (1978) Structure of the chicken's inner ear: SEM and TEM study. *Am J Anat* 153:251-272.